

Optimization of RNAV Departure Trajectories

with Respect to Environmental Criteria

Janite Quiran Parmanande

Thesis to obtain the Master of Science Degree in

Aerospace Engineering

Supervisors:

Prof. João Manuel Gonçalves de Sousa Oliveira

Prof. Pedro da Graça Tavares Alvares Serrão

Examination Committee

Chairperson: Prof. João Manuel Lage de Miranda Lemos

Supervisors: Prof. Pedro da Graça Tavares Alvares Serrão

Member of the Committee: Prof. António Aguiar

October 2016

Acknowledgements

First of all, I would like to express my sincere gratitude to my advisors, Professor João Oliveira and Professor Pedro Serrão, for both the opportunity of working with them and the continuous support, motivation and invaluable knowledge steering me in the right direction. The doors to their offices were always open for me whenever I had any questions.

I would also like to express my gratitude to my dear parents, siblings, significant other and family in general for the unconditional love and support throughout my whole life. Without them, I wouldn't have reached this far and wouldn't be the person I am today.

I thank my fellow classmates and friends I made throughout the years, for making this journey unforgettable.

I would finally like to thank Professor Alexandre Gonçalves for all the insight on the matter of Geographic Information Systems and Professor António Aguiar for all the flight data shared, without which this project wouldn't have been possible. I would also like to express my gratitude to Airspace Planners Américo Melo, Luís Martins and Vanda da Cruz from NAV Portugal and Environmental Specialists Sílvia Pereira and Jorge Mendeira from ANA for the valuable meetings and recommendations. Lastly, I would like to thank Lieutenant-Colonel Carlos Fernandes for the very much appreciated guided tour around Montijo Air Base.

A special mention goes to my cousins for helping me with the aesthetic details.

Resumo

Nos últimos anos, o tráfego aéreo tem visto um crescimento exponencial, resultado da crescente procura por transporte aéreo. Este aumento tem levado ao levantamento de questões ambientais focados em manter a aviação sustentável, sendo o ruído ligado à aviação um dos problemas mais importantes actualmente. Em resposta a estas questões, reguladores de aviação têm imposto novas regras e certificações para evitar que os níveis de ruído atinjam certos níveis, considerados indesejáveis já que podem levar a problemas de saúde.

Paralelamente, e relacionado com esta crescente procura, o Aeroporto Humberto Delgado de Lisboa prevê um crescimento de tráfego maior do que consegue suportar actualmente. Em resposta a esta preocupação, a solução proposta e em fase de desenvolvimento consiste na utilização da Base Aérea Nº 6 do Montijo - actualmente uma base militar - como aeródromo auxiliar de forma a expandir a capacidade do aeroporto de Lisboa.

Assim sendo, nesta dissertação, procedimentos de saída focados em minimização do impacto do ruído foram definidos para este aeródromo, como um estudo de cariz académico da componente de ruído deste projecto em desenvolvimento. Para este objectivo, um modelo de ruído detalhado foi desenvolvido, capaz de modelar qualquer trajectória desejada e de calcular os níveis de ruído a que as comunidades são sujeitas devido a essa trajectória. Complementarmente, um estudo das mesmas comunidades foi feito, de forma a estudar o impacto do ruído nas mesmas. Posto isto, Procedimentos de Minimização de Ruído (*Noise Abatement Procedures*) foram estudados e aplicados neste aeródromo, seguidos de uma comparação entre cada um destes procedimentos em termos do impacto nas comunidades.

Palavras-Chave: Ruído Aeronáutico, Procedimentos de Redução de Ruído, Montijo (LPMT), Portela+1

Abstract

In recent years, air traffic has shown an exponential growth, a result of the increasing demand for air transportation. This growth has led to environmental concerns regarding keeping air transportation sustainable, with aviation noise at the forefront of these concerns. To answer these concerns, aviation regulators have imposed new rules and certifications to make sure that noise levels do not overstep safety thresholds, as that would be hazardous to public health.

In parallel, and also as a consequence of the increasing demand for air transportation, Lisbon's main airport, Humberto Delgado, is expected to experience higher demand than it can currently deal with. One solution that is currently being explored in order to tackle this issue is the use of Air Base No. 6 of Montijo - currently a military air base - as an auxiliary aerodrome as a way to add to Humberto Delgado airport's maximum capacity.

With all of this in mind, in this dissertation, departure trajectories were designed for Montijo's Air Base with emphasis on Noise Abatement, as an academic study of the noise section of this ongoing project. For this purpose a detailed noise model was developed, capable of modelling any desired trajectory and calculating the noise levels it creates for nearby communities. Furthermore, an analysis was made to assess the impact noise has on those communities. After a thorough research on common Noise Abatement Procedures, some of these were applied and compared between themselves based on that criteria.

Keywords: Aviation Noise, Noise Abatement Procedures, Montijo (LPMT), Portela+1

Table of Contents

Acknowledgements.....	i
Resumo.....	ii
Abstract.....	iii
Table of Contents.....	iv
List of Tables.....	vii
List of Figures.....	ix
List of Abbreviations.....	xii
List of Symbols.....	xiv
1 Introduction.....	1
1.1 Context.....	1
1.2 Objectives	2
1.3 Structure	3
2 Theoretical Background.....	4
2.1 Sound and Noise.....	4
2.2 Noise Measurement.....	5
2.3 Noise Metrics	6
2.3.1 Single Event Noise Metrics	6
2.3.2 Cumulative Noise Metrics	8
2.4 Geographical Information System.....	9
2.5 ANP Database	10
2.6 Airport and Aircraft Operations	11
2.6.1 RNAV and RNP.....	12
2.6.2 Noise Abatement Procedures (NAP).....	13
2.6.3 SESAR.....	17
2.6.4 NextGen.....	18
3 ECAC Doc.29 Noise Model.....	19
3.1 Geometry.....	19
3.2 Aircraft Performance Calculations	21
3.3 Flight path segmentation	22
3.3.1 Ground track and flight profile	23

3.3.2	Ground Roll	27
3.3.3	Initial Climb.....	27
3.3.4	Accelerated Climb	28
3.3.5	Thrust Reduction.....	29
3.4	Single Event Noise Calculation	30
3.4.1	NPD Tables	30
3.4.2	Segment Noise Level L_{seg} and Event Noise Level L	31
3.4.3	Corrections.....	32
3.5	Cumulative Noise Calculation.....	33
3.6	Noise Contours.....	33
4	Parameters for the design of trajectories.....	34
4.1	Processing GIS	34
4.1.1	Sources of data.....	34
4.1.2	Software.....	36
4.2	Awakenings	37
5	Experimental Validation	39
5.1	Noise validation.....	39
5.1.1	Validation Process.....	39
5.1.2	Results	41
5.2	Trajectories validation	46
5.2.1	Validation Process.....	46
5.2.2	Results	48
6	Application to Montijo Airport	50
6.1	Population Analysis [GIS]	50
6.2	Lisbon's Terminal Airspace	51
6.2.1	Montijo Air Base.....	52
6.2.2	Danger, Restricted and Prohibited Areas	53
6.3	Aircraft, Movements and Schedules	53
6.3.1	Routes	54
6.3.2	Schedules and Aircraft.....	55
6.4	Procedures.....	57

7	Results and Discussion	59
	7.1 Standard Noise Abatement Procedures	59
	7.2 Custom Procedures.....	64
	7.3 Cumulative Noise Metric <i>LDEN</i>	67
	7.4 Additional Considerations.....	69
8	Conclusions and Further Research.....	72
	References	75
	Appendix.....	80
	A. Performance calculation parameters.....	80
	B. Noise as measured from Noise Monitoring Stations	82
	B1	82
	B2	82
	C. Modeled Flight Paths for Validation - TP348	83
	D. Validation Results.....	85
	E. Lisbon Restricted and Danger Areas	86
	F. RNAV SIDs for Lisbon (LPPT) RWY 03/35.....	87
	G. FlightRadar24 data - TP348	88
	H. Departure trajectories - FlightRadar24 data.....	89
	I. Flight Schedules.....	90
	J. Standard ANP Departure Procedures	91

List of Tables

Table 2-1 - Parameters for different forms of equivalent sound levels Leq according to Equation (2-15). [12]	9
Table 3-1 - Reference conditions for NPD data in the ANP database. [17]	21
Table 3-2 - Example of a standard procedure as described in the ANP database, for an ICAO-A procedure for an Airbus A320-211. [17]	23
Table 4-1 - Excerpt of GIS data for Portugal total area from 2011, taken from Portugal's Statistics National Institute. [37]	34
Table 4-2 - Excerpt of GIS data for Portugal total area from 2011, taken from Portugal's Statistics National Institute. [37]	35
Table 5-1 - Excerpt of flight parameters for flight TP544 with destination to Düsseldorf Airport (date not disclosed for confidentiality reasons).....	39
Table 5-2 - Excerpt from noise monitoring station data for the same flight TP544 with destination to Düsseldorf Airport.....	40
Table 5-3 - Results obtained for the first set of flight procedures.....	42
Table 5-4 - Results obtained for the second set of flight procedures.	42
Table 5-5 - Corrected errors for L_{max} in Stations 1, 3 and 7.....	44
Table 5-6 - Summary of the average errors for the corrections made for L_{max} in each station.....	45
Table 5-7 - Overview for the errors of L_{max} in the original and the corrected model.....	46
Table 5-8 - Standard deviation and variance for corrected and uncorrected models.....	49
Table 6-1 - ICAO airspace division and specifications overview.....	51
Table 7-1 - Thrust setting for each phase of the flight. [60]	70
Table A-1- Performance parameters intrinsic to the aircraft.....	80
Table A-2 - Procedural steps combination matrix.	80
Table A-3 - Excerpt of Jet Engine Coefficients Table for A320-211, as obtained from the ANP database [58].....	81
Table A-4 - Excerpt of Aerodynamic Coefficients table for A320-211, as obtained from the ANP database [58].....	81
Table B-1 - Set 1 Noise	82
Table B-2 - Set 2 Noise	82
Table C-1 - Procedural Steps to simulate flight TP348.....	83
Table D-1 - Results obtained for the procedures defined in the model for segmentation and noise validation.....	85

Table I-1 - Schedule as obtained from ANA for Ryanair and EasyJet.....	90
Table J-1 - ANP standard procedure (Default) for Airbus A320-211.....	91
Table J-2 - ANP standard ICAO-A procedure for Airbus A320-211.	91
Table J-3 - ANP standard ICAO-B procedure for Airbus A320-211.....	91

List of Figures

Figure 1-1 - Number of movements in Lisbon and Portugal. [5]	2
Figure 1-2 - Number of movements in Montijo Air Base. [5]	2
Figure 1-3 - Process for flight procedures design.	3
Figure 2-1 - Noise level curve vs time Lt , and some relevant parameters. [12]	7
Figure 2-2 - Interpolation in a noise-power-distance curve. [12]	10
Figure 2-3 - Position finding of an aircraft with NDB (on the left), VOR (in the middle), and VOR-DME (on the right). [19]	11
Figure 2-4 - Comparison between RNAV and RNP over conventional, ground-based navigation systems. [20].....	12
Figure 2-5 - PBN implementation's effect on Capacity. [20]	12
Figure 2-6 - Schematic representation on how adjustments in ground track (on the left) and profile (on the right) can reduce the noise impact on sensitive areas. [20]	13
Figure 2-7 - Schematic representation of the Fanning NAP. [1].....	14
Figure 2-8 - Radar tracking of flights before and after the implementation of RNAV. [26]	14
Figure 2-9 - Schematic representation of turn restriction ground tracks. [1].....	15
Figure 2-10 - Schematic representation of multi-turn NAP ground tracks. [1]	15
Figure 2-11 - NADP 1 and NADP 2 profile representation. [28].....	16
Figure 2-12 - Sequential phases from SESAR project. [29]	18
Figure 3-1 - The noise contour generation process. [12]	19
Figure 3-2 - East-North-Up (ENU) coordinate system. [34].....	20
Figure 3-3 - Local reference coordinate system x, y, z , centered on Montijo's aerodrome. [Google Maps].....	20
Figure 3-4 - Ground track-fixed co-ordinates system. [12]	20
Figure 3-5 - Aircraft-fixed coordinate system. [12].....	21
Figure 3-6 - Ground track geometry in terms of straight segments and turns and arcs segmentation. [12]	24
Figure 3-7 - Evolution of temperature and pressure in the International Standard Atmosphere model. [35]	26
Figure 3-8 - Aircraft-observer angles. [12].....	31
Figure 4-1 - Subsection 15060101308 (Arroteias, Alhos Vedros - Moita) from Portugal's Statistics National Institute database.	36

Figure 4-2 - The same subsection's location represented in Google Maps view.....	36
Figure 4-3 - Schematic representation of subsections (A and B) and grid cells (1-4).....	37
Figure 4-4 - FICAN proposed sleep disturbance dose-response relationship. [40].....	38
Figure 5-1 - Lisbon map with the location of the stations mentioned in Table 5-2. [Google Maps] ...	40
Figure 5-2 - Noise level error at monitoring stations.....	43
Figure 5-3 - Noise Level error at monitoring stations.....	43
Figure 5-4 - Graphical representation of the standard deviation obtained for L_{max} each station. ...	45
Figure 5-5 - Schematic representation of the evolution of wind intensity with height. [41]	46
Figure 5-6 - CAS and Altitude evolution throughout the flight, obtained through the real data available from flight TAP616.....	47
Figure 5-7 - Choosing the segment index (black circle) to initiate the turn.....	48
Figure 5-8 - Setting the turn to match the real flight path.	48
Figure 6-1 - Population density grid map for area of interest around Montijo.	50
Figure 6-2 - Montijo Air Base, as seen from Google Maps' satellite view.....	52
Figure 6-3 - Air Traffic distribution for LPPT for July 23 rd 2013. Data provided by NAV Portugal.....	54
Figure 6-4 - Distribution of SID Routes for the flights.....	56
Figure 6-5 - Distribution of Aircraft.....	56
Figure 7-1 - Full set of modeled trajectories for Airbus A320-211.....	59
Figure 7-2 - SEL contour for departure procedure on Lisbon map.	60
Figure 7-3 - SEL contour for departure procedure on Lisbon population density map.	60
Figure 7-4 - Flight profiles for ICAO-A and ICAO-B procedures.....	61
Figure 7-6 - Turn Restriction NAPs.....	62
Figure 7-7 - Multi-Turn NAPs.....	62
Figure 7-8 - Bar chart for the Awakenings parameter obtained for each trajectory modeled.....	62
Figure 7-9 - Comparison between MT1A and TR4B departure procedures.	63
Figure 7-10 - Optimal Flight Paths with respect to the Awakenings parameter.....	63
Figure 7-11 - Awakenings parameter for the optimal flight paths of each route.....	64
Figure 7-12 - Comparison between standard NAP and custom path to BUSEN.....	65
Figure 7-13 - Comparison between standard NAP and custom path to BUSEN.....	65
Figure 7-14 - Long Turn custom path, going around Danger area D10.....	66

Figure 7-15 - Comparison between Short Turn custom path, colored in green in Figure 7-13, and the Long Turn path going around area D10.....	66
Figure 7-16 - Comparison between the displacements for an aircraft following the two previously mentioned flights.	66
Figure 7-17 - Comparison between new short and long turn flight paths, with a safety margin for area D10.....	67
Figure 7-18 - Standard arrival trajectories modeled.....	68
Figure 7-19 - RWY1 arrival route - GIS map.....	68
Figure 7-20 - <i>LDEN</i> in area of interest based on the standard schedule found in Appendix I.....	69
Figure C-1 - Modeled and Real Flight Paths for TP348.....	83
Figure C-2 - Position Error in function of the ground distance traveled.....	84
Figure C-3 - True Airspeed error in function of the ground distance traveled.....	84
Figure C-4 - Noise-related Power parameter (Net Thrust) for Real and Modeled paths in function of ground distance.....	84
Figure D-1 - Noise related power parameter (net thrust) error in function of ground distance traveled.....	85
Figure E-1 - Restricted and Danger Areas in Lisbon TMA.....	86
Figure F-1 - RNAV SID for LPPT RWY 03/35.....	87
Figure G-1 - Trajectory for flight TP348, as obtained from Flightradar24.com on August 25 th 2016.....	88
Figure G-2 - Speed and Altitude over duration of flight graphs for flight TP348, as obtained from Flightradar24.com on August 25 th 2016.....	88
Figure H-1 - All departing flights from Ryanair.....	89
Figure H-2 - All departing flights from EasyJet.....	89

List of Abbreviations

<i>ABL</i>	Atmospheric Boundary Layer
<i>AFE</i>	Above Field Elevation
<i>AGL</i>	Above Ground Level
<i>AIP</i>	Aeronautical Information Publication
<i>AIS</i>	Aeronautical Information Service
<i>AMSL</i>	Above Mean Sea Level
<i>ANA</i>	Aeroportos e Navegação Aérea
<i>ANP</i>	Aircraft Noise and Performance
<i>ANSI</i>	American National Standards Institute
<i>ARP</i>	Airport/Aerodrome Reference Point
<i>ASA</i>	Acoustical Society of America
<i>ATC</i>	Airc Traffic Control
<i>ATM</i>	Air Traffic Management
<i>CAS</i>	Calibrated Airspeed
<i>CDA</i>	Continuous Descent Approach
<i>dB</i>	Decibel
<i>dba</i>	A-weighted decibel
<i>DME</i>	Distance Measuring Equipment
<i>EASA</i>	European Aviation Safety Agency
<i>ECAC</i>	European Civil Aviation Conference
<i>EEA</i>	European Environment Agency
<i>ENU</i>	East-North-Up
<i>EPN</i>	Effective Perceived Noise
<i>EUROCONTROL</i>	European Organisation for the Safety of Air Navigation
<i>FAA</i>	Federal Aviation Administration
<i>FICAN</i>	Federal Interagency Committee on Aviation Noise
<i>GIS</i>	Geographic Information System
<i>GPS</i>	Global Positioning System
<i>IAS</i>	Indicated Airspeed
<i>ICAO</i>	International Civil Aviation Organization
<i>IFR</i>	Instrument Flight Rules
<i>ILS</i>	Instrument Landing System
<i>INE</i>	National Statistical Institute
<i>INM</i>	Integrated Noise Model
<i>ISA</i>	International Standard Atmosphere
<i>ISO</i>	International Organization for Standardization
<i>LPPT</i>	Lisbon Humberto Delgado Airport
<i>LPMT</i>	Montijo Air Base
<i>MLS</i>	Microwave Landing System
<i>MSL</i>	Mean Sea Level
<i>NADP</i>	Noise Abatement Departure Procedure
<i>NAP</i>	Noise Abatement Procedure
<i>Navaid</i>	Navigational Aid
<i>NDB</i>	Non-Directional Beacon

<i>NextGen</i>	Next Generation Air Transportation System
<i>NPD</i>	Noise-Power-Distance
<i>NUTS</i>	Nomenclature of Territorial Units
<i>OECD</i>	Organization for Economic Cooperation and Development
<i>PBN</i>	Performance-Based Navigation
<i>PndB</i>	Perceived Noise decibel
<i>RNAV</i>	Area Navigation
<i>RNP</i>	Required Navigation Performance
<i>RWY</i>	Runway
<i>SESAR</i>	Single European Sky ATM Research
<i>SID</i>	Standard Instrument Departure
<i>STAPES</i>	System for Airport Noise Exposure Studies
<i>STAR</i>	Standard Terminal Arrival Route
<i>TAS</i>	True Airspeed
<i>TMA</i>	Terminal Control/Manoeuvring Area
<i>VFR</i>	Visual Flight Rules
<i>VOR</i>	Very High Frequency Omnidirectional Range
<i>WHO</i>	World Health Organization

List of Symbols

ρ	Air Density
σ	Standard Deviation
σ^2	Variance
F_n	Net Thrust per engine
F_n/δ	Corrected Net Thrust per engine
h	Aircraft altitude (AMSL)
L_A	A-weighted Sound Pressure Level
L_{AE}	Sound Exposure Level
L_{Amax}	Maximum value of L_A during an event
L_{DEN}	Day-Evening_Night Level
L_E	Single Event Sound Exposure Level
L_{EPN}	Effective Perceived Noise Level
L_{eq}	Equivalent Continuous Noise Level
L_{PNT}	Tone Corrected Perceived Noise Level
\log	Logarithm to base 10
p	Air Pressure
P	Power parameter in NPD variable $L(P,d)$
SEL	Sound Exposure Level
T	Air Temperature
t	Time
V	Ground Speed
x, y, z	Local Coordinates

1 Introduction

1.1 Context

Throughout the years, air traffic has been increasing exponentially and, even though making air transportation environmentally sustainable is not currently possible, it is possible to make it progressively more so. Climatic changes and local air quality concerns have become more frequent around the world, despite the fact that aviation contributes in less than 3% to greenhouse gas emissions [1]; similarly, aircraft noise is currently one of the most relevant public concerns.

A recent report by European environment and aviation agencies shows that the growth in European air traffic has outstripped technological and operational improvements over the past 25 years, thus leading to increased environmental pressures in the next years. This report - The European Aviation Environmental Report from 2016 - is a collaboration between the European Commission, the European Aviation Safety Agency (EASA), the European Environmental Agency (EEA) and EUROCONTROL. [2] According to the report, aircraft noise has been decreasing by around 4 dB per decade since 1960. Nevertheless, that improvement has been decreasing in recent years, which is leading to smaller and smaller improvements in population exposed to noise, while the number of flights is still increasing. The population exposed to noise levels above 55 dBA L_{den} ¹ is projected to increase by 15% up to 2035. [3]

With the concern that the air traffic growth may be able to surpass the introduction of new and better technologies, these concerns have been studied gradually and through different approaches with the intention of being mitigated and controlled. ICAO (*International Civil Aviation Organization*) proposed different interventional measures for noise mitigation, which, between the two adversities mentioned, will be the one that will be given more focus to.

Several methods have been developed to facilitate the study of noise, such as the calculation of Noise Contours to assess the impact of noise in different regions around an airport, based on different operations throughout the day. For these methods, it is necessary to use mathematical models capable of making simulations of any procedure based on real data to design realistic maps, avoiding the need to do practical tests of those procedures. There are different models for this effect, such as the INM (*Integrated Noise Model*), developed by the FAA (*Federal Aviation Administration*), the STAPES (*SysTem for AirPort noise Exposure Studies*), developed by EUROCONTROL, or, lastly, the one described in Doc.29 from ECAC (*European Civil Aviation Conference*), an intergovernmental organization established by ICAO and the Council of Europe. The latter will be described in detail and developed in this dissertation as a tool to calculate noise and create noise contours for a given flight procedure.

¹ L_{den} is a commonly used noise metric and will be described in Subchapter 2.3 - Noise Metrics. According to the World Health Organization, long-term exposure to levels above 55 dBA can lead to serious health issues.

As a complement to these maps, GIS (*Geographical Information Systems*) can be used as they contain valuable information about population on a certain area, allowing to clearly differentiate the areas in which the population density is higher and the ones where it is lower. Naturally, it is preferable to have a lower noise impact in areas with a higher density.

With all this information, it becomes possible to implement algorithms of optimization of procedures with respect to environmental, population and economic criteria.

1.2 Objectives

In Portugal, Lisbon's main airport Humberto Delgado has reached 20 million passengers transported in 2015, which represents an increase of 10.7% in relation to the previous year; the number of movements in the airport has been equally increasing, as shown in Figure 1-1. According to ANA, the Airport Authority of Portugal, an increase of the maximum number of movements per hour in Lisbon is to be expected for the near future, from the current 40 that the airport can operate to a total of 72. [4] On the contrary, the Montijo Air Base's traffic movements² has been declining since 2014, as can be seen in Figure 1-2. [5]

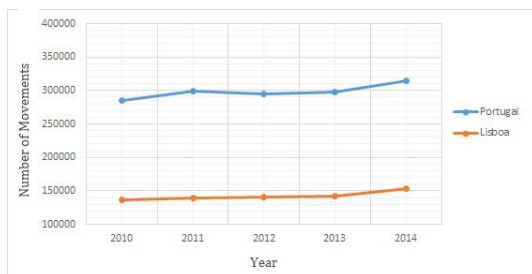


Figure 1-1 - Number of movements in Lisbon and Portugal. [5]

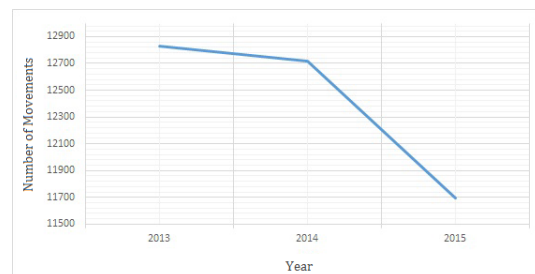


Figure 1-2 - Number of movements in Montijo Air Base. [5]

In response to this expected increase, the solution that has been most considered is the usage of Montijo's military airbase as an auxiliary airport to Humberto Delgado's. This on-going national project is currently known as "Portela³ +1".

As such, it is essential to make the necessary studies that can enable and validate this solution. Due to the fact that noise can have a bigger impact over populations near an operating airport, this dissertation has the main objective of optimizing the departure trajectories with the aim of minimizing the noise impact over nearby populations.

For this effect, a noise model based on Doc. 29 from ECAC will be developed, which will allow to make simulations for different aircraft with different specifications and assess the impact of noise for different operational procedures, in an efficient and practical way; this model will be used,

² Movements here include takeoffs, landings, missed approaches, and touch-and-go training operations.

³ Until May 2016, this airport was known as Aeroporto da Portela.

afterwards, alongside a geographical information system of the region of Lisbon to define realistically optimized trajectories with respect to community annoyance near the airport, followed by a thorough discussion of all the obtained results.

It's fundamental for any study in this theme to follow a defined plan, as schematically described in Figure 1-3.

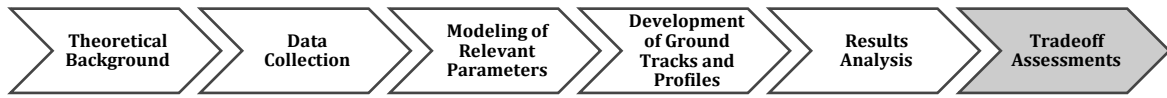


Figure 1-3 - Process for flight procedures design.

1.3 Structure

This chapter consisted on a brief summary on the current concern that any air traffic center is subjected to while designing a flight trajectory, and the description of the objectives of this dissertation.

Chapter 2 consists on the description of the state of the art in this matter, including a few core definitions of sound and noise, some of the most common noise metrics used currently. It is followed by the definition of some air control related terms, and describes in detail some of the most important noise abatement procedures applicable to different airports and their importance, with a higher focus on the departure procedures.

On Chapter 3, the ECAC noise model will be described in detail, starting by the definition of coordinate systems, followed by the concept of flight path segmentation and the general expressions for calculating noise levels during a takeoff operation, based on empirical tabulated data, and finishing with the description of the design of noise contour maps.

On Chapter 4, the process for the definition of new trajectories will be described, starting by explaining the processing of the GIS statistical data through QGIS software, followed by the introduction of the concept of Awakenings.

Chapter 5 will be focused on making a validation of the program developed and the results obtained, based on real data retrieved in regions near Humberto Delgado's Airport by dedicated stations.

Afterwards, Chapter 6 describes the functioning of the developed program, and the application of several different departure procedures on Montijo Airport, after gathering real world data to create realistic scenarios, both in terms of aircraft used and the scheduling of the flights.

Following the application, Chapter 7 shows the obtained results and discusses them thoroughly.

Finally, on Chapter 8, the conclusions of this dissertation are described, along with future work that can be done in this matter.

2 Theoretical Background

2.1 Sound and Noise

Sound is defined by ANSI/ASA S1.1-2013 as "(a) Oscillation in pressure, stress, particle displacement, particle velocity, etc., propagated in a medium with internal forces (e.g., elastic or viscous), or the superposition of such propagated oscillation. (b) Auditory sensation evoked by the oscillation described in (a)." [6] This means that sound is a longitudinal wave that needs a means to propagate, which is done by causing a series of successive compressions and rarefactions regions, resulting from variations of pressure on those areas. As such, they're represented by sinusoidal waves, associated with a frequency which represents the velocity with which the medium contracts and dilates, and an amplitude or energy, related to the intensity of that sound. The sound pressure is, as such, the difference between the average local medium pressure and the pressure in the sound wave, and is usually given by its root mean square value, which is an average over time and space of the square of that difference. These variations of pressure are given by Equation (2-1) for a point source at the origin in an unbounded infinite space.

$$p(r, t) = \frac{A}{r} \cos \left[\omega \left(t - \frac{r}{c} \right) \right], \quad (2-1)$$

Where:

p - Sound pressure at instant t and distance r [Pa];

A - Amplitude at source [N/m or J/m²];

r - Distance to source [m];

ω - Angular frequency [rad/s];

t - Time [s];

c - Speed of sound at medium [m/s].

There's a band of frequencies called audio spectrum, which is the audible frequency range at which humans can hear, and it spans from 20 Hz to 20 kHz; these values are different for each person and some of these deviations can be correlated to the person's age, due to the fact that throughout the years, the human ear loses sensitivity to the higher frequencies. On the other hand, the band of audible intensity can be measured through the sound pressures which the human ear is sensible to. The audible spectrum ranges from 20 μ Pa to 20 Pa. [7] Typically, this intensity is represented in a logarithmic scale given in dB, having the minimum audible sound pressure as reference, as shown in Equation (2-2):

$$L_p = 10 \times \log \left(\frac{p}{p_0} \right)^2 = 20 \times \log \left(\frac{p}{p_0} \right), \quad (2-2)$$

Where:

L_p - Sound pressure level [dB];

p - Sound pressure [Pa];

$p_0 = 20 \times 10^{-6}$ Pa - reference sound pressure.

In this scale, 0 dB corresponds to the hearing threshold, which is the minimum intensity to which the human ear is sensible, while 120 dB is the threshold of pain, which is defined as the least stimulus intensity at which a receiver perceives pain. [8]

With this, the concept of noise can be introduced, being defined as an unwanted or uncomfortable sound. Its impact is not a lasting one but it can have significant adverse effects on people living close to airports, such as interference in communication, sleep disturbance, annoyance responses, stress and even cardiovascular or psychological/physiological effects, which is why aircraft noise remains high on the agenda of public concern. [9]

It is important to mention that noise disturbance is difficult to evaluate due to the subjectivity associated, but there is a certain consensus that led to the definition of reference intensity values that should be avoided, since from those values onwards, the sound is considered uncomfortable for the average person. The World Health Organization's Night Noise Guidelines for Europe describes noise as the second largest environmental cause of health problems, following the impact of air quality, claiming that long-term average exposure levels above 55 dBA can lead to serious health issues such as high blood pressure and ischaemic heart disease. [10]

2.2 Noise Measurement

There are different scales used for the measurement of noise. Examples of these are the Perceived Noise decibel (PNdB), and the Effective Perceived Noise decibel (EPNdB), which incorporate different frequencies and durations of noise patterns, resulting from different velocities and operations. Nonetheless, there are two scales that stand out since they represent the perception of human ear to noise: these are the A-weighted Sound Level and the Tone-corrected Perceived Noise Level, that take into account the frequency spectra in different ways.

To reproduce the sensitivity of the ear to the mid frequencies, a decibel scale corrected by an A-weighted filter is used, in such way to reduce the low and high frequency components of the given sound. These levels are indicated by L_A and have units dBA. The mathematical definition of this filter is expressed in Equation (2-3). [11]

$$L_A(f) = L_p(f) + 20 \times \log \left[\frac{R_A(f)}{R_A(1000)} \right] \quad (2-3)$$

With R_A being given by:

$$R_{A(f)} = \frac{12200^2 f^4}{(f^2 + 20.6^2)(f^2 + 12200^2)(f^2 + 107.7^2)^{\frac{1}{2}}(f^2 + 737.9^2)^{\frac{1}{2}}} \quad (2-4)$$

On the other hand, the Tone Corrected Perceived Noise Level, L_{PNT} , is used for high precision measurements of aircraft noise, taking into account the complexities of human perception of noise by broad band sources containing pure sounds or other spectral irregularities; it is more focused for design and certification of aircraft, and is calculated through complex procedures of spectrums of 1/3 octave bands established by ICAO, which will not be described in this dissertation. [12] Noise impact

assessment requires the need to design noise contours, which are generally dependent on A-weighted scales, which is why a higher focus on this scale will be given.

The equivalent continuous sound level can also be defined, L_{Aeq} , representing the sensation with which the human ear effectively perceives sound during a time period T , and can be calculated using Equation (2-5). [7] [9] [13]

$$L_{Aeq} = 10 \times \log \left[\frac{1}{T} \int_0^T 10^{\frac{L_A}{10}} dt \right] \quad (\text{dBA}) \quad (2-5)$$

The European Committee also proposed as an indicator of ambient noise the so called Day-Evening-Night Level, L_{DEN} , based on L_{Aeq} throughout a whole day, with a 10dBA penalty for nighttime periods (from 23h00 to 07h00), and a 5dBA penalty for evening periods (from 19h00 to 23h00). [14]

According to the World Health Organization (WHO), the threshold of annoyance to continuous noise is 50 dBA for L_{DEN} , and few people are disturbed by values up to 55 dBA. On the other hand, for the Organization for Economic Co-operation and Development (OECD), values above 65 dBA of L_d are unacceptable – the black regions of noise –, and levels from 55 to 65 dBA do not ensure acoustical comfort to residents in those areas – the grey regions. [7] [10]

2.3 Noise Metrics

Other characteristics that should be taken into account during the study of aircraft noise, also representing the human perception of noise and being related to the exposure to a certain event, are the so called noise metrics. Two main metrics can be distinguished, describing (1) the noise in a single event, and (2) the total noise during long periods of time. While the former consists in an indicator of the sonority or intrusiveness of a singular event, the latter can be considered an indicator of the noise annoyance of a certain community, being a combination of single events distributed in time.

2.3.1 Single Event Noise Metrics

As mentioned, they're used to describe an acoustic event caused by a single aircraft movement. There are two scales frequently used, which can be determined both by measurements and by numerical calculations using adequate models, which will be described in more detail on Chapter 3: these are the (1) maximum sound level L_{max} , based on the maximum intensity during the event, and the (2) Sound Exposure Level L_E , based on the total energy of the event. This energy can be expressed as the product of the maximum intensity and an “effective duration” t_e of the event. As such, any event can be described by a noise level curve in function of time $L(t)$, as shown in Figure 2-1.

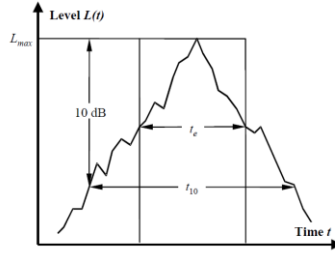


Figure 2-1 - Noise level curve vs time $L(t)$, and some relevant parameters. [12]

The effective duration t_e refers to the duration of an event with a constant value $L_{m\acute{a}x}$ which contains the same energy as the original curve $L(t)$.

Similarly, t_{10} refers to a "10 dB down-time", which is the period for which $L(t)$ is 10 dB below the maximum level L_{max} .

The integration of this curve results in the so called Single Event Sound Exposure Level L_E , which can be expressed by Equation (2-6).

$$L_E = 10 \times \log \left[\frac{1}{t_0} \int_{t_1}^{t_2} 10^{\frac{L(t)}{10}} dt \right], \quad (2-6)$$

Where t_0 corresponds to a reference time value.

The interval $[t_1, t_2]$ should be chosen in such way that it ensures that all the sound resulting from the event is comprised.

Using the definition of effective duration t_e , given by:

$$t_e \times 10^{L_{m\acute{a}x}/10} = \int_{t_1}^{t_2} 10^{L(t)/10} dt \quad (2-7)$$

Equation (2-6) can be rewritten as:

$$L_E \cong L_{m\acute{a}x} + 10 \cdot \log \left(\frac{t_e}{t_0} \right) \quad (2-8)$$

In this metric, particular importance should be given to three scales: (1) Maximum A-Weighted Sound Level $L_{A,m\acute{a}x}$, (2) Sound Exposure Level SEL , and (3) Effective Perceived Noise Level L_{EPN} , given respectively by Equations (2-9) to (2-12).

$$L_{AE} = 10 \cdot \log \left[\frac{1}{t_0} \int_{t_1}^{t_2} 10^{\frac{L_A(t)}{10}} dt \right], \quad t_0 = 1 \text{ s} \quad (2-9)$$

Where t_1 and t_2 are chosen in such way that $L(t)$ is 10 dB below $L_{A,m\acute{a}x}$.

$$L_{EPN} = 10 \cdot \log \left[\frac{1}{t_0} \int_{t_1}^{t_2} 10^{\frac{L_{PNT}(t)}{10}} dt \right], \quad t_0 = 10 \text{ s} \quad (2-10)$$

Similarly to Equation (2-8), the equations for L_{AE} and L_{EPN} can be rewritten as:

$$L_{AE} \cong L_{A,m\acute{a}x} + 10 \cdot \log \left(\frac{t_e}{t_0} \right), \quad t_0 = 1 \text{ s} \quad (2-11)$$

$$L_{EPN} \cong L_{PNT,m\acute{a}x} + 10 \cdot \log \left(\frac{t_e}{t_0} \right), \quad t_0 = 10 \text{ s} \quad (2-12)$$

Among these, both L_{AE} and $L_{A_{max}}$ can be measured directly using precise sound measuring equipment. Theoretically, L_{AE} would be preferred due to the fact that it takes into account both the duration of the event as well as its intensity; nevertheless, its measurements in aviation are susceptible to background noise interference. As such, the most commonly used metric to monitor airport noise is $L_{A_{max}}$. On the other hand, $EPNL$ is the most used metric for aircraft noise certification limits laid down by ICAO Annex 16, which all new civil aircraft have to meet. [15]

2.3.2 Cumulative Noise Metrics

The introduction of the concept of the cumulative noise metrics came in response to the difficulty to make informed comparisons of noise exposure changes over time.

As stated before, while single noise metrics can be considered indicators of the intrusiveness, loudness, or noisiness of individual aircraft noises, cumulative metrics are used to measure long-term noise by aggregating various single events in a way which can be turned into an indicator of the influence of annoyance over a community.

For this aggregation of single events to be done, it is necessary to identify the single event levels and the number of events. As such, long term aircraft noise exposure indices can be expressed in the form:

$$L + K \log N, \quad (2-13)$$

Where L is the average event level in dB, N is the number of events during the time period of interest, and K is a constant which quantifies the relative importance of noise level and number.

The energy principle is the basis of Equivalent Sound Level, L_{eq} and derived indices:

$$L_{eq} = \overline{L_E} + 10 \log N - \text{const.}, \quad (2-14)$$

Where $\overline{L_E}$ is the average single event level of the N events experienced during the specified time period. The constant term depends on that time interval (for 24 hours, it is $10 \times \log(\text{number of seconds in 24 hours})$).

As mentioned before, weightings into L_{eq} have been introduced to take into account the variation of noise sensitivity throughout the day. It is intuitive that noise is more tolerable during the morning and, with this in mind, modifications to L_{eq} can be adopted to describe environmental noise exposure. As such, the Day-Evening-Night Level L_{DEN} includes a 5dB evening weighting and a 10dB night weighting; this means that all noise occurring during the evening is augmented by 5dB and during the night by 10dB, before the full noise energy level is averaged for a period of 24 hours. For aircraft noise, it means that evening and night flights contribute as much to L_{DEN} as, respectively, three and ten identical daytime flights.

Time-weighted equivalent sound levels can be expressed in general by:

$$L_{eq,W} = 10 \times \log \left[\frac{t_0}{T_0} \sum_{i=1}^N g_i \times 10^{\frac{L_{E,i}}{10}} \right] + C \quad (2-15)$$

Where:

N is the number of aircraft noise events during the specified reference time period T_0 .

The level $L_{E,i}$ corresponds to the single event noise exposure level of the i -th noise event.

The coefficient g_i is a time-of-day dependent weighting factor, while the constant C is a normalizing constant.

Table 2-1 lists a number of time-weighted equivalent sound levels currently in use and the parameters needed for their calculation.

Table 2-1 - Parameters for different forms of equivalent sound levels L_{eq} according to Equation (2-15). [12]

L_{eq}	$L_{E,i}$ [dB]	t_0 [s]	C [dB]	T_0^4 [s]	g_i^5		
					day	evening	night
$L_{Aeq,24h}$	L_{AE}	1	0	$86400 N_{Tr}$	1	1	0
$L_{Aeq,day}^6$	L_{AE}	1	0	$57600 N_{Tr}$	1	0	0
$L_{Aeq,night}$	L_{AE}	1	0	$28800 N_{Tr}$	0	0	1
L_{DN}	L_{AE}	1	0	$86400 N_{Tr}$	1	1	10
L_{DEN}^7	L_{AE}	1	0	$86400 N_{Tr}$	1	3.162^8	10

$L_{Aeq,24h}$ is the 24-hour average sound level;

$L_{Aeq,day}$ is the 16-hour day-average sound level;

$L_{Aeq,night}$ is the 8-hour night-average sound level;

L_{DN} is the Day-night average sound level;

L_{DEN} is the Day-evening-night sound level.

It is particularly relevant to add that, for all these metrics, when designing a noise contour, these values correspond to outdoor areas, since conditions would vary greatly indoors according to the shape, size, orientation and layout of buildings and the types of construction, whether sound insulated as well as whether windows were open or closed.

2.4 Geographical Information System

To be able to make a realistic relationship between noise and community annoyance, it is necessary to make a study about that population in the area of study to complement the noise data. With this in mind, it is relevant to introduce the concept of Geographic Information Systems, which were defined by Dueker and Kjerne [1989] as "A system of hardware, software, data, people, organizations and institutional arrangements for collecting, storing, analyzing and disseminating information about areas of the earth." [16] What this means is that it is a system that allows people to accurately measure aspects of geographic phenomena and processes in any place on Earth, and representing those measurements in the form of a computer database. With this database, it is

⁴ T_0 is the product of the number of seconds of the part of the day and the number of days the scenario is defined for.

⁵ Day evening and night intervals are specified to accommodate local lifestyles.

⁶ $L_{Aeq,day}$ is defined for 16 hours of day and evening period .

⁷ L_{DEN} is defined for day, evening and night periods of 12h, 4h, and 8h by the European Commission.

⁸ $g_i = 3.162$ comes from $g_i = 10^{\frac{\Delta_i}{10}}$, with a level offset of $\Delta_i = 5$ dB for the evening period.

possible to process data to infer new data, discover new relationships by integrating different sources.

With GIS technology, it's possible to compare diverse information at different locations in order to discover how they relate to each other. These locations can be expressed in many different ways, such as latitude and longitude, and many different types of information can be compared and mapped, such as data about people like population, income, or education level. Once all of the desired data has been entered into a GIS system, they can be combined to produce a wide variety of individual maps, depending on which data layers are included.

2.5 ANP Database

To make an accurate noise assessment, a noise model will be developed, which allows to make simulations for different aircraft, with different specifications such as weight, engines, flaps configurations or power settings. For this effect, the ANP database is an international online data resource accompanying the ECAC Doc.29 3rd Edition and ICAO Doc 9911 guidance documents on airport noise contour modelling developed by Eurocontrol Experimental Centre and frequently updated, being the most commonly used database for noise modeling [17]. It contains aircraft and engine performance coefficients for a wide range of commercial aircraft; this information is supplied by the manufacturers and database managers themselves.

Relationships between the noise levels and slant distances⁹ for different engines and power settings can also be found on that database through NPD (Noise-Power-Distance) tables and curves, such as the one represented in Figure 2-2. This data is defined for reference conditions, such as the assumption of a steady flight at a reference speed in specified reference atmospheric conditions and in a specified flight configuration. As such, all these values have to be adjusted in accordance to the conditions to be modelled. [12] Further information about the reference conditions and the adjustments will be given in Chapter 3 – ECAC Doc.29 Noise Model.

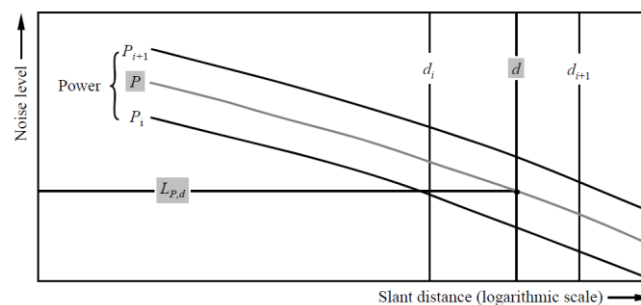


Figure 2-2 - Interpolation in a noise-power-distance curve. [12]

Lastly, it's important to mention that there is no practicable way in which the accuracy of the data entries can be systematically and independently checked, and some inconsistencies are most

⁹ The slant range is the distance between the observer and the aircraft.

likely to be found when comparing model predictions with measured data; nevertheless, the database is subject to constant updates, approved by the suppliers and database managers to keep it as accurate as possible. [12]

2.6 Airport and Aircraft Operations

As referred in the previous chapter, a solution to the noise concern is based on the improvement of the procedures around an airport. Research into the field of noise abatement procedures has been quite extensive.

Current procedures are, in general, based in the use of ground navigation aids stations, infrastructures, and aircraft navigation system which enable navigating from one navaid to another. Conventional nav aids are the ‘ground-based’ part of the navigation infrastructure. It refers to the navigation aids such as NDB (Non-Directional Beacon), VOR (Very High Frequency Omni-directional Range), DME (Distance Measuring Equipment), which define “airways” in the sky that aircraft can follow to complete a flight plan, as well as ILS (Instrument Landing System) and MLS (Microwave Landing System) [18].

Figure 2-3 shows how NDB, VOR, and VOR/DME stations can find the position of an aircraft.

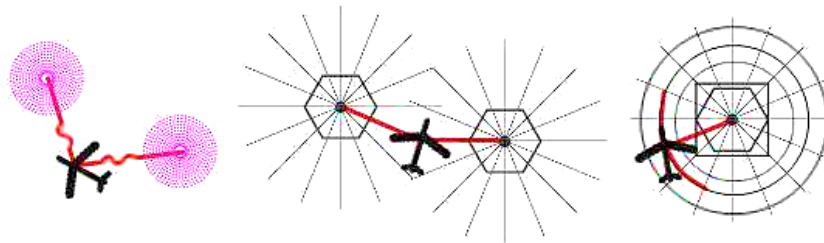


Figure 2-3 - Position finding of an aircraft with NDB (on the left), VOR (in the middle), and VOR-DME (on the right). [19]

Nonetheless, modern operations are moving towards a new concept - the Performance-based Navigation (PBN); it has the goal of facilitating airspace design, traffic flow and improved access to runways, providing a basis for designing and implementing new and more efficient flight paths. Additionally, this change allows for many more benefits, such as a increased safety and more control of gaseous emissions and noise levels. [20]

This modern navigation trend involves the development of instrument procedures that are not based on the conventional radio nav aids. The use of Area Navigation (RNAV¹⁰), which will be explained in the next section, in departure procedures to allow for a reduction of flight track dispersion in Standard Instrument Departures (SID) was proposed to better contain noise contours.

¹⁰ Area Navigation used to be called Random Navigation, hence the acronym RNAV.

2.6.1 RNAV and RNP

Area navigation (RNAV) is defined by Clausing [21] as “a method of instrument flight rules (IFR) navigation that allows an aircraft to choose any course within a network of navigation beacons, rather than navigate directly to and from the beacons. This can conserve flight distance, reduce congestion, and allow flights into airports without beacons.”

RNAV began as a means of navigation on a flight path from any point, or fix, to another. These fixes could be defined by a latitude and longitude, and an airplane’s position relative to them could be established using a variety of nearby navaids [20]. Fundamentally similar to RNAV, Required Navigation Performance (RNP) is another type of PBN, with the key difference that it includes an on-board performance monitoring and alerting. A schematic representation of RNAV and RNP specifications compared to conventional navaids navigation is shown in Figure 2-4.

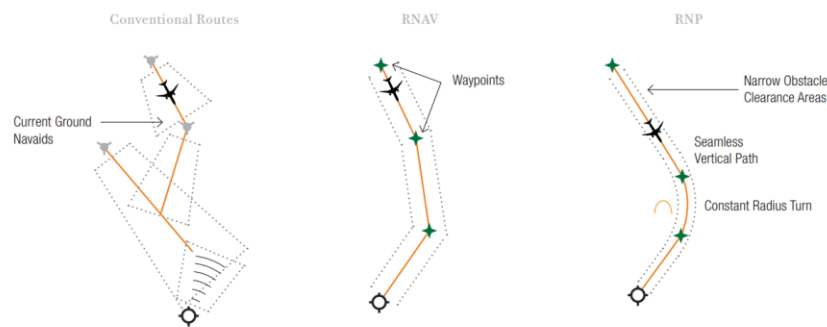


Figure 2-4 - Comparison between RNAV and RNP over conventional, ground-based navigation systems. [20]

The benefits that come with the implementation of PBN are numerous. One is better safety due to more accurate position tracking, with no accidents having been reported with the use of RNAV/RNP procedures; instead, most of the accidents occur during Non-Precision Approaches using conventional navaids rather than RNAV/RNP procedures [20]. Furthermore, delays in airports are diminished due to a better definition of parallel offset routes allowing better use of airspace, as shown in Figure 2-5, as opposed to conventional routes, which have limited flexibility due to vertical separation requirements. Additionally, it also offers environmental benefits by saving fuel, reducing CO₂ emissions and better avoidance of noise-sensitive areas due to better precision, allowing more efficient use of different procedures aimed to reduce noise impact, detailed in the next section.

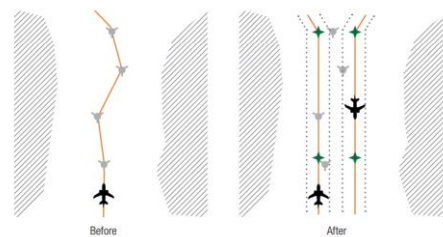


Figure 2-5 - PBN implementation's effect on Capacity. [20]

2.6.2 Noise Abatement Procedures (NAP)

Noise Abatement Procedures are a variety of flight procedures that can be situationally implemented with the aim of reducing or redistributing noise around an airport, both during approach and departure procedures, through different methods, as detailed in the remainder of this chapter and including its benefits and drawbacks.

Research into the field of NAPs has been quite extensive and commonly implemented during approach procedures; although it will not be explained in detail, the benefits of Continuous Descent Approaches (CDA), in combination with reduced flap approaches and higher ILS glide slope angles have been investigated and have been shown successful. [22] [23] [24] Nevertheless, there has been little discussion of the environmental and operational interdependencies of departure procedures, notably what are known as Noise Abatement Departure Procedures (NADP), which will be the main focus in this dissertation.

Knowing that the profile of a flight path is the vertical component of an aircraft trajectory (also known as its altitude), and the ground track is the projection of that trajectory onto the ground, there is a wide variety of methods to control a procedure in terms of noise impact, comprising of combined adjustments of the flight path's ground track and profile in the most diverse ways, along with adjustments in the power setting during the procedure, aimed to provide noise relief for some communities. A schematic representation of changes in ground track and profile is shown in Figure 2-6, following a RNAV specification for better accuracy and efficiency in these procedures.

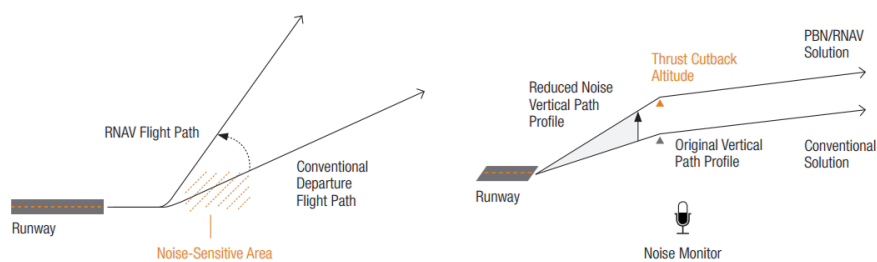


Figure 2-6 - Schematic representation on how adjustments in ground track (on the left) and profile (on the right) can reduce the noise impact on sensitive areas. [20]

It's important to note that aircraft operating procedures for noise abatement should comply with the provisions of ICAO Doc. 8168 (PANS-OPS), Volume I, Section 7. [25]

2.6.2.1 Ground Track

As shown in Figure 2-6, noise-sensitive locations such as areas with hospitals or school can be avoided with an optimized ground track with respect to those areas, by shifting the noise exposure towards other areas, ideally with low population densities. This is one of many ground track procedures that can be implemented in any airport, but it's not always possible to avoid all populated areas; furthermore, this optimization in terms of noise can come at the cost of a big increase of fuel consumption and emission of pollutant gas due to the longer path, making it necessary to make a proper balance to assess the tradeoffs.

2.6.2.1.1 Fanning

Another common procedure is the so called *Fanning*, which aims to make a balanced distribution of noise exposure over a broad area at the beginning of a departure procedure. It is implemented by FAA air traffic control to improving airport capacity¹¹ during periods with high traffic levels, due to the fact that the departure procedures are not coincident for sequential flights, allowing a higher number of flights to occur within a certain period of time. It consists in dividing the initial straight-out departure trajectory into different branches before converging them again after the initial climb, as shown in Figure 2-7. [1]

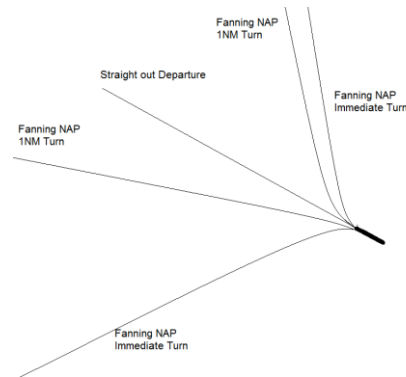


Figure 2-7 - Schematic representation of the Fanning NAP. [1]

Similarly to what was mentioned for the noise-sensitive locations avoiding trajectories, these procedures may not provide any benefit for fuel consumption and emissions. Furthermore, the immediate turns are not viable for larger aircraft types.

2.6.2.1.2 RNAV/RNP procedures

As mentioned before, RNAV/RNP departures can be an efficient method to provide noise relief for more sensitive locations due to its higher accuracy than conventional navigation. Nevertheless, the fact that the noise is contained in a certain area can be seen as an issue for the community below the RNAV trajectory, as it is subjected to much higher air traffic. Figure 2-8 shows the difference between conventional and RNAV departure routes tracked by a radar.

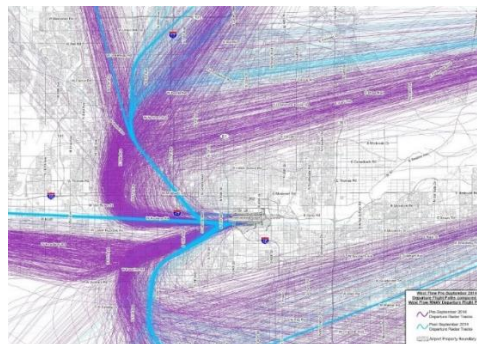


Figure 2-8 - Radar tracking of flights before and after the implementation of RNAV. [26]

¹¹ Airport capacity is related to the number of operations (both arrival and departures) that an airport can sustain in an hour time.

In purple, the conventional departure routes can be seen, in contrast to the high precision ones in blue, corresponding to RNAV departures, in the Phoenix Harbor Airport with data before and after September 18th.

2.6.2.1.3 Turn-restriction NAPs

It's common to implement turn-restriction NAPs, which put a constraint on the departure ground tracks used for a given runway at a given airport, meaning that the aircraft are kept flying at the runway heading until reaching a certain distance or altitude, after which it can turn towards the destination or fix. With this in mind, different tracks can be defined by making small changes in the turning point distance or altitude, making the aircraft turn sooner or later, and then converging in the same fix, as represented in Figure 2-9. Just like before, an increase in airport capacity and a reduction in emissions is expected for the most-direct track, but it can come at the cost of a higher noise impact, while the NAP turning point provides lower levels, but higher fuel consumption and lower capacity. This shows that a proper balance has to be made, and the decision to change procedures must come with a careful weighting among many different parameters.

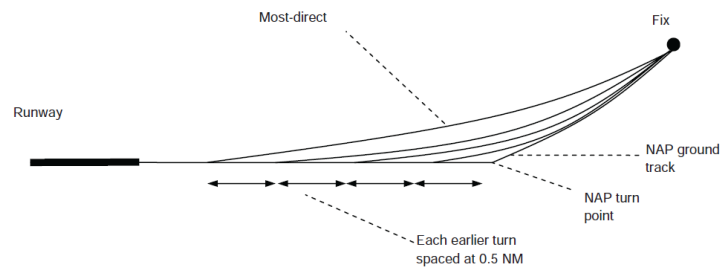


Figure 2-9 - Schematic representation of turn restriction ground tracks. [1]

2.6.2.1.4 Multi-turn NAP routing

A similar concept is the multi-turn NAP routing, designed to avoid densely populated and noise-sensitive areas near airports, in which at a certain point the ground track towards a constant fix can be modelled in different ways, from a most-direct route to the longest route, designed to go around a sensitive area, as shown in Figure 2-10.

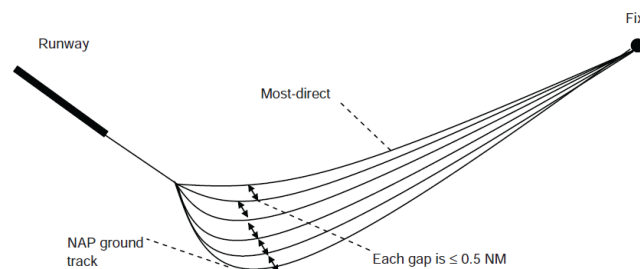


Figure 2-10 - Schematic representation of multi-turn NAP ground tracks. [1]

Any of these procedures can also be used when the airport is near an unpopulated area or a body of water, such as a river, the noise-related optimal route being extended towards that area so that the aircraft is able to climb to a certain altitude, before turning to its destination fix; nevertheless,

and yet again this detour can reflect an increase of fuel consumption and emissions due to the longer ground tracks, unless that body of water is located in the direction of the runway.

2.6.2.1.5 Temporal

Finally, it is important to mention that there isn't a fixed optimal ground track for any given area; it can vary with the time-of-day. There can be a higher flexibility to reduce noise in certain areas only during night-time periods, or conversely there can be areas where night-time noise has a low impact, such as elementary schools which are empty during those periods.

2.6.2.2 Profile

As mentioned, a flight path can be separated into two components and, as such, changes in ground track are not the only adjustments that can be done to optimize trajectories (see Figure 2-6). Furthermore, due to the fact that the noise impact due to the profile is easier to generalize as it can be modelled to follow a straight line for assessment purposes, two departure methods have been presented and recommended by the FAA's Advisory Circular. [27] The first of them is intended to provide noise relief for communities and noise sensitive areas located in close proximity to the airport - the close-in procedure -, while the second one aims to provide relief for communities farther from the airport - the distant procedure.

Similarly, ICAO has also promulgated their standard profile NADPs to ensure that the necessary safety of flight operations is maintained while minimizing noise exposure on the ground, where its NADP1 (or ICAO-A) procedure is aimed to provide noise reduction near the airport, as opposed to NADP2 (or ICAO-B) which is aimed for distant communities. According to ICAO's Doc.8168, Vol.1 - Flight Procedures, Appendix to Chapter 3, the primary differences consist in that the acceleration segment for flap/slat retraction is either initiated prior to reaching the maximum prescribed height or at the maximum prescribed height. To ensure optimum acceleration performance, thrust reduction may be initiated at an intermediate flap setting. [28]

Figure 2-11 shows a representation of both profiles overlapped and a comparison between the altitudes at which an aircraft following each of them reaches along its path can be seen. (*Taken from ICAO PANS OPS Volume 1 (Doc 8168-OPS/611)*).

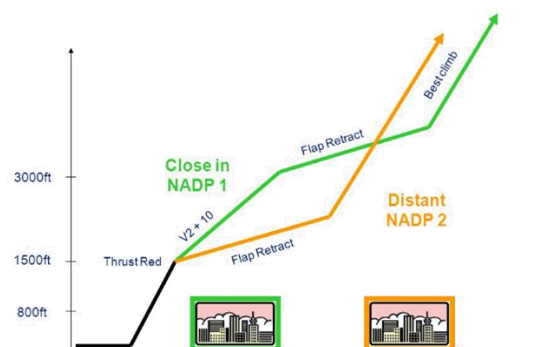


Figure 2-11 - NADP 1 and NADP 2 profile representation. [28]

2.6.2.2.1 Close-in – NADP 1

This procedure consists in a power reduction at or above a prescribed minimum altitude and a delay of the normal retraction of the aircraft's flaps until it reaches a clean-up altitude. By maintaining the deployment of flaps, it increases its climb gradient as compared to the conventional retraction, reaching a particular altitude at an earlier distance from the departure runway end; the concept behind this is to increase the vertical distance to the ground, reducing the noise levels close to the airport. Due to the fact that the flaps are still extended, the aircraft has to maintain its original climb speed until the clean-up altitude, where the aircraft accelerates and the flaps are retracted, maintaining a positive rate of climb and completing the transition to the normal enroute climb speed. [28]

2.6.2.2.2 Distant – NADP 2

In practice, this procedure is very much alike to the aircraft manufacturer's standard profile and many airlines implement it as their standard profile. As opposed to NADP 1, an aircraft following this procedure retracts its flaps/slats as soon as it reaches the minimum prescribed altitude, lowering its pitch angle and accelerating towards a set airspeed while maintaining a positive rate of climb. There is also a power reduction, performed when the aircraft either starts the flaps/slats retraction or when the zero flap/slat configuration is attained. Finally, at the prescribed altitude, the transition to normal enroute climb procedure shall be completed. [28]

Typically, the redistribution of noise away from the areas near the airport when an aircraft follows a NADP 1 profile comes with a larger noise reduction than the corresponding increase in areas farther from the airport. Nonetheless, the use of high lift devices to climb faster until a certain altitude creates lots of drag; as such, part of the power coming from the engines is used to compensate that drag, which translates into less excess power to climb. Conversely, in NADP 2 the aircraft can reach its most efficient climb speed earlier, becoming more efficient in terms of fuel savings, reason why most airlines and airports prefer implementing this procedure as opposed to NADP 1.

2.6.2.3 Ground-Based Measures

There is a wide variety of ground-based operational measures that come with many benefits in terms of noise impact, such as the use of a single engine during taxi in a runway, or the use of a preferential runway system that directs flights towards less sensitive areas; these will not be detailed in this dissertation as it is more focused on the flight procedures *per se*.

2.6.3 SESAR

It's important to mention SESAR, standing for Single European Sky ATM Research, which is an ongoing collaborative project to completely overhaul European airspace and its air traffic management. According to its website, it unites around 3,000 experts in Europe and beyond to develop the technologies and procedures that can enhance ATM performance, ensuring safety and fluidity over the next years.

With EUROCONTROL and the European Commission as founding members, it counts with a joint cooperation of several other companies, such as Airbus and even NAV Portugal, and is designed in three sequential phases, as represented in Figure 2-12 and detailed subsequently. [29]



Figure 2-12 - Sequential phases from SESAR project. [29]

1. Definition Phase – containing the content, development and deployment plans of the next generation of ATM systems, as delivered in its ATM Master Plan.
2. Development Phase – development of new technological systems, components and operational procedures required for the success of the project, as defined in the delivered plan from the previous phase.
3. Deployment Phase (currently in progress) – will see all the developed systems implemented, forming a new air traffic management infrastructure to guarantee high performance air transport activities in Europe.

Among other consequences, the increased efficiency in the ATM systems will allow for a better precision and accuracy while performing noise abatement procedures, along with the development of new and better technologies and equipment to reduce noise from source. The use of automated thrust reduction in noise-sensitive areas and the implementation of concepts such as the 4D Trajectory, which adds a fourth dimension - time - to the three spatial dimensions conventionally used, will translate into higher and more consistent reductions in noise levels, along with other benefits such as reduced emissions and costs, and increased airport capacity.

2.6.4 NextGen

Parallel to the European project SESAR, NextGen is a new ongoing National Airspace System developed by the FAA to be implemented across the United States between 2012 and 2025. It proposes to change its current ATC system, from a radar-based system with radio communication to a satellite based one. GPS technology will be used to obtain shorter routes, translating into time and fuel savings, along with reductions in traffic delays and increased airport capacity. Furthermore, the aircraft can be monitored and managed with higher safety margins by the controllers due to a more effective communication system, allowing for a reduction in separation distances. [30]

To finalize, it's relevant to add that the result of the changes to flightpaths for aircraft can result in many localities experiencing huge increases in air traffic over previously quiet areas, affecting some communities previously unaffected by noise. Some municipalities have already filed suits. It has also broken at least one historical agreement between a major airport and a municipality under one of its flightpaths. [31] [32]

3 ECAC Doc.29 Noise Model

As mentioned in the previous chapters, to be able to make an accurate assessment of the noise impacts on a community without the need to do practical experiments as they can become expensive, it is necessary to start by developing accurate models able to describe any desired procedure and create accurate noise level contours for each of them, in a quick and efficient way.

For this purpose, a model based on the recommendations present on the second volume of Document 29 by ECAC/CEAC [12] – Europe's largest and longest-standing aviation organization and part of the ICAO air transport global community, with the mission of promoting the continued development of a safe, efficient and sustainable European air transport system [33] – was developed. These recommendations establish a combination of logic and mathematics to obtain a physical model capable of calculating noise levels due to aircraft operations in any point. The deductions, assumptions and approximations done for the formulas presented go beyond the scope of this dissertation, and as such will not be thoroughly explained.

Typically, modelling systems comprise three main elements, starting by an input of airport and aircraft data, such as the runway heading and altitude and weather conditions, the aircraft's engines' and flaps' coefficients - found on an updated and complete database -, and a set of procedural steps to be modelled; this is followed by the application of the model, which processes the given input and converts it into an accurate and detailed flight path, which is then used to calculate the noise levels due to that flight in a grid of observers located in the ground, and create a noise contour around the given airport.

A generic schematic representation of this process is shown in Figure 3-1, and a detailed description of the steps in this process will be given in this chapter.

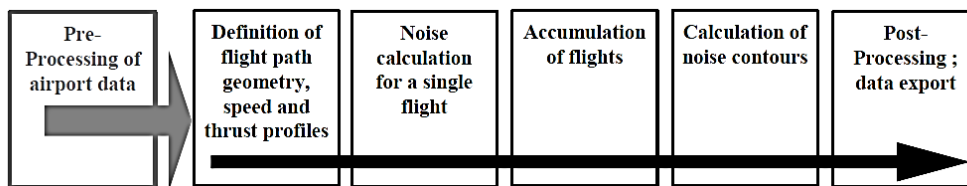


Figure 3-1 - The noise contour generation process. [12]

3.1 Geometry

Before forming any flight path, it is necessary to define the coordinate systems to be used. With this in mind, different systems will be used depending on the situation.

The fixed local coordinate system (x, y, z) is a Cartesian one, with its origin at the aerodrome reference point $(X_{ARP}, Y_{ARP}, Z_{ARP})$, where x points towards East, y points towards North, and z points Up - which is the Earth-bounded ground reference frame ENU (Earth-North-Up - see Figure 3-2). The system shown in Figure 3-3 will be the one in which the contours will be represented.

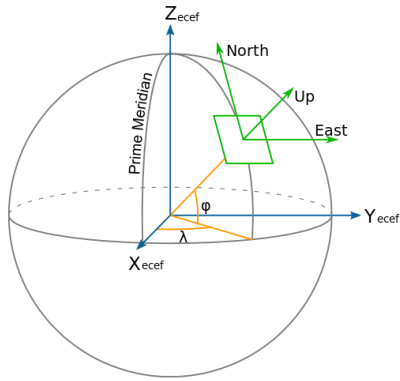


Figure 3-2 - East-North-Up (ENU) coordinate system. [34]

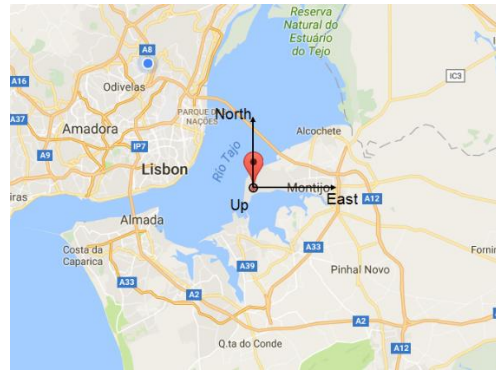


Figure 3-3 - Local reference coordinate system (x, y, z) , centered on Montijo's aerodrome. [Google Maps]

A second coordinate system is a one-dimensional system which follows the ground track, where its axis is the ground track distance s and has its center on the start of roll in the runway in use (see Figure 3-4). This will be the main system used while modelling the flight paths as it's specific for each ground track, representing a distance s measured along the track throughout the flight direction. In this system, any flight operation parameter – such as height, airspeed or power setting – is function of the distance s .

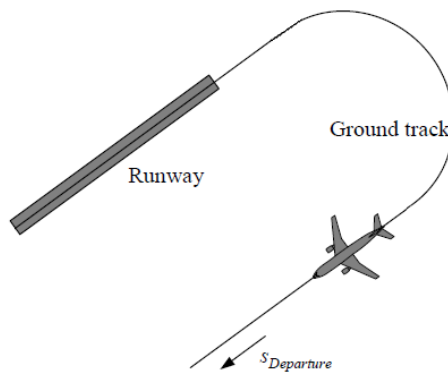


Figure 3-4 - Ground track-fixed co-ordinates system. [12]

Finally, a third and last reference system fixed to the aircraft will be used in situations where it's important to know the aircraft's attitude. This aircraft-fixed Cartesian coordinate system (x', y', z') has its origin at the actual aircraft location, with its x axis following the aircraft's longitudinal (roll) axis, y axis following the lateral (pitch) axis and z following its vertical (yaw) axis. Based on these axes, a set of angles can be defined; they are (1) the flight direction ξ , (2) the bank angle ε , and (3) the climb angle γ , which are represented in Figure 3-5 as described in Doc.29.

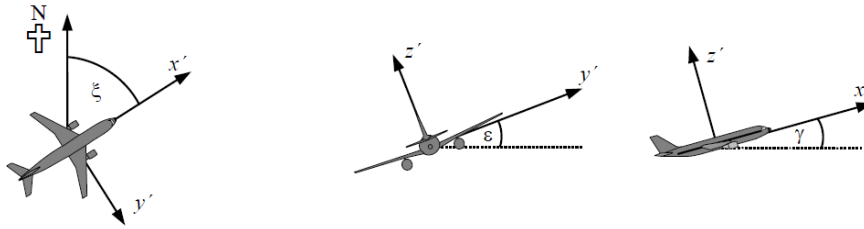


Figure 3-5 - Aircraft-fixed coordinate system. [12]

3.2 Aircraft Performance Calculations

Before moving towards the first step of the noise modeling process, it is essential to explain all the parameters necessary for aircraft performance calculations, as they will be needed throughout the rest of the process.

As mentioned before, all the aircraft performance parameters can be obtained in the ANP database. The calculations for performance require parameters that include not only coefficients intrinsic to the aircraft - such as the aircraft's weight and the number and location of engines - but also details on the procedure - which influence the power settings, flaps deflections, airspeeds, rate-of-climb; all of these parameters are shown in Appendix A.

The data contained in this database is normalized to standard reference conditions, as exemplified in Table 3-1 for the NPD data.

Table 3-1 - Reference conditions for NPD data in the ANP database. [17]

1) Atmospheric pressure	101.325 kPa
2) Precipitation	None
3) Wind speed	Less than 15 kt
4) Groundspeed	160 kt
5) Local Terrain	Flat, soft ground free of large structures or other reflecting objects within several kilometers of aircraft ground tracks.

One of the most important parameters needed for the definition of a flight path is the propulsive force produced by each engine of the aircraft. With this in mind, a relevant parameter to introduce is the so called net thrust F_n - it represents the component of engine gross thrust available for propulsion. For aerodynamic and acoustical calculations, it is adjusted to air pressure at mean sea level, being named as *Corrected net thrust*, F_n/δ , being given by:

$$\frac{F_n}{\delta} = E + F \cdot V_C + G_A \cdot h + G_B \cdot h^2 + H \cdot T \quad (3-1)$$

Where:

F_n is the net thrust per engine [lbf];

δ is the air pressure ratio, the ratio between the ambient air pressure at the aircraft's altitude and the standard air pressure at mean sea level $p_0 = 101.325$ kPa [35];

V_C is the calibrated airspeed [kt];

T is the ambient temperature at the aircraft's altitude [K]; and

E, F, G_A, G_B, H are engine thrust constants or coefficients [lb, lb.s/ft, lb/ft, lb/ft², lb/K, respectively], obtained from the ANP database.

An example of the engine coefficients needed for the calculation of the propulsive thrust parameter is found in Appendix A, for different power settings of an Airbus A320-211.

3.3 Flight path segmentation

In the first step towards the development of a noise model, it is necessary to define the aircraft's trajectory. In this context, a trajectory or flight path is defined as the full description of the motion of aircraft in space and time, being, along with the engine power parameter's¹² evolution throughout the flight, the information required to calculate the noise generated by an aircraft along its path at any point.

For this effect, there are two main algorithms to model its flight path: (1) segmentation and (2) simulation. The latter has an increased complexity and greater potential, by describing the real flight path of an aircraft through a series of discrete points in space after successive small intervals of time; nevertheless, this complexity translates into higher demand on computing capacity which leads to much higher processing times, reason why this algorithm isn't considered the best practice today [12]. Instead, the segmentation method is the recommended practice as it gives great results by accurately describing a flight path by approximating it by a series of contiguous straight segments both for the ground track and the profile of the aircraft. These segments' lengths have been optimized based on the aircraft's flight characteristics in each segment depending on the procedure in effect [12] - described in Subchapters 3.3.1 through 3.3.4 -, giving a good balance between computing times and noise accuracy. This method is based on the use of the comprehensive ANP database; nevertheless, it is necessary to make some adjustments and corrections due to sound propagation particularities, which will be detailed in Subchapter 3.4.3.

Within the method of segmentation, it is possible to determine a flight path and engine power in different ways, the main ones involving (1) analysis of measured flight data, and (2) synthesis from a series of procedural steps. Both of these are relevant for the model to be developed. The former, as expected, is based on the measurement of flight data with the use of radars to determine the aircraft's exact position coordinates along its path and the necessary equipment to measure the static pressure, engines' power setting, the calibrated and true airspeed and other relevant parameters, which will all be combined to model the flight path to be provided into the noise calculation stage; this method will be particularly relevant for the validation process of the developed model, as real measured flight

¹² In this model, the net thrust, which describes the propulsive effort generated by an aircraft engine, will be the noise-related power parameter to be used.

data will be used to compare with the modeled results. On the other hand, in the absence of radar data, the flight paths and related parameters have to be estimated based on procedural steps, such as instructions given to flight crews via AIPs and aircraft operational manuals, consisting on specific instructions on the power settings, flaps settings and operations to follow. Standard procedures have been developed for each aircraft and are also present on the ANP database, as represented in Table 3-2. [17]

Table 3-2 - Example of a standard procedure as described in the ANP database, for an ICAO-A procedure for an Airbus A320-211. [17]

ACFT_ID	Profile ID	Step	Step Type	Thrust Rating	Flap_ID	End Point Altitude (ft)	Rate Of Climb (ft/min)	End Point CAS (kt)
A320-211	ICAO_A	1	Takeoff	MaxTakeoff	1+F			
A320-211	ICAO_A	2	Climb	MaxTakeoff	1+F	1500.0		
A320-211	ICAO_A	3	Climb	MaxClimb	1+F	3000.0		
A320-211	ICAO_A	4	Accelerate	MaxClimb	1+F		812.1	186.1
A320-211	ICAO_A	5	Accelerate	MaxClimb	1		933.5	201.2
A320-211	ICAO_A	6	Accelerate	MaxClimb	ZERO		1119.7	228.2
A320-211	ICAO_A	7	Accelerate	MaxClimb	ZERO		1240.5	250.0
A320-211	ICAO_A	8	Climb	MaxClimb	ZERO	5500.0		
A320-211	ICAO_A	9	Climb	MaxClimb	ZERO	7500.0		
A320-211	ICAO_A	10	Climb	MaxClimb	ZERO	10000.0		

The segmentation process for the different operations that can be combined to produce a flight path will be detailed throughout this Subchapter, including the equations to calculate the flight profile, the required propulsion to follow the operation and the resulting airspeed, and all the necessary preliminary data from the ANP database.

3.3.1 Ground track and flight profile

As mentioned, any flight path is defined by a series of contiguous segments and flight parameters; these segments can be separated into two components, (1) its projection towards the ground, which results in the ground track, and (2) the evolution of its altitude along the distance traveled, which consists on its profile.

It's important to mention that the profile of a flight path depends on its ground track. For example, an aircraft's climb rate is lower in turns as compared to that in a straight flight, given that all other parameters such as thrust and airspeed are equal. Nevertheless, for noise modelling purposes, it's deemed more efficient to consider them independent, but still taking into account the aircraft's bank angle in both components, as it is related to parameters such as the directionality of sound emission. [12]

3.3.1.1 Ground Track

Designing a ground track is typically a simple process as it consists in a series of lines that are either straight - defined by length Δs and heading ξ -, or circular arcs - defined by change of heading $\Delta\xi$ and curve radius r , as shown in Figure 3-6. As also shown in the figure, for a segmentation model these arcs can be represented by a sequence of straight segments forming structured sub-arcs following Equations (3-2) to (3-4), while being in accordance with the flight profile.

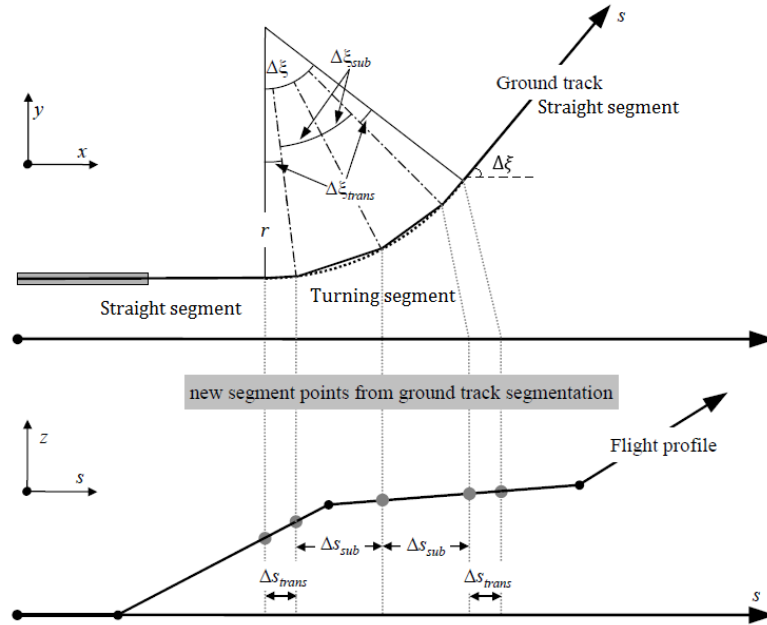


Figure 3-6 - Ground track geometry in terms of straight segments and turns and arcs segmentation. [12]

As shown in Figure 3-6, with the purpose of making the transition as seamless as possible without turning the curve into a computational burden, any curve is divided into sub-arcs, with the first and last sub-arc functioning as a transition arc. These transition sub-arcs are dictated by the bank angle and change of heading, and are not strictly defined in Doc.29's model; for simplicity purposes and since they have negligible effect on the final noise contours [12], it is assumed that the transition change of heading is constant and equal to $\Delta\xi_{trans} = 5^\circ$ for any turn. The remainder of the arc is then divided into n_{sub} sub-arcs according to the following equation:

$$n_{sub} = \text{floor}\left(1 + \frac{\Delta\xi - 2 \cdot \Delta\xi_{trans}}{30}\right), \quad (3-2)$$

Where $\text{floor}(x)$ is a function that rounds the input to the next smaller integer number.

Similarly, the change of heading of each sub-arc $\Delta\xi_{sub}$ is given by:

$$\Delta\xi_{sub} = \frac{\Delta\xi - 2 \cdot \Delta\xi_{trans}}{n_{sub}}, \quad (3-3)$$

Where n_{sub} has to be large enough so that $\Delta\xi_{sub} \leq 30^\circ$.

For an aircraft to make a turn and change its heading, it has to change its bank angle ε by tilting itself towards the side it wants to turn, as given by Equation (3-4). With this in mind, for an aircraft to make a seamless transition from straight flight to a steady turn, it would need an instantaneous change of bank angle which is not physically possible. This instantaneous change can be ignored and approximated by assuming a linear increase from its initial value at the beginning of the turn to its final value at a certain distance within the curve, which will be defined as the end of the transitioning sub-arc; this assumption is also followed for the end of the turn, in which the bank angle decreases linearly from the beginning of the transition sub-arc until the end of the turn.

$$\varepsilon = \tan^{-1} \left\{ \frac{2.85 \cdot V^2}{r \cdot g} \right\}, \quad (3-4)$$

Where:

V is the groundspeed [kt]

r is the radius of the turn [ft]

g is the acceleration due to gravity [ft/s²]

3.3.1.2 Flight Profile

As mentioned, the flight profile describes the aircraft's altitude along the distance traveled, along with the evolution of its airspeed, bank angle and engine power setting. To define an accurate flight profile which reflects the operations intended to represent, it's important to have reliable information on the atmospheric conditions, aircraft data and the operating procedures, such as the power settings and flaps settings. The synthesis of flight profiles from procedural steps yields both its geometry and the associated speed and thrust variations, by following the equations described throughout the rest of Section 3.2, as recommended by ECAC.

The flight profile is segmented, each segment being defined by a set of parameters at its beginning and end. As such, it is built in such way to meet the required conditions at the end of each segment - usually height and speed -, the end point of a segment being the initial point of the following one, which includes all the flight parameters too. These parameters include the aircraft's altitude z , its bank angle ε , its ground speed V , and its engine power P . Furthermore, for a generic point that is located within a segment, these parameters can be interpolated according to Equations (3-5) through (3-8).

$$z = z_1 + f(z_2 - z_1), \quad (3-5)$$

$$V = \sqrt{V_1^2 - f(V_2^2 - V_1^2)}, \quad (3-6)$$

$$P = \sqrt{P_1^2 - f(P_2^2 - P_1^2)}, \quad (3-7)$$

$$\varepsilon = \varepsilon_1 + f(\varepsilon_2 - \varepsilon_1), \quad (3-8)$$

With $f = \frac{s-s_1}{s_2-s_1}$.

The evolutions of temperature, pressure and density with height follow the International Standard Atmosphere (ISA) model, which was published by the International Organization for Standardization (ISO) as an international standard, ISO 2533:1975. [35] A graphic evolution of pressure and temperature is shown in Figure 3-7. According to this model, depending on the atmospheric layer in question, the temperature, pressure and air density are given by Equations (3-9) through (3-11).

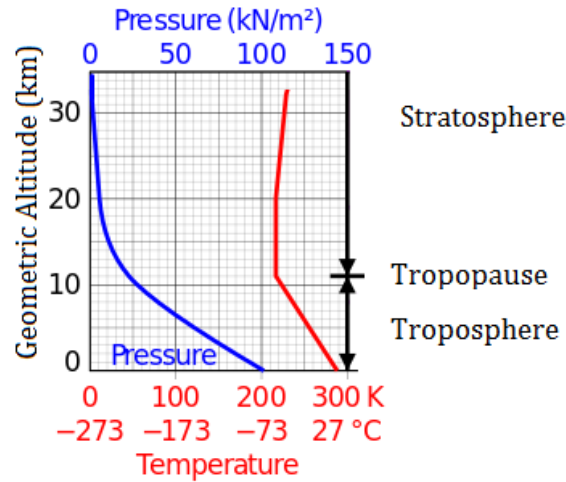


Figure 3-7 - Evolution of temperature and pressure in the International Standard Atmosphere model. [35]

As such, for the troposphere, i.e., $h < 11,000$ m:

$$T(z) = T_0 + \lambda_{trop}z \quad [\text{K}] \quad (3-9)$$

$$p(z) = p_0 \times \left(\frac{T}{T_0}\right)^{-\left(\frac{g}{R\lambda_{trop}}\right)} \quad [\text{Pa}] \quad (3-10)$$

$$\rho(z) = \rho_0 \times \left(\frac{T}{T_0}\right)^{-\left(\frac{g}{R\lambda_{trop}} - 1\right)} \quad [\text{kg/m}^3] \quad (3-11)$$

With:

$T_0 = 288$ K as the reference temperature at mean sea level ($h = 0$ m);

$p_0 = 101325$ Pa as the reference pressure at mean sea level ($h = 0$ m);

$\rho_0 = 1.225$ kg/m³ as the reference air density at mean sea level ($h = 0$ m);

$\lambda_{trop} = 6.5 \times 10^{-3}$ K/m as the temperature gradient for the troposphere.

For the purposes of noise calculation for departure procedures, it is irrelevant to model the atmospheric conditions above an altitude of around 12,000 ft as its impact is negligible.

Furthermore, despite the fact that wind velocity varies with height and time, for the purposes of noise modelling it will be considered that the aircraft is heading directly into a default headwind of 8 kt at all times, due to the fact that the ANP databases are given under that assumption as well. Doc.29 gives corrections to include any wind velocity, but these will not be followed in this

dissertation for simplicity. Likewise, no wind is taken into account for sound propagation calculations.

3.3.2 Ground Roll

During takeoff, an aircraft accelerates from rest at the start of roll point in the runway, where $s = 0$ ft, up to a set takeoff speed V_{TO} at a certain distance from the start of roll s_{TO} , usually around $V_{TO} \sim 155 - 190$ kt at $s_{TO} \sim 5000 - 8000$ ft.

This takeoff ground roll distance is given by Equation (3-12), being defined for reference ISA conditions and considering an 8 kt headwind.

$$s_{TO8} = \frac{B_8 \cdot \theta \cdot (W/\delta)^2}{N \cdot (F_n/\delta)} \quad (3-12)$$

Where:

B_8 is a coefficient appropriate to a specific aircraft/flap-deflection combination [ft/lbf], obtained from the ANP database;

W is the aircraft's gross weight at brake release [lbf]; and

N is the number of engines supplying thrust.

The ground roll is then segmented into n_{TO} parts based on the aircraft's groundspeed. Each segment has a difference of about $\Delta V \cong 10$ m/s to the subsequent one; for simplicity, it is assumed constant acceleration along the ground roll.

$$n_{TO} = \text{floor} \left(1 + \frac{V_{TO}}{10} \right). \quad (3-13)$$

As such, the change of velocity along a segment is:

$$\Delta V = V_{TO}/n_{TO}, \quad (3-14)$$

And the time on each segment:

$$\Delta t = \frac{2 \times s_{TO}}{V_{TO} \times n_{TO}}, \quad (3-15)$$

Finally, the length of each segment k is given by:

$$s_{TO,k} = (k - 0.5) \times \Delta V \times \Delta t = \frac{(2k - 1) \times s_{TO}}{n_{TO}^2}. \quad (3-16)$$

3.3.3 Initial Climb

Right after takeoff, the aircraft climbs with a constant airspeed until a set altitude. From the moment an aircraft leaves the ground, the properties of its noise propagation to the ground vary from point to point. A single segment for the climb section was shown to provide poor results in terms of noise accuracy; as such, it is recommended to divide it into segments, with the length of each being

influenced by lateral attenuation. This results in this section being segmented based on a set of height values, expressed subsequently, and following Equation (3-17).

$$z = \{18.9, 41.5, 68.3, 102.1, 147.5, 214.9, 334.9, 609.6, 1289.6\} \text{ meters}$$

Based on this set of heights, it should be identified which of them is closest upper bound to the section endpoint height, and then calculate each segment's height using:

$$z_{seg_i} = z \left[\frac{z_i}{z_N} \right], (i = 1, \dots, N), \quad (3-17)$$

Where:

z_{seg_i} is the height of the i^{th} segment of the climb section;

z_i is the i^{th} member of the set of height values;

z is the section endpoint height; and

z_N is the closest upper bound to height z .

As for any segment, the initial net thrust is put equal to the preceding one's net thrust, which is influenced by the aircraft's parameters, such as its airspeed, flap and power settings - which are constant within a section -, height and bank angle. On the other hand, at the end of each segment the net thrust is yet again given by Equation (3-1), and the distance traveled along the ground track Δs in each segment depends on the climb angle γ from the initial altitude z_{seg_i} to $z_{seg_{i+1}}$, using Equation (3-18).

$$\Delta s = \frac{(z_{seg_{i+1}} - z_{seg_i})}{\tan \gamma} \quad (3-18)$$

And the climb angle γ given by Equation (3-19), as taken from Doc.29:

$$\gamma = \arcsin \left(K \cdot \left[N \cdot \frac{F_n/\delta}{W/\delta} - \frac{R}{\cos \varepsilon} \right] \right), \quad (3-19)$$

Where:

K is a constant that depends on the calibrated airspeed which takes into account the effects on climb gradient of climbing into an 8 kt headwind and the acceleration inherent in climbing at constant calibrated speed (true airspeed increases as air density decreases with altitude);

R is the ratio of the aircraft's drag coefficient to its lift coefficient, appropriate to the flap setting; and

ε is the bank angle [rad].

3.3.4 Accelerated Climb

Usually - but not exclusively - following the initial climb, the aircraft accelerates from its current airspeed at the beginning of the procedural step until it reaches the defined airspeed, climbing at a defined rate of climb ROC [ft/min], both of them defined in the procedure to be followed, such as the one represented in Table 3-2. This accelerated climb section is recommended to be segmented by iterative processes; as for every segment, the initial conditions are those from the end of the preceding segment, while the altitude h_2 , true airspeed V_{T2} , end thrust $(F_n/\delta)_2$ and segment distance Δs are all calculated by iteration based on the distance and altitude at the end of the segment. As such, an initial end altitude to start the iteration process is guessed to be $h_2 = h_1 +$

250 ft, and then it is re-iterated by using Equation (3-21), until the difference between successive estimates is less than a tolerance value of 1 ft. On the other hand, the segment distance is estimated following Equation (3-20).

$$s_{seg} = 0.95 k^2 \frac{(V_{T2}^2 - V_{T1}^2)}{2} (a_{max} - G \cdot g) \quad (3-20)$$

Where:

0.95 is a factor to account for the 8 kt headwind when climbing at 160 kt;

k is a constant to convert kt to ft/sec = 1.688 ft/sec per kt;

$V_{T2} = V_{E2}/\sqrt{\sigma_2}$ is the true airspeed at the end of the segment, where

V_{E2} is the equivalent airspeed, which can be approximated to the calibrated airspeed V_{C2} at the end of the segment as defined in the procedure at low speeds and altitudes;

$\sigma_2 = \rho_2/\rho_0$ is the air density ratio at end altitude h_2 , with $\rho_0 = 1.225 \text{ kg/m}^3$.

$a_{max} = g \left[N \frac{F_n/\delta}{W/\delta} - \frac{R}{\cos \varepsilon} \right]$ is the maximum acceleration in level flight [ft/sec²]; and

$G \cong \frac{ROC}{60 k V_T}$ is the climb gradient.

Based on this estimate of Δs , the end altitude of the segment is given by:

$$h'_2 = h_1 + s \frac{G}{0.95} \quad (3-21)$$

The values of net thrust F_n/δ and V_{T2} change within every iteration because they are influenced by the height h_2 . Likewise, the bank angle ε is influenced not only by the radius of the turn but also by the airspeed, and as such it also varies with each iteration.

3.3.5 Thrust Reduction

An important factor for departure procedures is the use of reduced thrust instead of the maximum available, if the conditions allow it, in order to prolong engine life while also decreasing noise levels. This is a common occurrence in current practice and, as such, leads to more realistic noise contours. Typically, after the initial climb section, the aircraft reduces its power setting from takeoff thrust to climb thrust which can be sustained indefinitely. Nevertheless, for noise abatement purposes, it can be further reduced, which is referred to as deep cutback; for safety reasons, it cannot be reduced past a certain point [36]. This point, also known as engine-out reduced thrust, is determined by the performance of the aircraft, and is given by Equation (3-22).

$$\left(\frac{F_n}{\delta} \right)_{engine,out} = \frac{(W/\delta_2)}{N-1} \left[\frac{\sin(\arctan(0.01 G'))}{K} + \frac{R}{\cos \varepsilon} \right] \quad (3-22)$$

Where:

δ_2 is the pressure ratio at altitude h_2 ;

G' is the engine-out percentage climb gradient, which depends on the number of engines N :

= 0% for aircraft with automatic thrust restoration systems;

= 1.2% for aircraft with $N = 2$ engines;

= 1.5% for aircraft with $N = 3$ engines;

= 1.7% for aircraft with $N = 4$ engines;

3.4 Single Event Noise Calculation

After having trajectory defined by a sequence of points and the mentioned parameters at each of them, it is possible to finally start calculating noise levels received in different locations due to that single aircraft operation.

As mentioned in Subchapter 2.3 – Noise Metrics, the sound generated by a single aircraft movement that is received by an observer at a certain location is expressed as a single event noise level. The most common metrics used in modern aircraft noise indices are single-event sound exposure levels, L_E , which take into account all the sound energy in the events, and its exact values are given by Equation (2-6); however, it is also common to use the metric L_{max} which is the maximum instantaneous level in the event, as it's easier to model. Both of these will be calculated in this model in a different scale of noise, using the A-weighted filter to represent the human ear's sensitivity to different frequencies, resulting in the metrics L_{Amax} for the maximum level, and L_{AE} , given by Equation (2-9), for the sound exposure level.

3.4.1 NPD Tables

The calculation of noise levels in each segment is based on tabulated data from the international ANP database, which gives values for L_{max} and L_E as functions of propagation distance d and the noise-related power parameter $P \equiv F_n/\delta$, for different aircraft.

This data has to be corrected and adjusted, because its values refer to certain conditions, such as the airspeed, and due to the fact that it is under the assumption of infinite flight path instead of small segments. The values given in the table are thus baseline levels $L_{max}(P, d)$ and $L_{E\infty}(P, d)$. Furthermore, the data is tabulated for certain values of P and d , which means that it will be necessary to estimate the noise levels by interpolation. Due to the fact that the power parameter for which the noise levels are tabulated varies linearly and the propagating distance varies logarithmically, a linear interpolation is used between tabulated power settings, while a logarithmic one is used between distances, following Equations (3-23) and (3-24).

$$L(P) = L(P_i) + \frac{L(P_{i+1}) - L(P_i)}{P_{i+1} - P_i} (P - P_i) \quad (3-23)$$

$$L(d) = L(d_i) + \frac{L(d_{i+1}) - L(d_i)}{\log d_{i+1} - \log d_i} (\log d - \log d_i) \quad (3-24)$$

The adjustments to be made to the baseline values obtained from these tables take into account effects such as: (1) duration corrections ΔV , which are due to the fact that the NPD tables are defined for a reference flight airspeed; (2) installation effects $\Delta_I(\phi)$, which take into account the lateral directivity of the aircraft, as sound can be refracted and reflected by engines or airframes; (3) lateral attenuation $\Lambda(\beta, l)$, which takes into account the interaction between direct and reflected sound waves due to ground effect; and, finally, (4) the segment correction Δ_F , which takes into account the finite length of the segments. These will be detailed later in this Chapter.

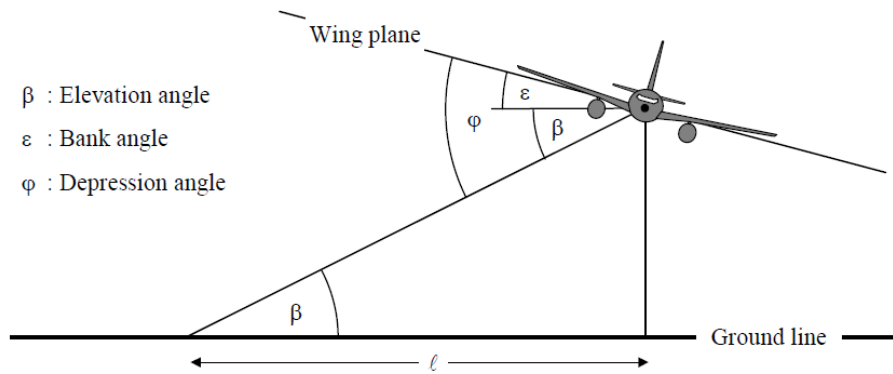


Figure 3-8 - Aircraft-observer angles. [12]

As can be seen in Figure 3-8, ϕ and β are angles that depend on the relative position of the aircraft and the observer, while l is the horizontal distance between the observer and the ground track.

3.4.2 Segment Noise Level L_{seg} and Event Noise Level L

After calculating the values of the correction parameters, the noise levels for each segment can be obtained and are given by Equation (3-25) and (3-26). Having found the values for each segment, it is finally possible to obtain the two most commonly used metrics: the maximum event level L_{max} is simply given by the maximum value of $L_{max,seg}$ among all segments, while the sound exposure level L_E is given by the decibel sum of the contributions of each segment's sound exposure level $L_{E,seg}$, as given by Equation (3-27) and (3-28):

$$L_{max,seg} = L_{max}(P, d) + \Delta_I(\phi) - \Lambda(\beta, l) \quad (3-25)$$

$$L_{E,seg} = L_{E\infty}(P, d) + \Delta_V + \Delta_I(\phi) - \Lambda(\beta, l) + \Delta_F \quad (3-26)$$

$$L_{max} = \max_i(L_{max,seg_i}) \quad (3-27)$$

$$L_E = 10 \log_{10} \sum_i 10^{L_{E,seg_i}/10} \quad (3-28)$$

It is relevant to mention that for each noise metric, the distance parameter d for the NPD tables is different. As such, when calculating the sound exposure level in each segment, the distance parameter is referred to as the minimum slant range d_p , given by the perpendicular distance from the observer to the infinite-length segment; on the other hand, when calculating the maximum level metrics, the NPD distance is the shortest distance d_s between the observer and the finite-length segment.

3.4.3 Corrections

3.4.3.1 Duration Correction

As mentioned, this correction takes into account non-reference speeds, since the data for NPD tables is obtained for a reference speed of 160 kt in a steady flight. As such, it is necessary to take into account the climb angle to obtain the horizontal component of the segment, $V_{seg} = V / \cos(\gamma)$, and the additive duration correction will be given by Equation (3-29).

$$\Delta V = 10 \log_{10} \left(\frac{V_{ref}}{V_{seg}} \right) \quad (3-29)$$

3.4.3.2 Engine Installation Correction

The airframe configuration and the location of the engines influence the properties of sound propagation by reflecting and refracting on the surfaces, resulting in a non-uniform directionality of sound radiated laterally; this parameter is influenced by the depression angle ϕ (see Figure 3-8) and by the location of the engines in the aircraft, i.e., if they're wing-mounted or fuselage-mounted engines. It is given by:

$$\Delta_I(\phi) = 10 \log_{10} \left[\frac{(a \cos^2 \phi + \sin^2 \phi)^b}{(c \sin^2 2\phi + \cos^2 2\phi)} \right] \quad (3-30)$$

With a , b , and c constants that depend on the engine location.

3.4.3.3 Lateral Attenuation

Typically, the noise levels at any lateral position are less than the ones immediately below the aircraft at the same distance. This lateral attenuation is due to interference between the direct sound waves and the ones that reflect from the surface, and can be approximated from empirical data, and given by Equation (3-31). [12]

$$\Lambda(\beta, l) = \Gamma(l) \Lambda(\beta), \quad (3-31)$$

Where $\Gamma(l)$ is a distance factor that depends on the lateral distance to ground track l , and $\Lambda(\beta)$ is long-range air-to-ground lateral attenuation level, which depends on the elevation angle β .

3.4.3.4 Finite segment correction

So far, all the adjustments assume the aircraft flying in a straight, steady level flight, along an infinite path. This last correction adjusts the level so that the values are respective to the finite segment only, and it's given by Equation (3-32).

$$\Delta_F = 10 \log_{10} F, \quad (3-32)$$

Where F is the energy fraction, which accounts for the pronounced longitudinal directivity of aircraft noise and is influenced by the distance between the observer and the aircraft and the noise levels in each segment.

3.5 Cumulative Noise Calculation

As stated before, the cumulative noise metrics are obtained by accumulating several single events throughout a period of time, resulting in the total noise exposure at that location.

As mentioned before, weightings to the obtained metrics are introduced to take into account the variation of noise sensitivity throughout the day. The metric to be calculated in the model will be the Day-Evening-Night Level L_{DEN} , which includes a 5dB evening penalty and a 10dB night penalty before the full noise energy level is averaged for a period of 24 hours. This sound levels metric can be expressed in general based in Equation (2-15) and Table 2-1, resulting in:

$$L_{DEN} = 10 \times \log \left[\frac{1}{86400} \sum_{i=1}^N g_i \times 10^{L_{E,i}/10} \right], \quad (3-33)$$

With $g_i = 1$ for if event i is during the diurnal period, $g_i = 3.162$ for an evening event, and $g_i = 10$ for a nocturnal event, for each of the N events.

3.6 Noise Contours

For any of these metrics, a noise contour can finally be drawn for assessment of noise impact around an airport area. For this effect, a fixed-spacing or regular grid of fictional observers can be created around the airport, and all of these metrics can therefore be calculated for each of those locations to result in a matrix containing noise data at structured locations around an airport. Each fictional observer is located at the center of each square in the grid and represents a local area. This information can then be used with the data obtained in the GIS to calculate the number of inhabitants in that same area, so that with a combination of these two data, a realistic assessment of noise impact in communities can be made. Due to the high number of parameters for the calculation of noise levels in one location, it is important to make a balance between both the total size of the grid and size of each square within the grid, and accuracy desired.

4 Parameters for the design of trajectories

After finishing the modeling of the noise received at any location for any desired trajectory flown by any aircraft, it's possible to finally compare different flight procedures and assess the impact they have on the communities near the airport area. To this effect, a specific parameter representing the sleep disturbance caused to a local community by a single flight operation will be used. This parameter is based on both the noise level received and the population density at a given location.

The aim is to reduce this parameter as much as possible around the airport by applying different noise abatement procedures and choosing the one which provides better results. As such, it is necessary to collect the information on population densities and to process it, to be able to calculate the relationship between aircraft noise exposure and sleep disturbance as described in this Chapter.

4.1 Processing GIS

4.1.1 Sources of data

There are different databases and sources of GIS data, containing different types of information. Typically, the data contained in a common census for a country is a diversity of information related to the number of buildings and the ages and genders of the population that make up for it. This diversity of information includes but is not limited to the number of buildings with x number of floors, the number of buildings built in y decade, the number of residencies with and without a sewer system and water, number of families, age and genders and if the individuals are working or unemployed, and much more, as exemplified in Table 4-1.

Table 4-1 - Excerpt of GIS data for Portugal total area from 2011, taken from Portugal's Statistics National Institute. [37]

N_INDIVDUOS_PRESENT	10282306
N_INDIVDUOS_RESIDENT	10562178
N_INDIVDUOS_RESIDENT_H	5046600
N_INDIVDUOS_RESIDENT_M	5515578
N_INDIV_RESIDENT_N_LER_ESCRV	499936
N_IND_RESID_DESEMP_PROC_EMPRG	539870
N_IND_RESID_EMPREGADOS	4361187
N_IND_RESID_PENS_REFORM	2339094
N_IND_RESID_SEM_ACT_ECON	3966482
N_IND_RESID_EMPREG_SECT_PRIM	133386
N_IND_RESID_EMPREG_SECT_SEQ	1154709
N_IND_RESID_EMPREG_SECT_TERC	3073092

GIS databases are set in tables, with each column being the parameter in study, and each row corresponding to the location of interest. Typically, the locations are distributed in different levels, each of them more specific than the previous one, and have designated codes, as can be seen in Table 4-2. The first level is the Country/Nation to which the data relates to.

A system was defined by Eurostat to divide the nations in three levels for statistical purposes: the Nomenclature of Territorial Units for Statistics (NUTS) system comprises three levels of the territory, which are the NUTS I, II and III. [38] On the first of these, it is described which of the National subdivision is the one in question. For example, in Portugal there are three Regions possible within the country: (1) Continental Portugal, (2) the Azores, and (3) Madeira; these are the NUTS I subdivisions of Portugal. Following it, the second major level - the NUTS II - describes the District in question, for example the District of Lisbon. Lastly, the third major level - NUTS III - describes the region within the district that's being studied, for example the "Península de Setúbal". [37] [38]

Moreover, each NUTS3 level can be divided into the different Municipalities in which it consists, and each Municipality can be subdivided in civil Parishes¹³. Finally, these parishes can be divided in Sections and Subsections, which are the most specific cells in the GIS data, and represent avenues and streets or other specific areas, as shown in Figure 4-1.

Table 4-2 - Excerpt of GIS data for Portugal total area from 2011, taken from Portugal's Statistics National Institute. [37]

ANO	GEO_COD	GEO_COD_DSG	NIVEL	NIVEL_DSG	N_INDIVIDUOS_PRESENT
2011	PT	PT	1	Total Nacional	10282306
2011	1	Continente	2	NUT1	9769564
2011	17	Lisboa	3	NUT2	2731459
2011	172	Península de Setúbal	4	NUT3	748700
2011	1506	Moita	5	Município	62833
2011	150601	Alhos Vedros	6	Freguesia	14266
2011	150602	Baixa da Banheira	6	Freguesia	20080
2011	(...)	(...)	6	Freguesia	(...)
2011	150601001		7	Secção	506
2011	150601002		7	Secção	396
2011	(...)		7	Secção	(...)
2011	15060100101		8	Subsecção	13
2011	15060100102		8	Subsecção	0
2011	15060100103		8	Subsecção	25
2011	(...)		8	Subsecção	(...)

The organization in the codes designation for each section can be seen in Table 4-2. For the Region in level 4, the first three numbers correspond to the first three levels' codes respectively;

¹³ In Portuguese, *freguesias*.

likewise, each Section starts with the code of its respective Parish, which starts with its respective Municipality's one.



Figure 4-1 - Subsection 15060101308 (Arroteias, Alhos Vedros - Moita) from Portugal's Statistics National Institute database.

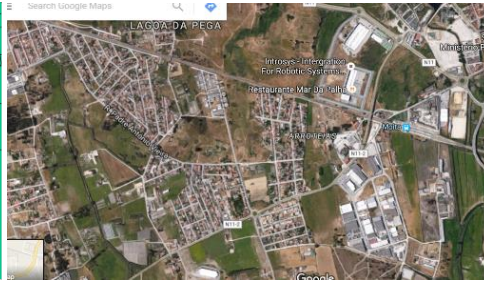


Figure 4-2 - The same subsection's location represented in Google Maps view.

In this dissertation, all this data was obtained from Portugal's National Institute of Statistics (INE), which contains all of the mentioned data from a study made in 2011 for all Municipalities, which means that information for all of the ones to be studied had to be collected individually. These files include all the information exemplified in Table 4-1 in comma-separated-values (.csv) files, and a detailed map of the municipality in a shapefile (.shp) file.

For the purposes of assessing the sleep disturbance due to noise, the most important parameters would be population density, the age of the individuals that make up the respective population as it can correlate to the sensitivity to frequency and intensity of the sound received, and possibly an average decade in which the buildings in the area were built, as newer buildings are built with materials that isolate sound more efficiently. Nevertheless, due to the difficulty to measure these correlations, for simplicity the only relevant parameter to be considered to obtain from the GIS is the number of individuals in each location.

4.1.2 Software

There are several programs to process GIS information from tables into an interactive interface. For this dissertation, due to its simplicity and being a free open-source program, the software QGIS (Quantum GIS) was used.

This program allows to import all the detailed maps from the shapefiles included in the database and show them in the interface using the "Add Vector Layer" function, while including information about the real areas and coordinates of each Section or Subsection and even the distances between any point. After importing each map, it is necessary to link and match the information from the tables in the .csv file to the respective municipality shapefile, through the use of the "Add Delimited Text" function. With these two functions, it is possible to check any information contained in the database in any location through the QGIS interface.

Keeping in mind that the aim here is to study the population density in certain areas, and based on the final step of the noise model developed - the noise contour grid -, it is convenient to represent this information in a regular grid, with the same spacing and coordinates as the one in the noise model, which can be done using the built-in function from QGIS Research Tools, "Regular Points".

With this representation, it is possible to connect the noise contour with the GIS map to see not only the noise level received by the fictional observer in any cell of the grid, but also the number of individuals that reside in that same cell. The population density in each cell can thus be easily obtained by:

$$\text{population density} = \frac{\text{nr of individuals in cell}}{\text{cell area}} \quad (4-1)$$

As shown in Equation (4-2), the number of individuals in each cell of the grid is given by the sum of the number of individuals in each subsection $n_{\text{subsection}}$ contained in the grid cell - partially or not -, multiplied by the area ratio a_{ratio} - given by the portion of area of the subsection within the cell -, divided by its total area. Naturally, if the subsection is fully contained in the cell, the area ratio will be equal to 1.

$$\text{nr of individuals in cell} = n_{\text{subsection}} \times a_{\text{ratio}} = n_{\text{subsection}} \times \frac{a_{\text{subsection in cell}}}{a_{\text{subsection}}} \quad (4-2)$$

A schematic representation is shown in Figure 4-3, for easier understanding.

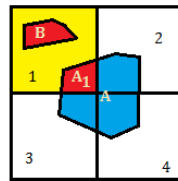


Figure 4-3 - Schematic representation of subsections (A and B) and grid cells (1-4).

As can be seen in Figure 4-3, Subsection A - the information available in the GIS - is contained in multiple grid cells. The portion of Subsection A contained in cell 1 is named A_1 . The number of individuals in A_1 is given by the total number of individuals in A, n_A , times the ratio $\frac{\text{Area}(A_1)}{\text{Area}(A)}$. Subsection B follows the same logic, but its area ratio is 1, and as such $n_{B1} \equiv n_B$. Finally, the total population density in Cell 1 is given by the sum of the number of individuals in A_1 and B_1 , divided by the area of Cell 1:

$$n_{\text{cell 1}} = \frac{n_{A_1} + n_{B_1}}{\text{Area}(A_1)}$$

4.2 Awakenings

The best criteria for choosing noise indicators is to predict its effects on the population. Two types of effects can be distinguished due to noise: (1) long-term ones, that contribute to the

development of chronic diseases and come from continuous exposure to high noise levels, the best indicator for these effects being cumulative metrics such as the L_{DEN} , and (2) short-term ones, with instantaneous effects such as sleep disturbance, and thus the best indicators are single event metrics such as the maximum level per event L_{Amax} or the single event sound exposure level SEL .

With the latter in mind, it is possible to introduce the concept of awakenings, which gives a measure to quantify the sleep disturbance based on empirical data, under the definition that it is the upper bound to the number of people expected to awake due to a single nighttime flyover. This relationship, shown in Equation (4-3), between aircraft noise exposure and sleep disturbance was based on research done by the Federal Interagency Committee on Aviation Noise (FICAN) in 1997. [24] [39]

$$\%Awakenings = 0.0087 \cdot (SEL_{indoor} - 30)^{1.79} \quad (4-3)$$

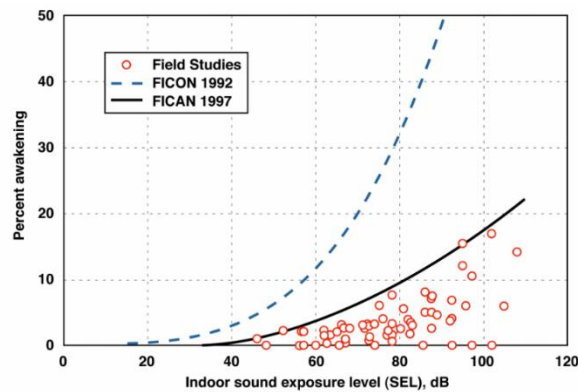


Figure 4-4 - FICAN proposed sleep disturbance dose-response relationship. [40]

This relationship, graphically shown in Figure 4-4, gives the percentage of expected awakenings in an area. This parameter can be combined with the population density in the same area from the GIS to obtain the exact number of people expected to awake due to a single nighttime flyover. It's relevant to mention that, since the individuals in question are assumed to be inside their home, the SEL value has to be corrected to the sound absorption of a typical home - which is around 20.5 dBA -, resulting in SEL_{indoor} . [24]

With this in mind, it's intuitive that flight paths that provide the lowest number of expected awakenings are considered better in terms of noise impact. Different noise abatement procedures such as the ones described in Section 2.6.2 will be modeled according to the definitions in Chapter 3, followed by the calculation of the awakenings parameter and comparing to assess which is more suitable to each route.

Simultaneously, the cumulative metric L_{DEN} will be calculated for the area near the airport throughout a full day, based on real current flight schedules - as will be detailed in Chapter 6 - and assuming different flight trajectories for each flight depending on their destination, in particular the awakenings-optimized ones, to confirm that these values are below the ones recommended by the World Health Organization.

5 Experimental Validation

In order to give meaning to any of the results obtained in any model, it is necessary to validate it first; in this case, it is essential to prove that the noise levels due to aircraft flights obtained from the model developed are accurate. For this purpose, noise levels due to real flights will be compared to model predictions to assess the accuracy of the developed model.

5.1 Noise validation

5.1.1 Validation Process

For this effect, real flight data for a few flights was obtained for Lisbon's Humberto Delgado Airport, along with the noise levels measured in dedicated noise monitoring stations for different noise metrics, for the purpose of comparing these real values to the ones obtained for the same flight procedures as modeled, assuming a fictional observer located on those stations.

This data was provided by TAP and ANA and includes two sets of three flights each. The first one corresponds to common departure procedures, contemplated in project ATAEGINA¹⁴, from Lisbon's main airport (IATA: LIS) Runway 03, with destinations to (1) Paris Orly Airport (IATA: ORY), (2) Germany's Düsseldorf Airport (IATA: DUS), and (3) Brussels Airport (IATA: BRU). The second set refers to modified procedures for noise studies, with destinations to (1) London Gatwick Airport (IATA: LGW), (2) Adolfo Suárez Madrid-Barajas Airport (IATA: MAD), and (3) Stockholm Arlanda Airport (IATA: ARN).

The data in each these files was organized in a spreadsheet with hundreds of values for different parameters, measured every 4 seconds throughout the flight since the aircraft taxi-in flight phase. As shown in Table 5-1, the flight path parameters include - but are not limited to - the aircraft's coordinates (on a geographic coordinate system), the aircraft's gross weight, its calibrated and true airspeeds, its heading and roll angles, and also parameters related to the engines - N_{11} ¹⁵ - and the flap settings.

Table 5-1 - Excerpt of flight parameters for flight TP544 with destination to Düsseldorf Airport (date not disclosed for confidentiality reasons).

HEIGHT	LATITUDE	LONGITUDE	CAS	TAS	HEAD	ROLL	N11	FLAP
0	38.768.860	-9.142.335	91.13	90.0	25.66	-0.352	83.500	10.42
0	38.769.127	-9.142.163	95.63	94.0	25.31	0.000	83.375	10.42
0	38.769.535	-9.141.991	103.00	99.0	25.31	-0.352	83.500	10.42
0	38.769.947	-9.141.788	105.13	104.5	26.02	-0.352	83.500	10.42

¹⁴ Airline TriAls of Environmental Green flight maNAgeMENT functions is a project which includes Portuguese companies such as NAV Portugal EPE, ANA-Aeropostos de Portugal and TAP, aiming at developing systems which enable environmentally sustainable flight operations. [64]

¹⁵ The N_1 is the rotational speed of the engine's low-pressure compressor (or fan) and turbine stages, and is given in %. It affects the noise-related power parameter *net thrust*.

On the other hand, the complementary file contained the noise levels measured in different noise monitoring stations for those two sets, as represented in Table 5-2. The locations of these stations can be seen in Figure 5-1, and the mentioned data can be found in Appendix B.

Table 5-2 - Excerpt from noise monitoring station data for the same flight TP544 with destination to Düsseldorf Airport..

Location ID	Location Description	Flight Number	Aircraft Type	L_{max}	L_{eq}	SEL	EPNL	Duration
7	Aeroporto	TAP544	A320	83,80	78,90	91,90	91,70	20
3	Camarate	TAP544	A320	77,10	71,60	87,60	88	39
1	Pirescoxe	TAP544	A320	69,60	67,30	79,70	78,20	17

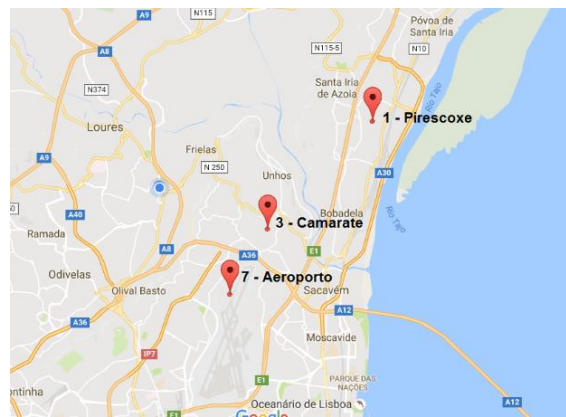


Figure 5-1 - Lisbon map with the location of the stations mentioned in Table 5-2. [Google Maps]

With this data, it's possible to reproduce the exact flight paths from recorded flight data into the developed noise model through the *analysis* method. The trajectory is thus given by a sequence of segments formed by the coordinates of the aircraft throughout its path, and it is unnecessary to make any further segmentation.

Despite the fact that there is a higher number of points in the data - due to the 4 second spacing between measurements -, it is only necessary to consider three fictional observers, each located in the station coordinates and therefore the computation times will stay short.

The power setting is obtained with the combined use of the ANP database and the N_1 parameter in the flight parameters table, following a modified version of Equation (3-1): [12]

$$\frac{F_n}{\delta} = E + F \cdot V_C + G_A \cdot h + G_B \cdot h^2 + H \cdot T + K_3 \left(\frac{N_1}{\sqrt{\theta}} \right) + K_4 \left(\frac{N_1}{\sqrt{(\theta)}} \right)^2, \quad (5-1)$$

Where:

K_3 and K_4 are constants derived from engine data encompassing the N_1 speeds of interest;
 θ is the ratio of the absolute total temperature at the engine inlet to the absolute standard air temperature at mean sea level.

Due to the fact that the noise calculation is based on the use of NPD tables, the only essential pieces of information to calculate noise levels are (1) the noise related power parameter - as given by Equation (5-1) for each point -, and (2) the distance parameter - related to the fictional observers' location and the flight path and (3) the airspeed, for correction purposes. The resulting noise values can then be compared to the real ones to assess the accuracy of the noise model.

5.1.2 Results

Due to the lack of information about the weather conditions for the dates at which the flights occurred, standard conditions for air temperature, pressure and density were assumed.

The real flight paths were then individually inputted in the model along with the power parameter N_1 in each segment, and thus calculated the noise at the station locations. The only information regarding the aircraft on these flights is that it is an Airbus A320 for all procedures, its model being unspecified. Nonetheless, by analyzing the Flight Numbers (such as TP348) on FlightRadar24, it could be noted that TAP operates mostly with A319-111 and A320-214 models; as such, the ANP database for the latter will be used for modelling purposes.

The coordinates of the noise monitoring stations are:

- 7 - Aeroporto: 38.790561 N -9.134764 W, 364 ft height;
- 3 - Camarate: 38.806572 N -9.122324 W, 279 ft height;
- 1 - Pirescoxe: 38.834433 N -9.089842 W, 20 ft height.

The results for each flight are found in Table 5-3 and Table 5-4.

The error or residual between the modeled noise levels and the real ones at each station was then calculated through Equation (5-2), and the variance through Equation (5-3). Analyzing these errors allows to predict further errors in other flights and thus empirically correct the noise levels for any defined procedure; ideally, a higher number of real results is needed to improve the error prediction algorithm.

$$error = L_{real} - L_{modeled} \text{ [dBA]} \quad (5-2)$$

$$var = \sigma^2 = \frac{1}{N} \sum_{i=1}^N (x_i - \mu)^2 \text{ [dBA]} \quad (5-3)$$

With:

x_i each error of the respective measurement done by the model;

$\mu = 0$ (assuming the noise levels measured by the stations are absolutely correct, the expected value for the error is 0); and

$i = 1, \dots, N$ each measurement for all flights, and $N = 6 \times 3 = 18$. This variance is numerically equal to the average total deviation squared σ^2 .

Table 5-3 - Results obtained for the first set of flight procedures.

Flight	Station	Real L_{max} (dBA)	Modeled L_{max} (dBA)	L_{max} error (dBA)	Real SEL (dBA)	Modeled SEL (dBA)	SEL error (dBA)
TP616	7	82,8	84,39	-1,59	91,1	94,2	-3,13
	3	75,7	77,8	-2,1	87	88,7	-1,7
	1	71,6	67,55	4,05	80,7	81,6	-0,87
TP544	7	83,8	84,47	-0,67	91,9	94,1	-2,19
	3	77,1	78,92	-1,82	87,6	90,6	-3
	1	69,6	72,05	-2,45	79,7	84,7	-4,95
TP434	7	83,7	83,61	0,09	91,5	93,7	-2,23
	3	79,4	82,22	-2,82	88,8	92,9	-4,07
	1	74,8	73,44	1,36	84	85,8	-1,79

Table 5-4 - Results obtained for the second set of flight procedures.

Flight	Station	Real L_{max} (dBA)	Modeled L_{max} (dBA)	L_{max} error (dBA)	Real SEL (dBA)	Modeled SEL (dBA)	SEL error (dBA)
TP348	7	84,9	84,67	0,23	92,5	94	-1,51
	3	80,3	82,11	-1,81	89,8	92,7	-2,93
	1	68	67,32	0,68	79,1	81,7	-2,58
TP1024	7	82,8	83,16	-0,36	90,7	93,7	-2,96
	3	78,4	81,73	-3,33	87,9	92,9	-4,97
	1	67,4	66,96	0,44	77,1	81,7	-4,63
TP784	7	83,9	83,33	0,57	92,9	93,5	-0,62
	3	78,9	82,46	-3,56	88,8	93,6	-4,83
	1	74	74,76	-0,76	83,7	86,9	-3,17

Although there is not enough diversity in real noise levels available data, it was the most reliable way to validate the model and have an estimate of its accuracy for observers located at any distance from the flight path. The modeled values give a maximum deviation of around 5dB from the real value which, despite not being perfect, is enough to serve the purposes of this analysis given the lack of further information such as weather conditions, wind speed and direction or humidity.

An analysis on these errors was made by plotting them in function of the aircraft's height and ground distance traveled, as shown in the subsequent graphs.

Noise Levels Error vs Height

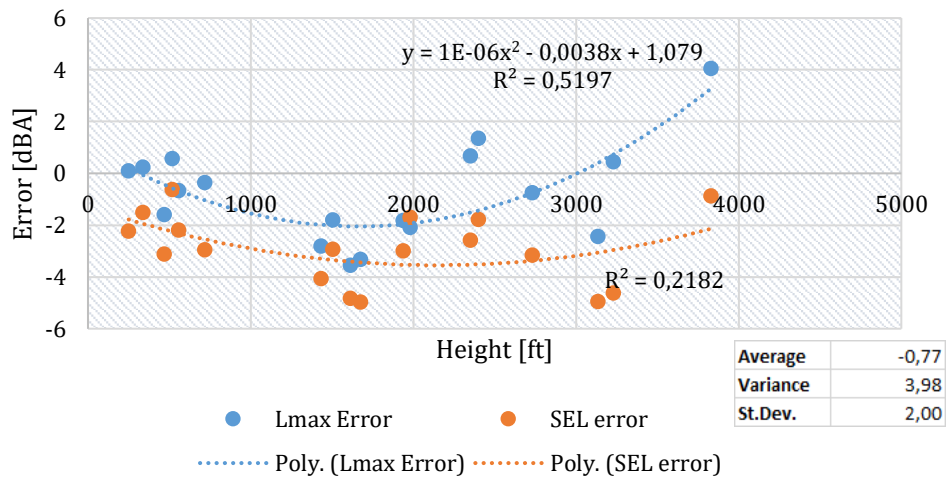


Figure 5-2 - Noise level error at monitoring stations.

Noise Levels Error vs Ground Distance

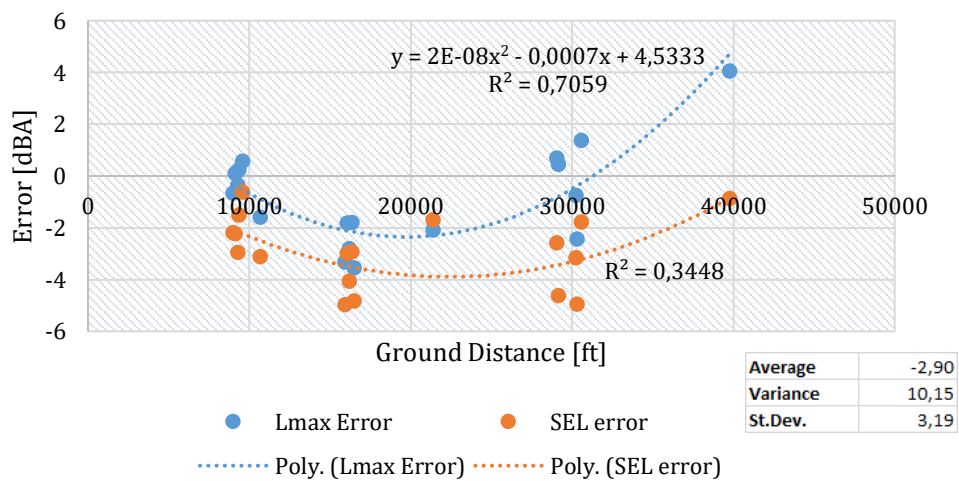


Figure 5-3 - Noise Level error at monitoring stations.

As mentioned, the number of exact results is not high enough to make significant inferences; furthermore, the available data is restricted to these three stations, therefore any conclusion taken from these results and graphs are only significant for this interval - which corresponds to altitudes up to approximately 4,000 ft and a ground distance of up to 40,000 ft for an aircraft following any common departure procedure. With this in mind, a small trend is noticeable in Figure 5-2 and Figure 5-3, in which the noise level errors are shown in a scatter plot for all six flights in the three locations where the monitoring stations are set. It is possible to see that during the first half of the interval, up to an altitude around 1,000 ft (or 10,000 ft of ground distance), the noise model gives good results, with errors lower than 1 dBA for L_{max} and 3 dBA for the SEL. Due to the fact that the SEL is a measurement of the total energy throughout the flight path rather than the maximum level due to a

single point, the error for this metric will be generally bounded in a smaller interval: as can be seen, its error ranges from -5 dB to -1 dB, as opposed to L_{max} which shows errors from -3 dB to up to +5 dB. The fact that SEL takes into account the several segments that compose the flight path makes it so that the lower errors obtained in the first half of the path compensate for the higher ones in the rest of the flight.

A regression model was made using a second degree polynomial function to predict the error associated with the noise model for the referred interval based on both the height and the ground distance. It is important to stress that due to the lack of available data, higher values for the coefficient of determination (R-squared) parameter, which typically defines how well the regression model predicts future outcomes, were not possible. Nonetheless, this error prediction algorithm is expected to increase the noise modelling accuracy regarding the noise levels within this interval on further procedures.

Table 5-5 - Corrected errors for L_{max} in Stations 1, 3 and 7.

Flight	St.	Initial error (dBA)	Corrected error 1 (dBA)	Corrected error 2 (dBA)
TP616	7	-1,59	-1,27	-0,99
	3	-2,1	0,43	-0,67
	1	4,05	3,48	-3,55
TP544	7	-0,67	-0,06	-0,61
	3	-1,82	0,71	-0,31
	1	-2,45	-1,36	-4
TP434	7	0,09	-0,2	0,22
	3	-2,82	-0,56	-1,3
	1	1,36	3,69	-0,22
TP348	7	0,23	0,26	0,46
	3	-1,81	0,5	-0,27
	1	0,68	3,01	-0,57
TP1024	7	-0,36	0,63	-0,2
	3	-3,33	-0,87	-1,81
	1	0,44	1,29	-0,63
TP784	7	0,57	0,97	0,78
	3	-3,56	-1,15	-2,02
	1	-0,76	1,12	-2,39
$\sum_i abs(error_i)$		28,69 (av: 1.59) ($\sigma^2=3.98$)	21,56 (av: 1.20) ($\sigma^2=2.55$)	21 (av: 1.17) ($\sigma^2=2.61$)

Table 5-6 - Summary of the average errors for the corrections made for L_{max} in each station.

Station	Original	Correction 1 (height)	Correction 2 (ground distance)
A-7	mean = -0.29 $\sigma = 0.76$	mean = 0.05 $\sigma = 0.71$	mean = -0.06 $\sigma = 0.61$
B-3	mean = -2.57 $\sigma = 2.67$	mean = -0.16 $\sigma = 0.75$	mean = -1.06 $\sigma = 1.27$
C-1	mean = 0.55 $\sigma = 2.06$	mean = -1.87 $\sigma = 2.57$	mean = -1.89 $\sigma = 2.42$

Where both the mean and the standard deviation σ are given in dBA. Figure 5-4 shows a graphical representation of this table.

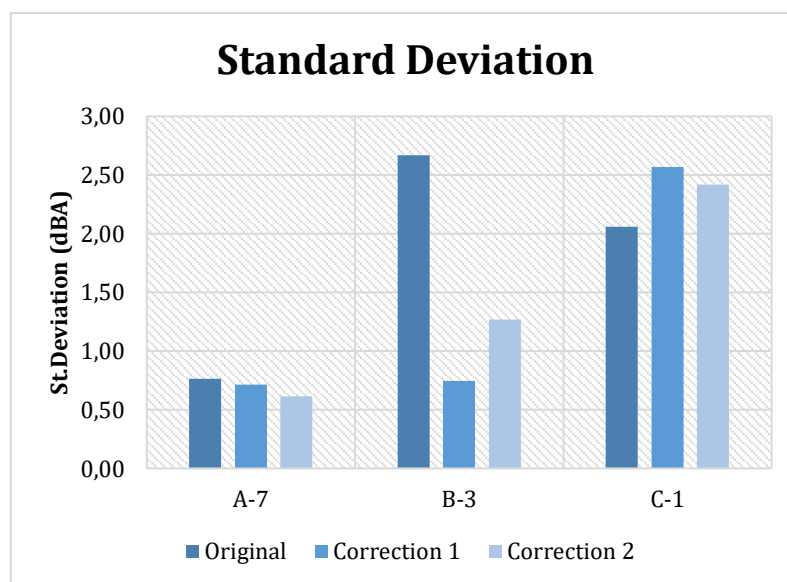


Figure 5-4 - Graphical representation of the standard deviation obtained for L_{max} each station.

As can be inferred from Table 5-3 to Table 5-6 and Figure 5-4, the higher modeling errors are found for locations near Station 3, where the aircraft is flying at around 1,000–2,000 ft. The most likely cause for these deviations is wind effects, as the described model assumes an 8 kt headwind for the whole flight. As can be seen in Figure 5-5, there is a larger wind velocity gradient closer to the ground (that is, below 2,000 ft AGL), which is a part of the atmospheric boundary layer (ABL); above these altitudes, the wind speed is not significantly influenced by height.

Nonetheless, despite the highest wind gradient being close to the ground, the noise levels errors for altitudes near Station 7 - where the aircraft is flying below 1,000 ft - are negligible; this is due to the fact that the closer proximity between the aircraft and the noise stations leads to wind speed not affecting sound propagation as much.

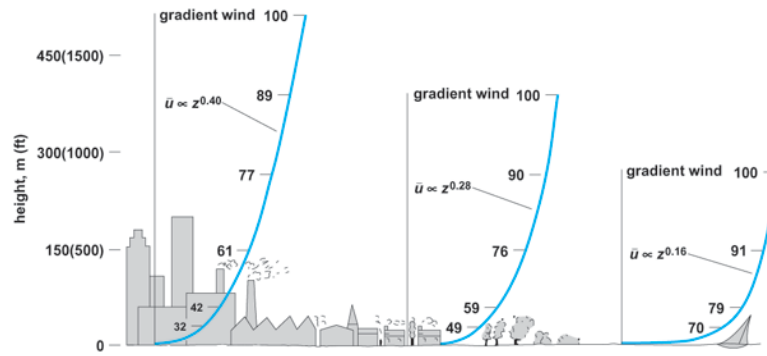


Figure 5-5 - Schematic representation of the evolution of wind intensity with height. [41]

Due to this fact, the correction based on height led to negligible improvements (~ 0.05 dBA) at lower altitudes, but much more significant improvements (~ 2 dBA) at slightly higher altitudes around 1,500–2,000 ft. Above these heights, the polynomial regression obtained does not represent the wind gradient anymore, leading to higher errors. For this reason, the final correction function to be applied on the noise model is the height-based empirical correction up to around 2,000 ft, while leaving the remainder of the model left uncorrected as the obtained results and errors have no correlation with wind. A summary of the obtained results is given in Table 5-7.

Table 5-7 - Overview for the errors of L_{max} in the original and the corrected model.

Overview		Original Model	Corrected Model
Mean [dBA]	$\mu = \frac{1}{N} \sum_i error_i$	-0.77	0.15
St. Deviation [dBA]	σ	2.00	1.33
Variance [dBA²]	σ^2	3.98	1.77

It's important to mention that wind conditions are not the only factor influencing the results. Parameters such as the air pressure, temperature and density were all calculated for reference ISA conditions, and they heavily influence both the engine power parameter calculation and sound propagation properties. Furthermore, the NPD tables were also designed for reference humidity conditions, which similarly have a high influence on atmospheric sound absorption.

5.2 Trajectories validation

5.2.1 Validation Process

The previous section could provide a good estimate on the accuracy of the noise levels calculated by the model for a real trajectory consisting on many points through an *analysis* method. Nonetheless, it is still necessary to assess the reliability of noise levels calculated through a trajectory modeled by *synthesis*, following a defined set of procedures such as the one described in Table 3-2.

For this effect, it will be aimed to model the flights described in the previous section through a set of procedural steps, so that the program developed can create a flight path that resembles the real flight as best as possible. Given the fact that not only the true position - both ground track and profile - of the aircraft is available, but also the aircraft's airspeeds and engine parameters, it is possible to make an initial guess for the procedure followed by the aircraft. This set of procedural steps can then be readjusted through trial-and-error by fine-tuning the parameters that define each step of the procedure - for example the end airspeed in an accelerated climb procedure and/or its rate of climb. The aim is to make a balance to minimize the errors of the position, airspeed and power parameter simultaneously; this balance is defined by the introduction of a cost function that should be minimized and takes into account these three parameters with equal weightings. The atmospheric conditions used are, yet again, the international standard ones due to lack of more detailed information.

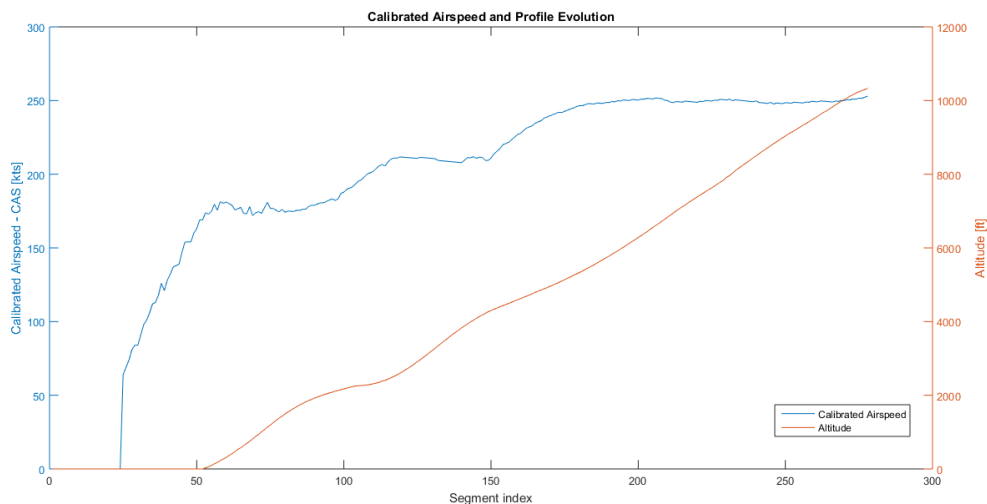


Figure 5-6 - CAS and Altitude evolution throughout the flight, obtained through the real data available from flight TAP616.

For this purpose, knowing the evolution of the profile and the calibrated airspeed of the aircraft throughout its flight, as shown in Figure 5-6, it's simple to infer an initial guess for the procedural steps to model the flight. On the example shown, it's possible to conjecture that the aircraft takes off at around 180 kt CAS, climbing at constant airspeed up to around 2000 ft, and accelerates to around 220 kt CAS followed by a climb to 4000 ft at that airspeed, and finally accelerating to 250 kt and climbing at constant speed from then onwards; this will be the initial guess for this flight. This set of procedural steps is then adjusted by trial-and-error to minimize the resulting deviations in relation to the real flight.

This set of procedures only covers the profile of the modeled flight; nevertheless, the calculation of the profile is also function of the bank angle - which is associated with the ground track - and, as mentioned in Chapter 3, the model described by ECAC suggests considering the profile and ground track independent for simplicity. However, to solve this flaw, an iterative approach to model the flight was taken. In the initial guess for the profile, a straight path is assumed with bank angle

equal to zero throughout the whole flight. Afterwards, the flight segments in which turns are made can be chosen by the user in the program; this path is visually represented in real time on a map, overlapped with the real path, as seen in Figure 5-7 and Figure 5-8, making it simple to choose the most accurate segments. Along with this turn, the bank angle also changes in that segment. After this path is defined, the set of procedures is re-iterated, this time with the correct bank angles throughout the flight.

Likewise, the position and airspeed errors can be checked, and adjustments made in the procedural steps and/or the ground track, to minimize these errors as much as possible.

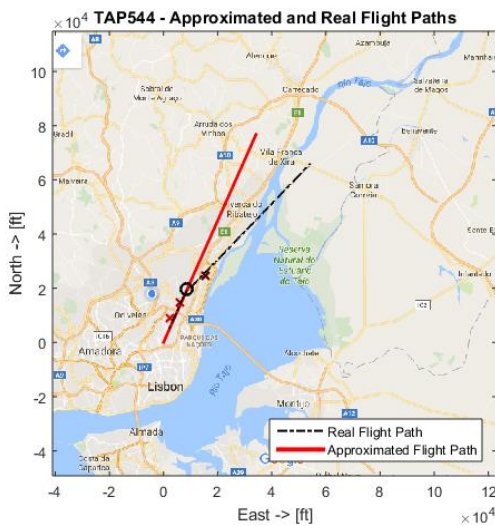


Figure 5-7 - Choosing the segment index (black circle) to initiate the turn.

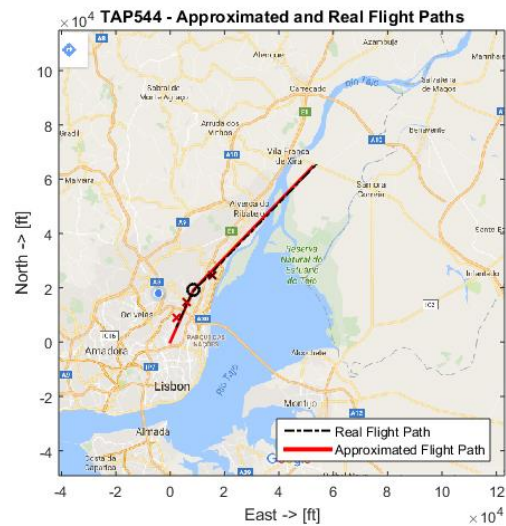


Figure 5-8 - Setting the turn to match the real flight path.

It is important to keep in mind that it is not possible to minimize all of these parameters at the same time. For example, having a modeled trajectory very close to the real one can come at the cost of the airspeeds having high deviations to the real ones at equivalent points along the trajectory. As such, for purposes of noise validation, it will be aimed to minimize as much as possible all of the mentioned parameter errors specifically near the noise monitoring stations, at the cost of having slightly higher errors in areas farther from these locations.

5.2.2 Results

Based on Figure 5-6 and following the method described, a set of procedural steps was defined for each flight, and the respective position, velocity and power error graphs along the path were calculated; an example can be found in Appendix C. The full table with the results obtained for the validation process can be found in Appendix D both with and without the empirical correction described in the previous section. In the errors column, X corresponds to positional error, S

corresponds to true airspeed error, and P corresponds to power parameter error¹⁶. A graphical representation of the power parameter error along the path is also shown.

Table 5-8 provides a summary for the obtained results and, as can be seen, the errors obtained are slightly higher than the ones from the previous section. This is due to the fact that both the flight trajectory and the aircraft's airspeed - both of which correlate with its power parameter - are not exactly the same as the real ones. For example, the procedural steps designed to model Flight TP616 have a net thrust around 3,000 kN below the real one at Station 1; this leads to a much lower noise level as interpolated from the NPD tables, resulting in an 8 dBA error. If a better approximation could have been made to model this flight, this error would have been significantly inferior.

Table 5-8 - Standard deviation and variance for corrected and uncorrected models.

	St.Deviation (dBA)	Variance (dBA²)
Uncorrected	2.85	8.11
Corrected	2.20	4.86

The empirical corrections applied provide slightly better results in relation to the original model, reducing the standard deviation by 0.65dBA.

Overall, according to the available data measured by noise monitoring stations, the flight path and noise models developed show results with a good degree of accuracy, making it possible to make an accurate noise impact study for virtually any flight and any location desired, such as Montijo's Air Base.

¹⁶ Note that noise related power parameter is, in fact, a measure of net thrust and is thus given in kN.

6 Application to Montijo Airport

After defining the process to design trajectories as described in Chapter 4 and validating the tools to be used for this process in Chapter 5, it's finally possible to actually begin to apply these tools for the purposes they were designed.

For this effect, it will initially be described the area of interest - the airbase of Montijo -, namely the population analysis from the GIS around Lisbon (see area in Figure 3-3), followed by the description of its ARP¹⁷ and its runways. The constraints to which special attention will be needed, such as airspeed restrictions at certain flight levels and separation minima will be mentioned, along with the areas dedicated to military use, in which civil aircraft cannot fly. Afterwards, a small analysis will be made in order to define the aircraft to be used, which will be based on the airlines to be considered - the lowcost airlines -, followed by the definition of a flight scheduling program based on current patterns, including the destination of each flight and the respective SIDs based on statistical data. Finally, the set of procedures for each flight to be applied for noise abatement purposes will be thoroughly described, following the structure shown in Table 3-2.

6.1 Population Analysis [GIS]

Using the QGIS software in conjunction with the data obtained from the INE, it was possible to obtain a grid containing the population density around Lisbon, as shown in Figure 6-1. The grid created has a 1km x 1km area in each cell and the population density values are based on an average number of individuals in each Section that belongs in the grid cell. The color gradient represents the population density obtained from QGIS, with a background for the same area of interest as seen in Google Maps. The area in red indicates the location of Montijo's airbase.

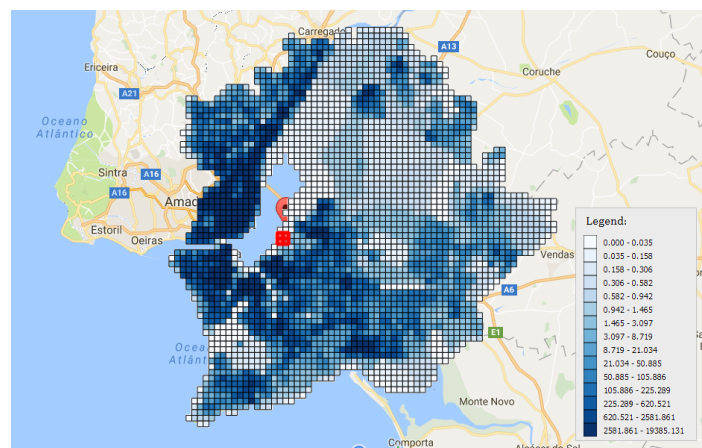


Figure 6-1 - Population density grid map for area of interest around Montijo.

¹⁷ ARP (Airport/Aerodrome Reference Point) is the approximate geometric center of all the usable runways, representing the center point of an airport. [65]

As described in Subchapter 4.1, the smallest or most-specific levels in the GIS are the Sections and Subsections - which have irregular shapes, as can be seen in Figure 4-1, and the totality of those produce the full map of the area of interest. When trying to represent the data in an equivalent regular grid, a square cell in it can consist in several parts of different Sections and/or Subsections and thus the number of individuals is calculated by a weighted sum of the number of individuals of each of them that are within the square cell, according to Equation (4-2); this is also done in QGIS. Afterwards, it's possible to define a color gradient based on the number of individuals calculated for clarity, resulting in the grid map represented in Figure 6-1.

6.2 Lisbon's Terminal Airspace

Airspace can be formally divided in classes as per ICAO airspace classification scheme [42]. Under this classification, there are various classes for controlled airspace and for uncontrolled airspace, and they are designated fundamentally in accordance to services provided and flight requirements. [43]

Besides having to follow instrument flight rules (IFR) - all aircraft must be IFR unless VFR authorized [44] -, any aircraft flying within controlled airspace has to follow a set of rules, such as Separation Minimums and airspeed constraints. These rules exist to facilitate safe navigation of aircraft in controlled airspace, while also serving to reduce exposure to wake vortex turbulence. ICAO Doc.4444 specified a minimum vertical separation for IFR flights as 1,000 ft below FL290 and 2,000 ft above, except when Reduced Vertical Separation Minima (RVSM) apply. [45] [46] Table 6-1 shows a summary for the airspace classes as defined by ICAO. [43]

Table 6-1 - ICAO airspace division and specifications overview.

Class	Controlled	IFR	VFR	Separation	Speed Limitation
A	Yes	Yes	No	Provided for all flights	Not applicable
B	Yes	Yes	Yes	Provided for all IFR to IFR /VFR	Not applicable
C	Yes	Yes	Yes	Provided for IFR to other IFR	250 kt IAS below 10000ft AMSL (for VFR only)
D	Yes	Yes	Yes	Provided for IFR to other IFR	250 kt IAS below FL100
E	Yes	Yes	Yes	Provided for all IFR to other IFR	250 kt IAS below FL100
F	No	Yes	Yes	Provided for all IFR to other IFR where possible	250 kt IAS below FL100
G	No	Yes	Yes	Not provided	250 kt IAS below FL100

Within the Lisboa FIR, the airspace is classified as "C", "D" and "G", depending on the location. Namely, the airspace classification "D" is currently allocated to restricted areas such as Montijo's

LPR26A, while they're used for military purposes; when the air traffic service provided is delegated to civilian units, the airspace classification changes to "C" for these areas. [47]

6.2.1 Montijo Air Base

As mentioned, the airport in study is the Montijo Air Base¹⁸ (ICAO: LPMT) which is currently a Portuguese Air Force's military air base located in Montijo, near Tejo river (see Figure 3-3), aimed for maritime patrol, anti-submarine warfare, and search and rescue operations, being in use since 1953. [48]

As can be seen in Figure 6-2, this air base consists of two intersecting runways: (1) Runway 1/19, with 2,147 m (7,044 ft) length and an asphalt surface; (2) Runway 08/26, with 2,440 m (8,005 ft) and a surface in concrete. Its ARP coordinates are (38° 42' 13.90" N, 009° 02' 09.30" W), and it has a 14 m (46 ft) elevation AMSL. [49]

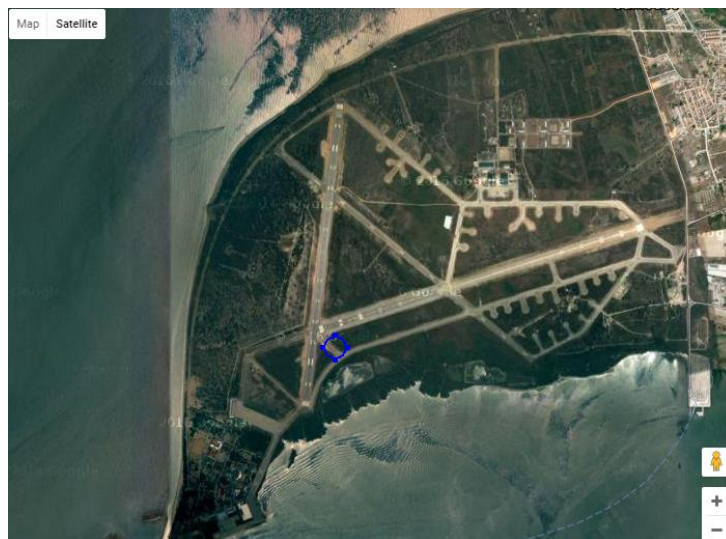


Figure 6-2 - Montijo Air Base, as seen from Google Maps' satellite view.

The plan to use this air base as an auxiliary aerodrome to Lisbon's main airport assumes the use of runway 01/19 as the main one, being roughly parallel to Humberto Delgado's runway 03/21, the most frequently used one in the airport. Not only is the use of RWY01 convenient based on the fact that Portugal has predominantly Northern winds, but also the usage of runway 06/28 would be incompatible with aircraft approaching or taking off from Humberto Delgado's runway 21 due to possible interference. Furthermore, the installation of an ILS (Instrument Landing System) in runways 01/19 is intended for increased safety, and the creation of a parking platform for aircraft from the different airlines, along with a civil terminal is being considered. [4] It's relevant to mention that this redefinition in Lisbon's airspace will require the approval of EUROCONTROL and EASA. [4]

¹⁸ In Portuguese: *Base Aérea do Montijo*, or *Base Aérea N.º6* (BA6)

6.2.2 Danger, Restricted and Prohibited Areas

Apart from the previously mentioned rules, there are also airspace restrictions and warnings, such as areas with military activities with potential risk to General Air Traffic. Three main categories can be differentiated: (1) danger areas, within which dangerous activity may occur at specified times mostly operated by military authorities, making it unsafe for civil aircraft to fly over the area [42]; (2) restricted areas, in which the flight of aircraft is restricted in accordance to specific conditions [50]; lastly, (3) prohibited areas, within which the flight of aircraft is strictly prohibited. [50] All these areas' vertical and lateral dimensions and limits are available in national AIPs¹⁹, along with the hours of operation where applicable.

It is frequent for many danger and restricted areas to be inactive for long periods of time, which makes the airspace become inefficient as it's not being used for military nor civil purposes. As such, the concept of Flexible Use of Airspace (FUA) has been developed to optimize the use of airspace within Europe; the airspace is, thus, no longer considered exclusively civil or military, but considered as one continuum instead. Its use is shared through enhanced civil/military co-ordination that ensures that the airspace segregation is temporary and based on real use for specified time periods. [51] [52]

As can be seen in the Lisbon TMA chart - included in Appendix E -, the airspace around Lisbon is limited with many danger and restricted areas, specifically near Montijo Air Base. This will limit the departure procedures to implement trajectory-wise; in particular, the D10 zone is a danger area located right next to the air base, and as such should be given special attention for flights aiming to turn east after taking off. It's important to note that the restricted area LPR26A-Montijo will be overlooked due to the assumption that the Air Base will no longer be used for military purposes only, allowing for civil navigation with no restrictions for the purposes of this dissertation.

6.3 Aircraft, Movements and Schedules

Before finally start designing departure routes, it is necessary to establish assumptions regarding aircraft types and flight destinations, which will determine the route to follow after taking off. There is a set of SID termination points towards which an aircraft can choose to fly, depending on the flight plan and ATC tactical instructions.

With this in mind, and based on the fact that this aerodrome is expected to be used by the low-cost airlines that currently fly from and to Humberto Delgado's airport, some assumptions will be made and will be detailed next.

¹⁹ Aeronautical Information Publication is defined by ICAO as a publication containing aeronautical information essential to air navigation. [70]

6.3.1 Routes

There are several termination points to which an aircraft can aim to fly to during a departure procedure. Each of them has their own SID (Standard Instrument Departure) route - a published flight procedure followed by an aircraft immediately after taking off from an airport aimed to simplify clearance delivery procedures while striking a balance between obstacle avoidance, noise abatement if necessary and airspace management considerations. [53] Each of these points is a reference point, usually - but not necessarily - associated with existing navigational aid stations and is most often used to indicate a change in direction, speed or altitude along the desired path. The RNAV SID charts for Lisbon LPPT can be found in Appendix F, as obtained from the online AIP provided by NAV Portugal.

It is relevant to note that due to the fact that the Montijo Air Base is not currently in use for civil navigation, the commercial flights' departure procedures to study haven't been thoroughly defined yet. As such, and due to its proximity to the Air Base, data for Humberto Delgado's airport will be used as the foundation to the design of trajectories for the former, and the SID termination points will be the same under the Lisbon TMA.

The map for the Lisbon TMA containing the Inbound, Outbound and Transit Routing can be seen in Appendix E, followed by the Standard Departure Charts for RWYs 03-35 - both Standard and RNAV -, all of which contain the mentioned waypoints for the area of interest. It can be seen that, for LPPT RWYs 03-35, there are 11 different SIDs, with 9 of them being RNAV. Due to this abundance, a flight path noise optimization process will not be studied for all of them; with this in mind, the SID termination points for which flights paths will be modeled and designed will be chosen based on statistical data, centered on those which are most frequently used during departure procedures for Humberto Delgado's airport as seen in Figure 6-3.

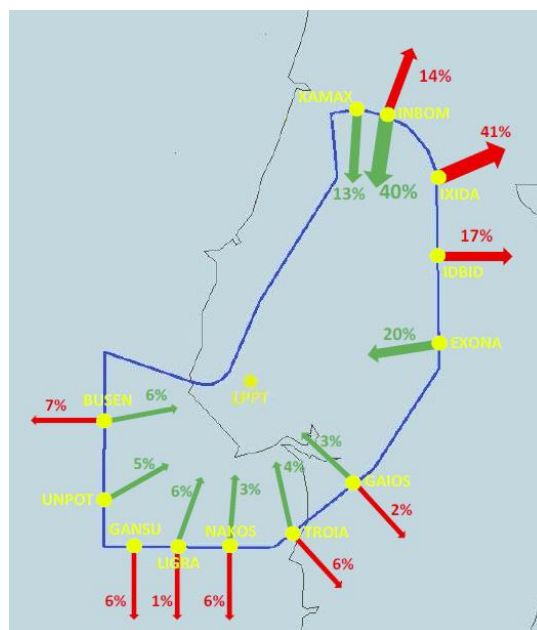


Figure 6-3 - Air Traffic distribution for LPPT for July 23rd 2013. Data provided by NAV Portugal.

As can be seen, the majority of the flights that depart from LPPT outwards of the Lisbon TMA head North and East, towards waypoints IXIDA (41%), IBDIB (17%) and INBOM (14%). Flights that have as destination the Autonomous Regions of Madeira or the Azores turn West passing through BUSEN (7%), while flights towards southern areas fly through the remaining points, roughly uniformly distributed. Based on this data, the routes to be considered will follow these four waypoints, along with two extra ones - GANSU and GAIOS - for potential flights that would head South or Southeast.

Lisbon Humberto Delgado Airport's departures list on August 26th was sampled from ANA Aeroportos website for the low cost carriers Ryanair and EasyJet flight numbers [54]. Afterwards, data for these flights was collected through the use of the website Flight Radar 24 [55], which is a Swedish internet-based service that shows real-time aircraft flight information on a map, including its trajectory, the aircraft model, and also airspeed and altitude graphs (which can be relevant when trying to reproduce these flight paths) for those flights. A total of 21 flights from EasyJet and 19 from Ryanair were found, with different destinations and departure routes, which can be inferred by comparing each trajectory with the RNAV SID charts from NAV, in Appendix F.

An example of data for flight TP348 departing from LIS with destination to LGW (London - Gatwick) is shown in Appendix G, as obtained in FlightRadar24.

6.3.2 Schedules and Aircraft

For the purposes of calculating the cumulative noise metrics such as the Day-Evening-Night Level, L_{DEN} , it is essential to define, along with the flight path, the time of day at which each flight is occurring. Based on the same assumptions as before, schedules can be made based on statistical or historical data by looking up for information relative to the mentioned low-cost airlines during the period of one day.

For scheduling and route-choosing purposes, from all the collected data the only relevant ones are (1) the operating aircraft, which is actually defined by the airline in question - Ryanair operates with Boeing 737-8AS for all flights collected, whereas EasyJet typically operates with Airbus A320-214 and A319-111 aircraft [55] -, (2) the destination - which correlates to the route the aircraft will follow after taking off - and (3) the time of day at which the flight occurred. A graphical analysis for the flights collected is found in Figure 6-4 and Figure 6-5, which shows the distribution of SID routes and aircraft used for each flight; it's possible to see that the most frequent exit route is through IXIDA. The departure trajectories for all these flights can be seen in Appendix H.

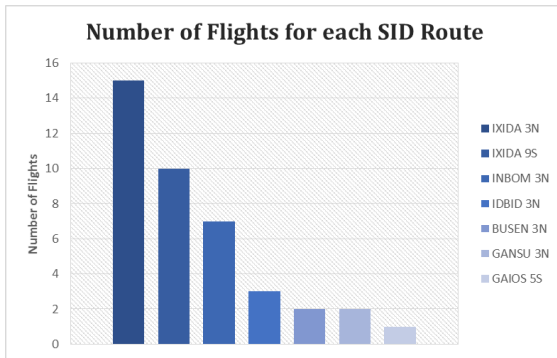


Figure 6-4 - Distribution of SID Routes for the flights.

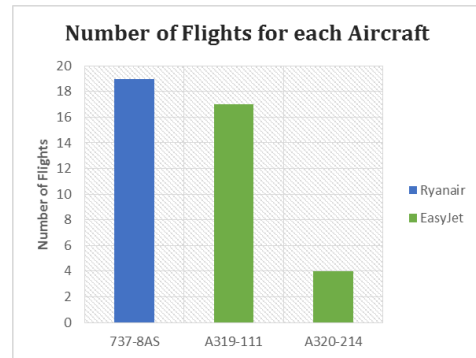


Figure 6-5 - Distribution of Aircraft.

The suffixes at each waypoint are to distinguish the different routes towards the same point. For example, IXIDA 3N is for an aircraft taking off from runway 3 or 35 to the North, while IXIDA 9S is a route towards the same point when the aircraft departs from runway 21. All of these routes, as mentioned, are found in Appendix F.

It's relevant to mention that these specific schedules are unlikely to correspond to the reality for LPMT since they're applied to Lisbon's main airport LPPT, which is in charge of several other flights from many more airlines. When this "Portela+1" project goes forward, a full rescheduling process will be made for both airports; this process involves technicalities that go beyond the scope of this dissertation. Thus, this is the schedule to be followed under the assumption that if it can be at work in the higher-traffic airport LPPT, then it can in LPMT too. Regardless, it can serve the purposes of this dissertation as a generic real schedule.

The information found in ANA's website, containing full flight schedules, destinations, and airlines for the previously mentioned flights can be found in Appendix I, and will be used as reference for L_{DEN} calculation purposes.

Furthermore, due to the fact that some of these aircraft models aren't found in the ANP database, the most similar aircraft available were chosen for modeling purposes; as such:

- Boeing 737-8AS is a Boeing 737-800 series aircraft, with AS being the designation that Boeing gave to aircraft of this series operated by Ryanair. The 737800 models are contained in the ANP database. [56]
- Airbus A320-214 is an Airbus A320-200 series aircraft; the two last digits (x14) of the series are engine variants, and the code A320-214 represents an A320-200 powered by CFM International (1) at 120.1kN (4). This aircraft is not available in the ANP database, and as such the A320-211 model will be used, which is also powered by CFM International, but at 111.2 kN. [57]
- Airbus A319-111 is an Airbus A319-100 series aircraft, powered by CFM International (1) at 97.9 kN (1). This aircraft is also not available in the ANP database, and thus the model A319-131 will be used, which is powered by International Aero Engines (3) also at 97.9 kN (1). [57]

6.4 Procedures

Taking into account all these considerations, it is finally possible to start defining detailed procedures and calculating realistic noise levels for the modeled flights, followed by the calculation of the awakenings parameter as a way to objectify the noise annoyance to the communities near an airport for each of those flights.

In an initial phase, only flights departing from LPMT's RWY01 will be modeled, by defining different routes heading towards the most common waypoints, which will be the ones seen in Figure 6-4, for the three aircraft referred. As such, for each of these points, a standard route will be made, by following the SIDs available for LPPT's Runways: for example for IXIDA 3N, the aircraft flies towards point PT412, from which there are three routes it can follow with one of them being IXIDA. For LPMT RWY01, a similar RNAV SID trajectory will be followed, going to PT412 initially and then turning towards IXIDA. This approach will be followed for the different routes as a standard one, serving as a template for comparison purposes for the subsequent paths modeled towards the same point; these subsequent paths will consist on the application of different Noise Abatement Procedures to that template. Profile-wise, standard departure profiles are detailed in the ANP database for each aircraft following the structure in Table 3-2, along with NADP-1 and NADP-2 profiles following the ICAO PANS-OPS guidance; the standard profile set of procedures has been modified to standardize power cutback to climb power at 1,000 ft AFE²⁰, and can be found in Appendix J for Airbus A320-211. [58] This way, the ground track in each of these trajectories will be designed independently of the profile, which makes the design process much simpler while leading to good results, product of the variety of combinations of ground track and profile noise abatement procedures that can be applied.

The process behind the design of procedures is based on the following organized steps:

1. Creating a standard trajectory that flies towards the first point in the LPPT SID, as described previously for IXIDA 3N, from which it then turns towards the desired point to which the SID refers to;
2. Profile-wise, each aircraft follows the standard profile procedure described in the ANP database for the aircraft in question. This is now referred to as *Path_{standard}* for aircraft 1.
3. Apply different ground track noise abatement procedures to *Path_{standard}*:
 - a. Turn restriction NAPs, which will be applied mostly to procedures where the aircraft, after taking off from RWY1, has to make a turn - e.g: GAIOS 3N or BUSEN 3N. In these procedures, the aircraft will turn sooner or later as represented in Figure 2-9;

²⁰ Above Field Elevation is the height referencing the highest point on the airfield.

- b. Multi-turn NAPs, applied to any route. In these procedures, the aircraft will follow different trajectories towards a converging point, as represented in Figure 2-10;
 - c. Fanning NAPs, although less important for two reasons: (1) one of the main purposes of the implementation of this concept is not only a fairer distribution of noise in a wider area but also an increase of the airport's capacity and runway throughput, which is not an issue in LPMT due to the lack of sequential departures; and (2), especially for departures from RWY1, the area right in front of the runway is a body of water - Rio Tejo - which is ideal for climbing as there is no community beneath the path, while turning both left or right will lead the aircraft into high population density areas.
4. For each set of procedures obtained in steps 1 to 3, different profile procedures will be applied, based on the ICAO-A and ICAO-B procedures described in the ANP database for the aircraft in use;
 5. Repeat steps 2-4 for other aircraft;
 6. The total awakenings parameter will be calculated for every single one of these combinations of flight paths;
 7. After comparing this parameter, the flight path with the lowest value for each SID route and aircraft will be selected as the optimal trajectory towards that point operated by that specific aircraft.
 8. The schedules presented will be thoroughly followed, creating a set of flights in the model that fly towards the optimal SID trajectories for each of the routes indicated in the schedule, and the cumulative noise metrics L_{DEN} and L_{DN} will be calculated.

It's important to mention that, as will be mentioned in the next chapter, some approximations were made for the ground track modeling during turns: these curves were approximated by straight paths of different lengths, rather than the recommended ones as represented in Figure 3-6.

Moreover, for these procedures to be valid for civil aircraft, area R26A Montijo, a restricted area aimed for Air Exercises by the military unit with limits between the Surface (SFC) and 2,000 ft AMSL according to the AIP effective 18 August 2016 published by NAV [47] (available in Appendix E), was disregarded as LPMT is contained in that area.

One last thing to notice is that this set of procedures designed ignore the interference between flights departing or approaching LPPT and those to LPMT. Portela+1 is an ambitious project that requires a great communication between the two airports and traffic controllers to minimize interference and increase efficiency. Further ATC simulation studies are required to assess traffic compatibility between these two airports.

7 Results and Discussion

7.1 Standard Noise Abatement Procedures

The approach to analyze departure procedures started by designing two sets of trajectories for each of the six different exit points. These sets correspond to Turn Restriction NAPs and Multi-Turn NAPs, with three to four different iterations of the NAP being modeled for each set of NAPs. Furthermore, from the six exit points, three head North while the remaining three head South. Profile-wise, each of these trajectories were modeled following an ICAO-A procedure and an ICAO-B procedures; due to the similarities between the ANP Default Procedure and the ICAO-B Procedure, the former was disregarded for this study. In summary, each trajectory is defined by and categorized into (1) Runway, (2) SID Termination Point, (3) NAP, (4) iterations of the NAP, and (5) profile procedure.

A total of 154 trajectories were initially modeled following this approach, and Figure 7-1 shows all of these projected over the map of Lisbon [Google Maps]. All paths were modeled for an Airbus A320-211.

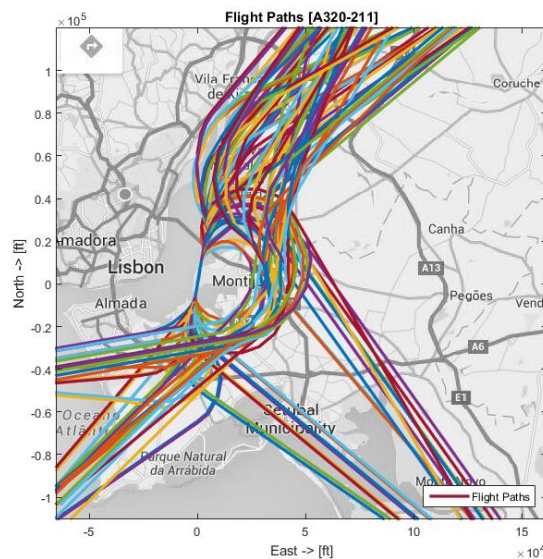


Figure 7-1 - Full set of modeled trajectories for Airbus A320-211.

All three routes towards North are initially close to each other, typically heading towards waypoint PT412 before diverging towards the respective exit route. Due to the fact that the shown map only focuses on the departure procedure *per se*, these routes are not as distinguishable between themselves as the ones heading towards South.

After designing the trajectory, the noise model allows the creation of a noise contour to assess the areas which are the most affected by the flight path being studied. Figure 7-2 shows the noise contour for the single event Sound Exposure Level metric and the respective flight path for an A320-211 aircraft heading towards BUSEN, after departing from RWY1 following an ICAO-A procedure. As this study is focused on the noise impact on nearby communities, it is important to analyze the noise

contours taking into account population information. As such, Figure 7-3 shows the same contour, projected over a grid map with the corresponding population densities, as obtained from the available GIS data. The population density grid map is found in Figure 6-1 with the respective units; as mentioned previously, darker areas correspond to higher densities.

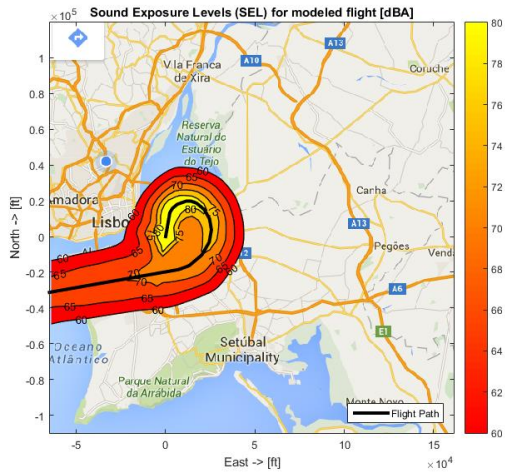


Figure 7-2 - SEL contour for departure procedure on Lisbon map.

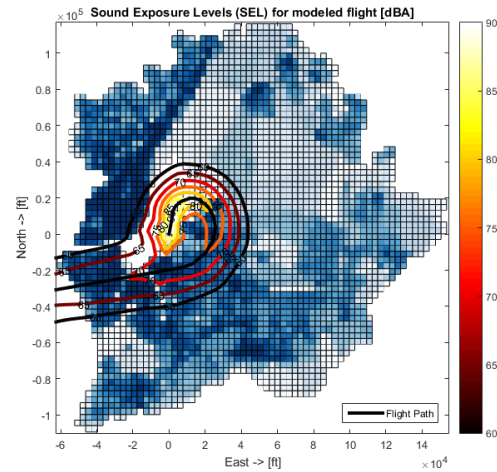


Figure 7-3 - SEL contour for departure procedure on Lisbon population density map.

In Figure 7-3, the modeled path initiates turn at 3,000 ft AMSL and crosses areas with high population densities, specifically after the initial turn when heading straight towards BUSEN. At this point, the aircraft is flying at around 8,000 ft AMSL with a True Airspeed of ~282 kt. Despite still climbing, the high population density area leads to a higher community annoyance, resulting in a total of 9061 Awakenings, i.e., number people awakened due to a single event flyover for this path.

For flights departing from RWY1, the initial area after taking off is not considered critical as the aircraft flies over a body of water - the Tejo River - and only then turns right; as such, it is deemed more important to follow a procedure focused on reducing noise in areas distant from the airport. Figure 7-4 plots the flight profile for both ICAO-A and ICAO-B procedures for this path.

It is important to mention that it is not possible to model ICAO-A and ICAO-B flight paths with the exact same ground track. This is due to two interrelated facts: (1) when an aircraft is turning, its climb rate is lower than it would be in a straight path (see evolution of climb angle γ with bank angle ϵ in Equation (3-19)); and (2) for a constant bank angle in a turn, the curve radius increases with airspeed (see Equation (3-4)). Since aircraft following ICAO-B procedures accelerate earlier in the procedure, the airspeed will be higher in the turn when compared to an equivalent turn made when following an ICAO-A procedure, and therefore the curve will be slightly wider, as shown in Figure 7-5. This ICAO-B procedure resulted in a total of 8038 Awakenings, a reduction of around 10% as compared to the former one. Nonetheless, this difference does not take into account only the profile procedure, but also ground track differences, providing better results both due to the fact that (1) the aircraft is flying at a higher altitude in critical areas and (2) the wider curve inadvertently moved the flight path away from areas with a higher population density.

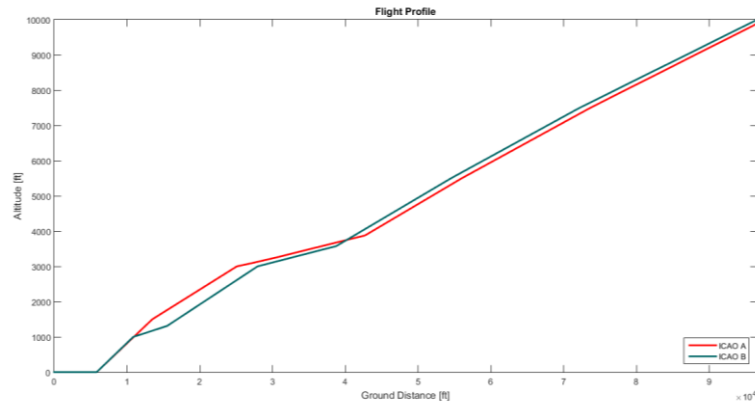


Figure 7-4 - Flight profiles for ICAO-A and ICAO-B procedures.

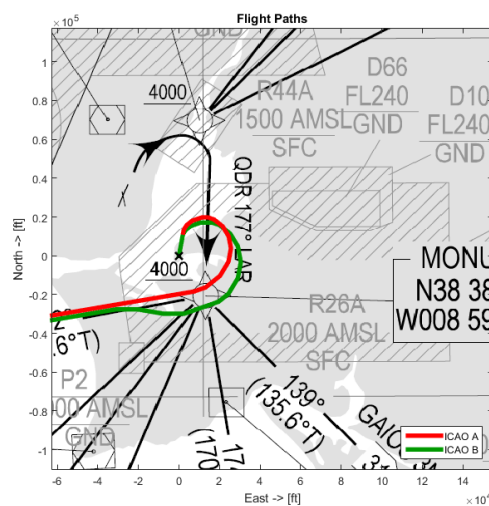


Figure 7-5 - Ground track for the modeled ICAO-A and ICAO-B departure procedures.

Despite not having been mentioned, all flights modeled comply with airspace rules, not overstepping danger and restricted areas' boundaries. Figure 7-5 shows the flight paths projected over RNAV SID for LPPT RWY 03/35, showing the path towards the SID termination point BUSEN and the restricted areas around Montijo. As previously noted, area R26A Montijo was disregarded for the purposes of these studies.

Following this approach for every SID termination point route, an algorithm was made to analyze all of the modeled trajectories towards each point and to select the one which provided the lowest value for the Awakenings parameter. Figure 7-6 and Figure 7-7 show the two sets of NAPs and the respective trajectories modeled for an A320-211 aircraft departing from RWY1 towards IXIDA. As before, the Awakenings parameter was calculated for each of these trajectories, with the obtained results shown in Figure 7-8. The first half shows the results for an ICAO-A procedure, while the second half corresponds to the equivalent ICAO-B procedures, as represented by the A and B labels in the horizontal axis.

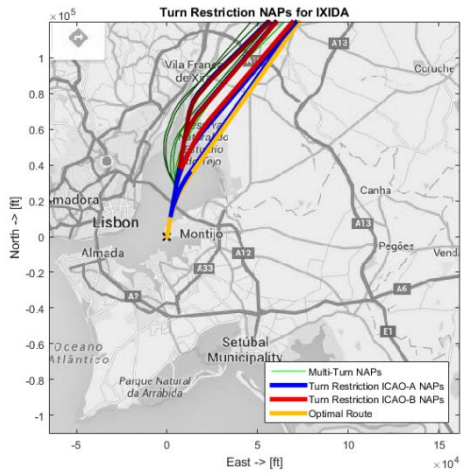


Figure 7-6 - Turn Restriction NAPs.

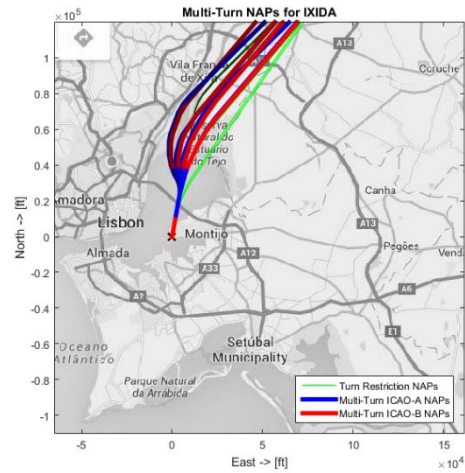


Figure 7-7 - Multi-Turn NAPs.

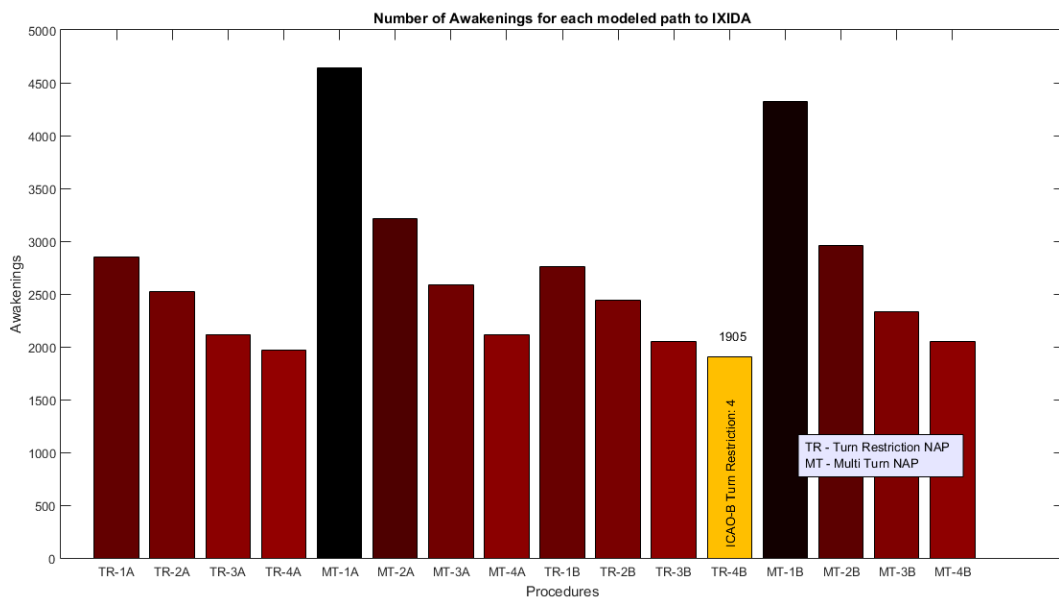


Figure 7-8 - Bar chart for the Awakenings parameter obtained for each trajectory modeled.

The optimal route was highlighted in yellow, corresponding to a flight that makes the turn as soon as possible, shortly after reaching an altitude of 1,000 ft and resulting in 1905 Awakenings. Conversely, the flight path named MT-1A which in Figure 7-7 corresponds to the leftmost path, results in 4643 Awakenings; flight TR-4B thus results in less than 50% of observed awakenings compared to flight MT-1A. This contrast is due to the fact that the latter flies closer to the Greater Lisbon area, which is characterized by its high population densities; the path TR-4B is optimal in terms of Awakenings as it turns away from this area, resulting in a lower community impact, as can be inferred from Figure 7-9.

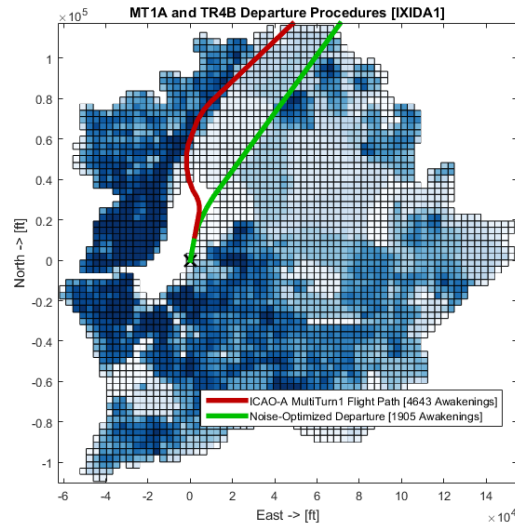


Figure 7-9 - Comparison between MT1A and TR4B departure procedures.

Extending this method to all of the termination points, the trajectories with optimal number of Awakenings for each route were selected, and are shown in Figure 7-10. Figure 7-11 shows a bar chart with the respective Awakenings parameter for each route; both runways are represented and are labeled by the corresponding number in the horizontal axis. In this chart, the first half of the results corresponds to the flights departing from RWY1, while the second one represents the flights departing from RWY19. A clear contrast can be seen between these two in terms of Awakenings; this is due to the facts that when departing from RWY1, (1) the aircraft climbs over a body of water, and (2) the areas specifically to the Northeast of the airport have low population densities. Conversely, when an aircraft departs from RWY19, it flies over areas with relatively high population densities, resulting in a higher Awakenings parameter.

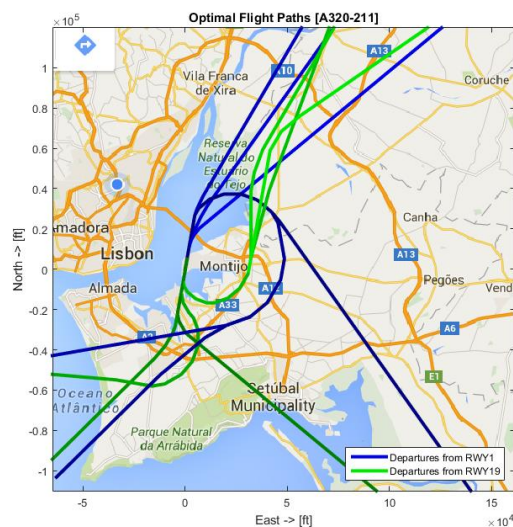


Figure 7-10 - Optimal Flight Paths with respect to the Awakenings parameter.

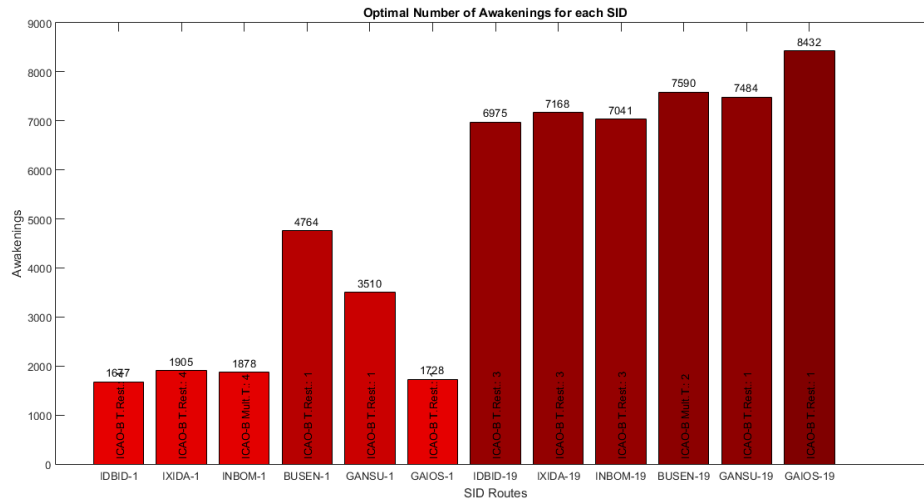


Figure 7-11 - Awakenings parameter for the optimal flight paths of each route.

7.2 Custom Procedures

As previously mentioned, in this initial stage the flight paths modeled followed Turn Restriction and Multi-Turn NAP iterations exclusively. However, it is possible to obtain flight paths further optimized in terms of noise annoyance by designing the trajectories based on population density information, rather than follow any of the previously mentioned NAPs specifically. These trajectories were modeled in this second phase, following ICAO-A and ICAO-B procedures.

Following the example from Figure 7-5 of a flight departing from RWY1 towards BUSEN, a new iteration of this route was made. An aircraft following this path initiates the turn at 1,500 ft AMSL and has a wider curve while climbing and heading towards BUSEN, which leads both to (1) a higher climb rate due to the lower bank angle during the turn and (2) a slight shift away from the high density area located at the northwest corner of the peninsula. The comparison between the two flights is shown in Figure 7-12 and Figure 7-13, plotted over a population density map and a SID chart respectively. As can be seen in Figure 7-13, it is not possible to have a wider turn as that would lead to flying over the restricted area D10 during the turn.

This new path leads to an improvement of around 30% in terms of Awakenings when compared to the one considered optimal when applying standard NAPs in the previous section, reducing the number of Awakenings from 4764 to 3273. Nevertheless, while the aim is to avoid every high population density area, in reality such paths may not be viable when taking into consideration other equally important parameters such as fuel consumption and gaseous emissions; thus, a balance has to be made between all these criteria. For this purpose, a new parameter was introduced aiming to roughly represent both fuel consumption and emissions. This parameter measures the displacement of the aircraft from the Start-of-Roll until the end of the departure procedure, which for this purpose is considered the point where the aircraft reaches an altitude of 20,000 ft. With this,

it is possible to check how far the aircraft has traveled along its route towards its destination and compare it between different procedures flying towards the same exit point. In this case, the optimal path towards BUSEN in terms of Awakenings takes slightly longer to reach its destination due to its wider turn in the initial climb. Hypothetically, if two aircraft departed at the same time following these two trajectories, the aircraft following the Noise-Optimized Custom path would end its procedure flying around 10,000 ft behind the one flying the Standard path. This means that it will have a slightly higher fuel consumption and particles emission to reach the same point.

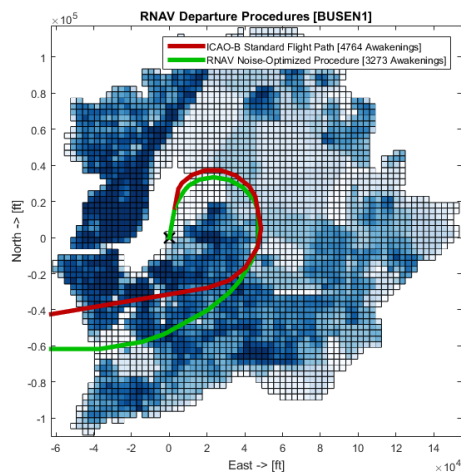


Figure 7-12 - Comparison between standard NAP and custom path to BUSEN.

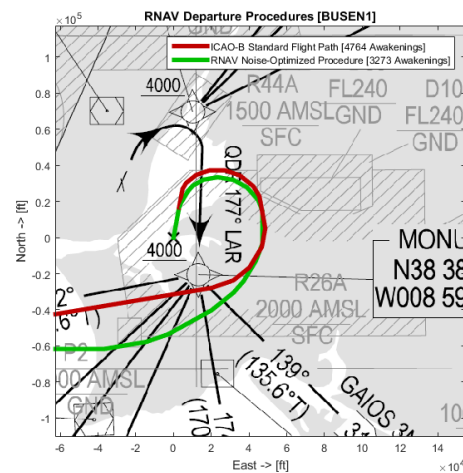


Figure 7-13 - Comparison between standard NAP and custom path to BUSEN.

While this difference may not be significant in terms of fuel consumption and emissions in this example, it can be more noteworthy when comparing two trajectories with more noticeable differences in ground track. For instance, for the same exit route, an even wider turn could be made, going around the danger area D10 and thus climbing over areas with lower population densities, as shown in Figure 7-14 and Figure 7-15. This path would lead to a further improvement of approximately 27% when compared to the optimal short turn trajectory, reducing the number of Awakenings from 3273 to 2387. Nonetheless, this improvement comes at the cost of a displacement difference of almost 200,000 ft in ground distance traveled as shown in Figure 7-16; i.e., an aircraft following this procedure would end up approximately 200,000 ft (60 km) behind an aircraft following the previously mentioned procedure, which would lead to a much more significant impact in terms of fuel consumption and emissions.

A small Awakenings error should be taken into account due to the GIS data boundaries: as can be seen in Figure 7-14, part of the flight trajectory – and thus noise contour – goes outside the population densities information, not being taken into account as a consequence. These areas observe a Sound Exposure Level of around 60–65 dBA, and thus, according to Equation (4-3), the population percentage affected in each cell of the grid is around 0.50%. Assuming that approximately 400 cells are outside the boundaries, with an average population density of 25 individuals/cell, then an error of roughly 50 individuals is associated with the obtained value.

of 20° is used between 1,000 ft and 3,000 ft for a smooth transition. These recommendations for noise study, also suggested by NAV Portugal, go according to ICAO's Doc.8168. [59]

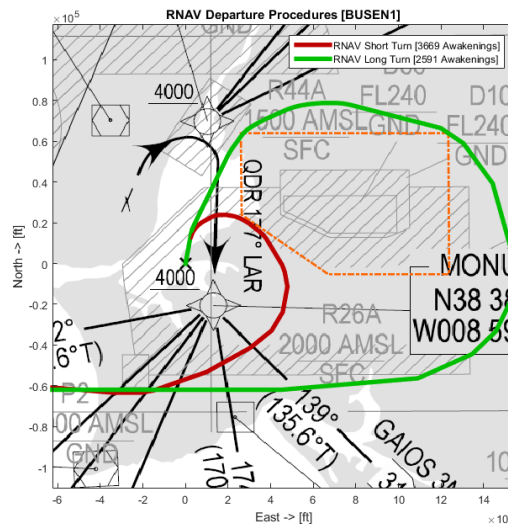


Figure 7-17 - Comparison between new short and long turn flight paths, with a safety margin for area D10.

Similarly, the long turn provides with a lower Awakenings parameter, with a 30% reduction from 3669 for the short turn, to 2591 for the longer one, coming at the cost of a higher fuel consumption and emissions due to the longer path to the exit route. As before, a small error is associated to these values due to the GIS information boundaries.

7.3 Cumulative Noise Metric L_{DEN}

Finally, for the calculation of the Day-Evening-Night Level, the schedule mentioned in the previous chapter was taken into account to define the time-of-day dependent weighting factor g_i , for the calculation of L_{DEN} as according to Equation (3-33). The optimal paths obtained for each route were used, as according to the historical data obtained for August 26th, shown in Appendix I.

Furthermore, since it is a parameter that takes into account all flights that occur in a 24-hour period, the flights approaching the aerodrome should be taken into account as well. For this purpose, two different simple RNAV standard arrival procedures were designed, one for each runway. Both are assumed to depart from airports in Europe, and as such come from East, as seen in Figure 7-17 and Figure 7-18. Details about the aircraft's flight such as its altitude, airspeed and power parameter were interpolated based on an example given in Doc.29 for a Boeing 737300, while its ground track was modeled using the departures segmentation model developed; the bank angle during turns was also calculated according to the segmentation model, with its values being the symmetric of those obtained, since the aircraft in the model is flying in the opposite direction to the one desired.

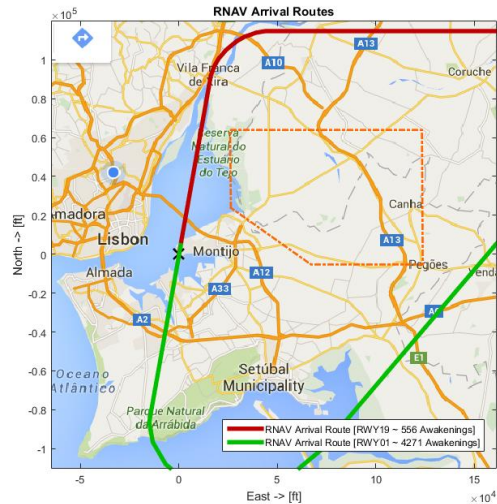


Figure 7-18 - Standard arrival trajectories modeled.

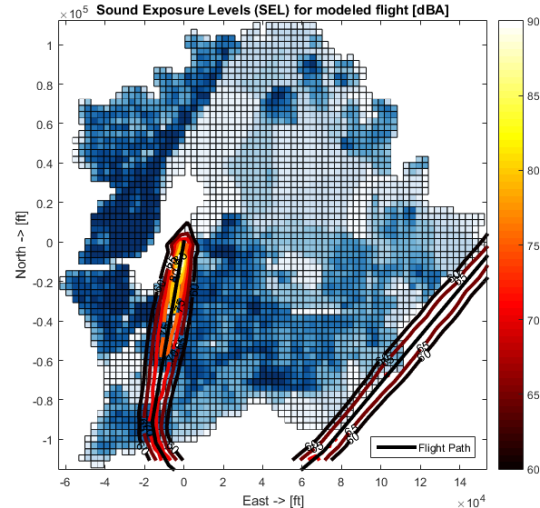


Figure 7-19 - RWY1 arrival route - GIS map.

These arrival routes start with a descent procedure from 6,000 ft to 3,000 ft with a descent angle of 3° , whilst maintaining 250 kt CAS. This step is followed by a deceleration at constant altitude to 148.6 kt CAS over a distance of 25,000 ft, and a descent at 3° at an altitude of 2,500 ft. The aircraft decelerates to 139 kt while descending, until finally reaching the touchdown roll point, where it sets its thrust at 60% maximum for 3,000 ft, after which the procedure ends.

A big contrast in terms of community annoyance can be seen between the arrival route for RWY01 and the one for RWY19. Since the route towards RWY19 is made by flying over a body of water, the population affected by aircraft noise for this path is very low, resulting in a total of 556 Awakenings. Conversely, when approaching RWY01, the aircraft flies over several areas with a relatively high population density, reason why the resulting parameter is much higher (4271 Awakenings).

Figure 7-20 shows the noise contour for the Day-Evening-Night Level based on the schedule for August 26th for EasyJet and Ryanair airlines for the departure procedures. The SID termination points selected based on FlightRadar data as mentioned in the previous chapter and, for each of these routes, the optimal flight path using NAPs was chosen. Furthermore, a total of 40 arrival procedures were assumed. 30 of them were assumed to be flying during day-time, 7 during the evening, and the remaining 3 during night-time; moreover, 30 made their approach operation towards RWY01 according to the green path shown in Figure 7-18, while the remaining 10 landed in RWY19; a higher number of flights was modeled towards RWY01 since the common wind conditions benefit this runway, for the aircraft to travel with a headwind. As can be seen in the figure, areas with an L_{DEN} higher than 65 dBA are either located in the aerodrome or in the Tejo River, which leads to no issues in regards to community annoyance. Nonetheless, there is a small region south of Montijo where the noise levels are higher than 55 dBA, which despite not being ideal, is inevitable due to its proximity to the aerodrome.

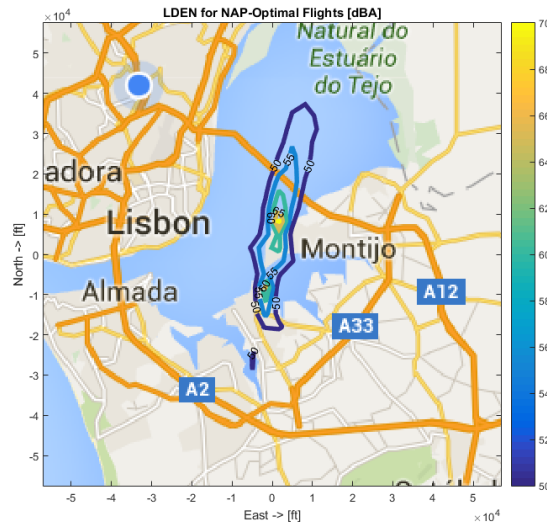


Figure 7-20 - L_{DEN} in area of interest based on the standard schedule found in Appendix I.

7.4 Additional Considerations

It's important to mention that the Awakenings parameter is no more than a concept. It is based on empirical data from studied done by FICAN as a way to quantify a subjective parameter; as such, it does not mean that N individuals will actually wake up from sleep, especially when taking into account that most flights are not made during the night-time period. Nonetheless, this concept allows making an efficient study for relative community annoyance.

As mentioned, it's important to notice that, realistically speaking, keeping in mind aspects such as fuel consumption and gaseous emissions is essential for designing new procedures; these aspects can be correlated to the total distance traveled s . Therefore, it is possible that the route with the best results for the awakenings parameter comes at the cost of consuming a higher amount of fuel, which may not be viable in reality. It is, thus, important to make a balance between all these parameters.

In reality, according to the Advanced Emissions Method III (AEMIII) [60], a method developed by EUROCONTROL to calculate aircraft emissions, the total amount of species emitted is given by:

$$Total\ Emissions = N \times \sum_i EI_i \times W_{f_i} \times t_i \times 10^{-3}, \quad (7-1)$$

Where:

N is the number of engines;

t is time of the flight segment;

EI corresponds to the Emission Indices as obtained from ICAO's Emissions Databank [61], corrected after different criteria such as the Mach number and atmospheric conditions;

W_f is the aircraft fuel flow in the corresponding flight segment.

Furthermore, ICAO categorized the different phases of a flight according to the aircraft thrust setting, as defined in Table 7-1. Since the departure phase corresponds to the operating modes where the power setting is the highest, these phases will affect greatly the aircraft's fuel consumption and, thus, the particles it emits to the air.

Table 7-1 - Thrust setting for each phase of the flight. [60]

Operating Mode	Throttle Setting (% of max thrust)
Take-off	100%
Climb-out	85%
Approach	30%
Taxi/Ground Idle	7%

This method goes beyond the scope of this dissertation and was not thoroughly explored, but it is essential for the design of trajectories as it complements the noise study.

The accuracy of the results obtained in the developed noise model is dependent on the grid spacing and consequently the number of cells used for the fictional observers' grid. Naturally, a higher number of cells implies exponentially higher computation times, which is an inconvenience, considering the fact that the model is used "iteratively" by making small changes in trajectories and profiles and analyzing the effects of changes as a dose-response relationship.

Due to the high complexity resultant from the high number of parameters that can be changed in each operation in a single procedure to obtain different results – such as the power and flaps settings, the climb and accelerated climb parameters (rate of climb, and end altitude for climb or end airspeed for accelerated climb), and the exact ground track trajectories –, the implementation of a direct optimization algorithm was disregarded for this dissertation. The method followed was instead based on the implementation of the most common Noise Abatement Procedures - described in Subchapter 2.6.2 - and the use of the recommended profile procedures available in the ANP database for each aircraft.

The ground tracks turns were modelled in a slightly different way than the one suggested in Doc.29 and described in Chapter 3. Instead of a steady curve being divided into structured, uniformly distributed line segments, it is similarly approximated by straight lines, but with varying lengths instead. This approximation was made due to difficulties found during the development of the flight path segmentation section of the model, while attempting to link the profile with the ground track (which would be independently segmented in accordance to Figure 3-6). These difficulties arose from the fact that the procedural step number within the procedure could change - more than once - in the middle of a curve, which would come with different flight parameters such as the rate of climb in the middle of the curve. This was a programming issue to which an exact solution was not found and would lead to significant position (and consequently noise levels) errors if not fixed. It was bypassed by dividing the turns into segments with changes of heading of $\Delta\xi = 5^\circ, 10^\circ$ or 20° , as selected by the user, with a corresponding aircraft bank angle of $\varepsilon = 5^\circ, 15^\circ$, or 25° respectively (nonetheless, in the last set of flights modeled mentioned in Chapter 7.2, the bank angle during turns was only influenced by the altitude, being equal to $15^\circ, 20^\circ$ or 25° as previously stated). The length of each segment depends on the length of a real equivalent arc - which follows Equation (7-2) -, considered the minimum length allowed to model a physically possible turn.

$$arc = R \times \Delta\xi_{radians} \quad (7-2)$$

Where the radius R follows Equation (3-4) solved in order to R .

This is essentially the method recommended by Doc.29, but with a different segmentation process, easier to control with procedural step changes rather than uniformly distributed straight lines independently of the step.

The Awakenings error associated with the GIS information boundaries comes from an assumption following patterns in the GIS map, shown in Figure 6-1. Since each cell has an area of 1 km^2 , the limits of the available data go from ~ 0 individuals/ km^2 at the southeastern corner, to ~ 50 individuals/ km^2 at the northeastern corner. As such, an average of 25 individuals/ km^2 was considered as the upper bound for the population density in each cell for determining the Awakenings uncertainty.

Lastly, the standard arrivals procedures were modelled in a simple way solely for the purposes of L_{DEN} calculation. The aircraft used was a Boeing 737300 rather than any of the three aircraft mentioned in the previous chapter. Furthermore, missed approaches and holding procedures – where the aircraft awaits for instructions from the ATC – were not taken into account.

8 Conclusions and Further Research

There are many aspects to study alongside with noise abatement, in a collective project which involves the cooperation of specialists in different subjects to obtain balanced results. It's impossible to focus exclusively on noise, or any other parameter for that matter, to create realistically viable procedures, because low noise impact on communities can come at the cost of a high fuel consumption and emissions indices of Greenhouse Gases, which is unreasonable both economically and environmentally.

Including the impact of emissions and fuel consumption is a first step to complement this dissertation's topic, through the implementation of, for instance, the Advanced Emission Model III (AME III) which, similarly to the mentioned ANP databases and NPD tables for noise calculation, is based on ICAO's Engine Exhaust Emission Databank which consists in a database for aircraft and engines containing fuel burn rates and emission indices provided by external sources, which can be used and corrected to calculate accurate values for engine emissions for any given flight. [62]

Scheduling optimization can also have a big impact on reducing cumulative noise levels such as the day-night level. Due to the many considerations that have to be taken into account to create a realistic schedule, a simple one based on statistical data for LPPT was used instead, solely for purposes of L_{DEN} calculation.

Runway throughput and airport capacity modeling can also be implemented to complete the developed model to take into account yet another aspect that has to be studied throughout the development of any airport project, and the Portela+1 is no exception. Nevertheless, due to the fact that the number of movements will typically not surpass a maximum of 12 movements per hour, which is the limit for LPMT [5], this parameter is not essential or detrimental for its success.

Implementing the impact of air humidity, and realistic temperatures and wind speeds will also lead to more accurate results, closer to real values. This can be achieved through the use of information from METARs, which are standard formats for reporting weather information; these reports are mainly used by pilots and flight planners, and are continuously made and updated by the airport or meteorological station in periods of 30 minutes to an hour, containing a detailed description of the weather as observed.

Similarly, taking into account the topography of the area of interest can make the model much more accurate. Unfortunately, the altitude data obtained from the Digital Elevation Model over Europe (EU-DEM) from the European Environment Agency [63] to be integrated in the GIS map through QGIS proved to be inaccessible, with the altitudes being displayed as "Not a Number". As such, such information was disregarded, with the area of interest being considered plain and with a constant altitude of 0 ft instead. Nonetheless, at the area of interest the altitude is actually approximately plain and 0 ft, with some slight variations specifically at the southern area of the peninsula, where it goes up to ~1640 ft (Serra da Arrábida), and at a small region of Greater Lisbon area where it can go up to ~750 ft (Serra de Monsanto).

Moreover, this dissertation does not include approach procedures as they involve different technicalities. Implementing these procedures into the model is naturally important to assess the noise impact near an airport and to include in the cumulative noise calculations, and is equally a first step to further develop this model.

The awakenings parameters is an attempt to objectify a community impact, which is subjective and typically unquantifiable, through statistical data. Many characteristics are standardized for the areas in which the studies were made on, and can differ in different ones. For instance, the sound absorption coefficient of the different materials of which a typical house consists of in Portugal might differ from the ones from which the data was taken from. Furthermore, it assumes that the noise levels affect young people in similar ways that it affects elderly people, while in reality older people are less sensitive to higher frequency sounds and higher sound levels as their ears lose sensitivity throughout the years. This can be taken into account by further exploring the GIS capabilities, as it contains both information about the buildings construction and the population age distribution, just like it contains the information used in this dissertation about population density. At the same time, it's possible to calculate sound levels for different frequencies for any given segment in a flight path. Sound propagation through air suffers from attenuation in levels due to the atmosphere, and different frequencies of sound can have different attenuation rates. These attenuation rates can also be found in the ANP database, usually given in dB/100m, and can further correct the values of the noise metrics calculated to become more precise, while also allowing the implementation of a awakenings parameter that takes into account the age of the individuals, as it influences the frequency sensibility.

Similarly, the room for adapting this awakenings parameter or include new parameters, is quite vast. As such, in a next stage for this project, it's even possible to take into account other subjects unrelated to aviation noise, such as the real estate. An interesting concept to implement could be the avoidance of flying over richer areas or areas where house prices is higher, prioritizing procedures over other regions. Or, following the inverse logic, lowering house prices in areas where noise levels are typically higher while increasing them in areas where it's negligible.

Despite the fact that all these procedures are following RNAV standards with proper equipment, an aircraft following one of these procedures can actually be slightly displaced from the designed procedure's ground track. These differences are typically negligible for an RNAV procedure, but can be taken into account through ground track dispersion methods, which are based on past experience from the study airport, generally via an analysis of radar data samples. [12] This is done by creating subtracks with progressively increasing lateral deviations from the main track towards both sides, and associating a percentage of movements in each subtrack based on the radar data samples analysis; naturally, the center/main track has the highest percentage distribution, while farther subtracks have progressively lower percentage distributions.

The real noise levels data available for model validation purposes, provided by TAP Portugal for 6 different flights, was obtained by noise monitoring stations in only 3 specific locations. As such,

while it can give a reasonable indication of the error associated with the noise calculation portion of the model, all these locations are relatively close to one another, and thus the results obtained *might* have a low error at those locations but higher errors at different ones. A higher number of results, as measured by noise monitoring stations in more diversified locations would allow a more significant and efficient model validation process, and would allow for further experimental adjustments to the model to obtain more accurate noise levels results in the subsequent flight paths designed.

It's important to mention that assumptions such as only Ryanair and EasyJet airlines will be expected to transfer to LPMT, despite being fair assumptions for the purposes of this dissertation, may not correspond to reality. There are more, less known, airlines that are expected to be transferred to this aerodrome, providing one daily flight to a single destination - such as Everjets, a Portuguese airline based at Funchal that operates flights in and out of Madeira to the mainland Portugal, or Iberia, a Spanish airline based in Madrid, providing flights to its main bases of Madrid-Barajas Airport and Barcelona El Prat Airport. Conversely, it's possible that broader airlines such as EasyJet refuse to transfer its flights currently going to LPPT to LPMT, due to the distance from Montijo to Lisbon's main area - also known as "Grande Lisboa" - which might have a negative impact on the number of customers, who will require transportation to Greater Lisbon.

Taking into account the interference between flights departing and approaching LPPT will have a huge impact in any procedure for either aerodrome; as well as aircraft approaching LPMT itself. A re-structuration of the airspace in Lisbon's TMA will be made (or rather is currently in progress) taking into account factors such as this one, and danger/restricted areas, and a new study can be made by reiterating the process of designing flight paths in this dissertation, but with the new updated rules and charts. Furthermore, excellent cooperation between NAV Portugal and Portuguese Air Force is essential for the success of this project.

Finally, it's important to mention that most information regarding the Portela+1 project is confidential. Even during the valuable meetings with Airspace Planners and Environmental Specialists from NAV Portugal and ANA, accurate information regarding the current project was not shared, which is why many assumptions had to be made for this dissertation based on current public information, which might be outdated considering the re-structuration of the airspace currently in progress.

References

- [1] Airport Cooperative Research Program, "ACRP Report 86 - Environmental Optimization of Aircraft Departures," Transportation Research Board of the National Academies, Washington,DC, 2013.
- [2] Aviation Environment Federation, "First EU-wide report on aviation's environmental impacts shows growing challenges," 3 February 2016. [Online]. Available: <http://www.aef.org.uk/2016/02/03/first-eu-wide-report-on-aviations-environmental-impacts-shows-growing-challenges/>. [Accessed 12 August 2016].
- [3] European Environment Agency (EEA); European Aviation Safety Agency (EASA); EUROCONTROL, "European Aviation Environmental Report 2016," EEA, 2016.
- [4] Expresso, "Expresso | Aeroporto do Montijo à vista," 6 January 2016. [Online]. Available: <http://expresso.sapo.pt/economia/2016-01-06-Aeroporto-do-Montijo-a-vista>. [Accessed 20 March 2016].
- [5] Lieutenant-Colonel C.Fernandes, Interviewee, *Private Communication*. [Interview]. 4 April 2016.
- [6] American National Standard / Acoustical Society of America, "Acoustic Terminology," in *ANSI/ASA S1.1-2013*, ANSI/ASA, 2013.
- [7] ANA Aeroportos de Portugal, "Plano de Acções de Gestão e Redução de Ruído para o Aeroporto de Lisboa - Resumo Não-Técnico," ANA, Lisbon, 2014.
- [8] J. R. Franks and M. K. M. C. J. Stephenson, *Preventing Occupational Hearing Loss - A Practical Guide*, National Institute for Occupational Safety and Health, 1996.
- [9] EUROCONTROL, "Environmental issues for aviation | Eurocontrol," EUROCONTROL, 2016. [Online]. Available: <http://www.eurocontrol.int/articles/environmental-issues-aviation>. [Accessed 20 4 2016].
- [10] World Health Organization, "Night Noise Guidelines for Europe," WHO, 2009.
- [11] Cross Spectrum, "Frequency weighting equations," 6 September 2004. [Online]. Available: <http://www.cross-spectrum.com/audio/weighting.html>. [Accessed 22 July 2016].
- [12] European Civil Aviation Conference, "Report on Standard Method of Computing Noise Contours around Civil Airports," in *ECAC.CEAC Doc.29*, (3rd Edition). ECAC, 2005.
- [13] A. A. Trani and J. Roa, "Airport Planning and Design: Aircraft and Airport Noise," Virginia Tech - Air Transportation Systems Laboratory, 2012.
- [14] L. H. C. H. P. Nicolopoulou-Stamati, *Environmental Health Impacts of Transport and Mobility*, Springer, 2005.
- [15] International Civil Aviation Organization, "Environmental Protection - Aircraft Noise," in *Annex 16 - Vol.I*, ICAO, 2005.
- [16] K. Dueker and D. Kjerne, *Multipurpose cadastre: Terms and definitions*, Falls Church, VA: Technical Papers, 1989.
- [17] EUROCONTROL, "ANP - Eurocontrol Experimental Centre," EUROCONTROL, 26 January 2009. [Online]. Available: <https://www.aircraftnoisemodel.org>. [Accessed 8 August 2016].
- [18] Eurocontrol, "Conventional Nav aids | Eurocontrol," Eurocontrol, [Online]. Available: <http://www.eurocontrol.int/articles/conventional-navaids>. [Accessed 26 April 2016].

- [19] Flight Gear, "Radio Beacons - Flight Gear," [Online]. Available: http://wiki.flightgear.org/Radio_beacons. [Accessed 4 August 2016].
- [20] D. Nakamura and W. Royce, "Operational Benefits of Performance-Based Navigation," Boeing, 2008.
- [21] D. J. Clausing, *The Aviator's Guide to Navigation* (4th ed.), New York: McGraw-Hill, 2006.
- [22] J. N. T. e. a. Clarke, "Continuous Descent Approach: Design and Flight Test for Louisville International Airport," *Journal of Aircraft*, vol. 41, no. No.5, 2004.
- [23] M. Van Boven, "Development of Noise Abatement Approach Procedures," in *10th AIAA/CEAS Aeroacoustics Conference*, Manchester, UK, 2004.
- [24] S. Hartjes and H. G. Visser, "Optimization of RNAV Noise and Emission Abatement Departure Procedures," 9th AIAA Aviation Technology, Integration, and Operations Conference, South California, 2009.
- [25] International Civil Aviation Organization, "Aircraft Operations," in *Doc.8168*, ICAO, 2013.
- [26] Kathryn, "Kathryn's Report," [Online]. Available: http://www.kathrynsreport.com/2015_06_25_archive.html. [Accessed August 2016].
- [27] Federal Aviation Administration, Advisory Circular - Noise Abatement Procedures, U.S: FAA, 1993.
- [28] International Civil Aviation Organization, "Flight Procedures, Vol.1," in *Doc.8168*, (5th Edition). ICAO, 2006.
- [29] European Commission, "Welcome to the SESAR project," [Online]. Available: <http://ec.europa.eu/transport/modes/air/sesar/>. [Accessed August 2016].
- [30] P. H. Appel, "Impacts of the LightSquared Network on Federal Science Activities," in *Committee on Science, Space, and Technology*, 2011.
- [31] USA Today, *Phoenix sues FAA over Flight Path changes*, Arizona: USA Today, 2015.
- [32] CBS News, *FAA new ATC system causing major noise pollution*, CBS News, 2015.
- [33] ECAC-CEAC, "About ECAC - ecac-ceac.org," ECAC, [Online]. Available: <https://www.ecac-ceac.org/>. [Accessed August 2016].
- [34] Digital Imaging and Remote Sensing Image Generation (DISRIG), "Coordinate Systems," 10 April 2016. [Online]. Available: <http://www.dirsig.org/docs/new/coordinates.html>. [Accessed 8 August 2016].
- [35] International Organization for Standardization, *Standard Atmosphere - ISO 2533:1975*, ISO, 1975.
- [36] International Civil Aviation Organization, "Noise Abatement Procedures, Vol.1 Part V.," in *Doc.8168 "PANS-OPS"*, ICAO, 2004.
- [37] Instituto Nacional de Estatística, "CENSOS," Statistics Portugal, 2011. [Online]. Available: <http://mapas.ine.pt/download/index2011.phtml>. [Accessed 11 April 2016].
- [38] Instituto Nacional de Estatística, "Nomenclatura das Unidades Territoriais para fins Estatísticos," INE, 2002.
- [39] Federal Interagency Committee on Aviation Noise, "Effects of Aviation Noise on Awakenings from Sleep," FICAN, 1997.
- [40] N. P. Miller, "How Many People Could be Awakened by a Full Night of Aircraft (or other) Noise Events?," Harris Miller Miller & Hanson Inc., 2009.

- [41] E. Plate, "Aerodynamic Characteristics of Atmospheric Boundary Layers, AEC Critical Reviews Series," U.S. Department of Energy, 1971.
- [42] International Civil Aviation Organization, "Air Traffic Services," in *Annex 11 to the Convention on International Civil Aviation*, (13th Edition). ICAO, 2001.
- [43] SKYbrary, "Classification of Airspace," 24 January 2014. [Online]. Available: http://www.skybrary.aero/index.php/Classification_of_Airspace. [Accessed 9 September 2016].
- [44] Federal Aviation Administration - Safety, "Airspace Made Easy," 6 June 2012. [Online]. Available: https://www.faa.gov/files/events/ea/ea03/2012/ea0345029/airspace_made_easy.pdf. [Accessed 22 August 2016].
- [45] SKYbrary, "Separation Standards - SKYbrary Aviation Safety," 8 December 2015. [Online]. Available: http://www.skybrary.aero/index.php/Separation_Standards. [Accessed 22 August 2016].
- [46] International Civil Aviation Organization, "Air Traffic Management," in *Doc.4444 - Procedures for Air Navigation Services*, (15th Edition). ICAO, 2007.
- [47] NAV Portugal, E.P.E., "eAIS Package for PORTUGAL," 18 August 2016. [Online]. Available: <https://www.nav.pt>. [Accessed 20 August 2016].
- [48] Força Aérea Portuguesa, "Base Aérea Nº 6 | Força Aérea Portuguesa," 2016. [Online]. Available: <http://www.emfa.pt/www/unidade-19-base-aerea-n-6>. [Accessed 22 August 2016].
- [49] World Aero Data, "World Aero Data: MONTIJO -- LPMT," 2016. [Online]. Available: <http://worldaerodata.com/wad.cgi?id=PO88904&sch=LPMT>. [Accessed 22 August 2016].
- [50] International Civil Aviation Organization, "Rules of the Air," in *Annex 2 to the Convention on International Civil Aviation*, (10th Edition). ICAO, 2005.
- [51] SKYbrary, "Danger Area - SKYbrary Aviation Safety," 8 October 2014. [Online]. Available: http://www.skybrary.aero/index.php/Danger_Area. [Accessed 8 August 2016].
- [52] EUROCONTROL, "Flexible Use of Airspace | Eurocontrol," [Online]. Available: <http://www.eurocontrol.int/articles/flexible-use-airspace>. [Accessed 24 August 2016].
- [53] US Airforce, "Chapter 9: IFR Departure Procedures," in *US Airforce Manual 11-217V1*, US Airforce, 2005.
- [54] ANA Aeroportos de Portugal; VINCI Airports, "ANA Aeroportos de Portugal," [Online]. Available: <http://www.ana.pt/en-US/Pages/Homepage.aspx>. [Accessed 25 August 2016].
- [55] Flightradar24 AB, "Flightradar24.com - Live flight tracker!," Launched in 2006. [Online]. Available: <https://www.flightradar24.com/>. [Accessed 23 June 2016].
- [56] T. Pither, *The Boeing 707, 720 and C-135*, England: Air-Britain (Historians) Ltd, 1998.
- [57] PLANE-SPOTTER.com, "Deciphering the AIRBUS Codes," 2006.
- [58] Aircraft Noise and Performance (ANP), "ANP Database Version 2.0," EUROCONTROL, 28 December 2012.
- [59] International Civil Aviation Organization, "Aircraft Operations, Vol.II.," in *Doc.8168 - Procedures for Air Navigation Services*, (1st Edition). ICAO, 2006.
- [60] F. Jelinek and S. C. a. J. Smith, "EEC Report EEC/SEE/2004/004: Advanced Emission Model, Validation Report," EUROCONTROL Experimental Centre, 2003.

- [61] International Civil Aviation Organization, "ICAO Engine Exhaust Emissions Databank," in *Doc.9646-AN/943*, ICAO, 1995.
- [62] EUROCONTROL Experimental Centre, "Advanced Emission Model (AEM3) v1.5: Validation Report," EUROCONTROL, 2004.
- [63] European Environment Agency, "Digital Elevation Model over Europe (EU-DEM) - European Environment Agency," 09 October 2013. [Online]. Available: <http://www.eea.europa.eu/data-and-maps/data/eu-dem#tab-european-data>. [Accessed 11 April 2016].
- [64] Community Research and Development Information Service (CORDIS), "European Commission: CORDIS: Projects & Results Services: Airline Trials of Environmental Green flight maNagement functions," 12 May 2014. [Online]. Available: http://cordis.europa.eu/project/rcn/191513_en.html. [Accessed 20 August 2016].
- [65] National Geodetic Survey, "ARP Computation," [Online]. Available: <http://www.ngs.noaa.gov/AERO/arpcomp/arpframe.html>. [Accessed 22 August 2016].
- [66] Committee on Aviation Environment Protection, "The seventh meeting of the Committee on Aviation Environment Protection (CAEP/7)," 2007.
- [67] Haris Miller Miller & Hanson Inc., "Basic Aircraft Noise Terminology," March 28 2012. [Online]. Available: https://www.lawa.org/uploadedFiles/lax/noise/presentation/noiseRT_090311_Noise%20101%20Presentation.pdf. [Accessed 22 July 2016].
- [68] W. P. Vermeer, H. Vos, J. Steenbekkers, F. v. d. P. (. & Associ e) and K. Groothuis-Oudshoorn, "Sleep Disturbance and Aircraft Noise Exposure: Exposure-dose relationships," Division Public Health, Leiden, Netherlands, 30 June 2002.
- [69] Federal Aviation Administration, "Civil Utilization of Area Navigation (RNAV) Departure Procedures," FAA, 2007.
- [70] International Civil Aviation Organization, "Aeronautical Information Services," in *Annex 15 to the Convention on International Civil Aviation*, (13th Edition). ICAO, 2010.
- [71] International Civil Aviation Organization, "Balanced Approach to Aircraft Noise Management," ICAO, 2014. [Online]. Available: <http://www.icao.int/environmental-protection/pages/noise.aspx>. [Accessed 10 July 2016].
- [72] International Civil Aviation Organization, "Assembly Resolutions in Force. Doc 9790," ICAO, 2011.
- [73] International Civil Aviation Organization | Destination Green, "ICAO Noise Standards by Neil Dickson, Environment Branch," ICAO Symposium on Aviation and Climate Change, 2013.
- [74] Federal Aviation Administration, "Next Generation Air Transportation System," FAA, [Online]. Available: <https://www.faa.gov/nextgen/>. [Accessed August 2016].
- [75] National Geographic, "National Geographic - Encyclopedia," National Geographic, [Online]. Available: <http://nationalgeographic.org/encyclopedia/geographic-information-system-gis/>. [Accessed August 2016].

Appendix

A. Performance calculation parameters

Table A-1- Performance parameters intrinsic to the aircraft.

Aircraft	Weight	Engine	Engine Location	Engine Coefficients	Flap Coefficients
737800, A320-211, A319-131, ...	(Weight)	CFM563, CFM656, V2522A, ...	Wing-mounted	E, F, Ga, Gb, H	B, C, D, R
			Tail-mounted	K1, K2, K3, K4 (for General Thrust Rating)	

Each aircraft is associated with its own engine and engine location, weight, and wing-related and flap-related coefficients, all of which heavily influence its performance and are inherent to the aircraft. For example, by operating with an A320-211, all the coefficients for performance calculations are automatically defined by the database. Nonetheless, the performance is also influenced by the procedure being followed, which in turn is not definite and can virtually be consisted of any procedural steps desired. Any combination of the following parameters is possible.

Table A-2 - Procedural steps combination matrix.

Procedure	Step Type	Thrust Rating	Flap ID	End Point Altitude [ft]	Rate of Climb [ft/min]	End Point CAS [kt]
Default	Takeoff	(General)	1, 5, 15, ZERO (or equivalent)	Height (for Climb only)	ROC (for Accelerate only)	CAS (for Takeoff and Accelerate)
ICAO-A	Climb	MaxTakeoff				
ICAO-B	Accelerate	MaxClimb				

It's possible to create any procedure based on combinations of these parameters that comprise the procedural steps. Similarly, each of these is associated with the performance coefficients mentioned above, but they depend on the procedural step. For example, the MaxTakeoff and MaxClimb Thrust Ratings for any given engine have defined coefficients, but are different between themselves. Note that the General Thrust Rating is only usable when the engine's rotational speed data is available, as is the case during the validation based on real data.

Table A-3 - Excerpt of Jet Engine Coefficients Table for A320-211, as obtained from the ANP database [58].

Aircraft ID	Thrust Rating	E (lb)	F (lb/kt)	Ga (lb/ft)	Gb (lb/ft²)	H (lb/°C)
A320-211	MaxClimb	16859.1	-4.38	0.183576	2,99E-06	0
A320-211	MaxTakeoff	23652.9	-22.93	0.295879	5,46E-06	0

Table A-4 - Excerpt of Aerodynamic Coefficients table for A320-211, as obtained from the ANP database [58].

Aircraft ID	Flap ID	B (ft/lb)	C/D (kt/√lb)	R
A320-211	1			0.066827
A320-211	1+F	0.007701	0.394884	0.071403
A320-211	ZERO			0.056281

B. Noise as measured from Noise Monitoring Stations

B1

Table B-1 - Set 1 Noise

Date Time	Start Date Time	Max Date Time	Operation Number	Location	Airport Desk	Runway	Flight Number	Tail Number	Airline	Aircraft Type	Max Lev	Leq	SEL	EPNL	Duration
15-01-2016 07:37	15-01-2016 07:38	15-01-2016 07:38	290853800	7	Aeroporto	3	TAP616	CSTNP	TAP	A320	82,80	77,40	91,10	90,30	23
15-01-2016 07:37	15-01-2016 07:38	15-01-2016 07:38	290853800	3	Camarate	3	TAP616	CSTNP	TAP	A320	75,70	71,10	87	86	39
15-01-2016 07:37	15-01-2016 07:39	15-01-2016 07:39	290853800	1	Pirescove	3	TAP616	CSTNP	TAP	A320	71,60	67,70	80,70	79,30	20
03-02-2016 08:06	03-02-2016 08:06	03-02-2016 08:07	290863986	7	Aeroporto	3	TAP544	CSTNS	TAP	A320	83,80	78,90	91,90	91,70	20
03-02-2016 08:06	03-02-2016 08:07	03-02-2016 08:07	290863986	3	Camarate	3	TAP544	CSTNS	TAP	A320	77,10	71,60	87,60	88	39
03-02-2016 08:06	03-02-2016 08:08	03-02-2016 08:08	290863986	1	Pirescove	3	TAP544	CSTNS	TAP	A320	69,60	67,30	79,70	78,20	17
01-03-2016 07:14	01-03-2016 07:15	01-03-2016 07:15	290878251	7	Aeroporto	3	TAP434	CSTNT	TAP	A320	83,70	79,80	91,50	91,40	15
01-03-2016 07:14	01-03-2016 07:15	01-03-2016 07:16	290878251	3	Camarate	3	TAP434	CSTNT	TAP	A320	79,40	73	88,80	88	38
01-03-2016 07:14	01-03-2016 07:16	01-03-2016 07:16	290878251	1	Pirescove	3	TAP434	CSTNT	TAP	A320	74,80	69,80	84	82,70	26

B2

Table B-2 - Set 2 Noise

Date Time	Start Date Time	Max Date Time	Operation Number	Location	Airport Desk	Runway	Flight Number	Tail Number	Airline	Aircraft Type	Max Lev	Leq	SEL	EPNL	Duration
26-01-2016 07:37	26-01-2016 07:38	26-01-2016 07:38	2,91E+08	7	Aeroporto	3	TAP348	CSTNT	TAP	A320	84,90	80,50	92,50	92,80	16
26-01-2016 07:37	26-01-2016 07:39	26-01-2016 07:39	2,91E+08	3	Camarate	3	TAP348	CSTNT	TAP	A320	80,30	74,30	89,80	90,30	36
26-01-2016 07:37	26-01-2016 07:40	26-01-2016 07:40	2,91E+08	1	Pirescove	3	TAP348	CSTNT	TAP	A320	68	66,80	79,10	78,30	18
05-02-2016 07:09	05-02-2016 07:10	05-02-2016 07:10	2,91E+08	7	Aeroporto	3	TAP1024	CSTNV	TAP	A320	82,80	77,50	90,70	90,10	21
05-02-2016 07:09	05-02-2016 07:10	05-02-2016 07:11	2,91E+08	3	Camarate	3	TAP1024	CSTNV	TAP	A320	78,40	72,30	87,90	86,90	36
05-02-2016 07:09	05-02-2016 07:11	05-02-2016 07:12	2,91E+08	1	Pirescove	3	TAP1024	CSTNV	TAP	A320	67,40	65,60	77,10	76	14
25-02-2016 09:29	25-02-2016 09:30	25-02-2016 09:30	2,91E+08	7	Aeroporto	3	TAP784	CSTNS	TAP	A320	83,90	80,30	92,90	93,20	18
25-02-2016 09:29	25-02-2016 09:30	25-02-2016 09:30	2,91E+08	3	Camarate	3	TAP784	CSTNS	TAP	A320	78,90	73,10	88,80	88,70	37
25-02-2016 09:29	25-02-2016 09:31	25-02-2016 09:31	2,91E+08	1	Pirescove	3	TAP784	CSTNS	TAP	A320	74	70,90	83,70	82,50	19

C. Modeled Flight Paths for Validation - TP348

In the following graphs, the crosses in the map represent the noise measuring stations, while the vertical dashed lines represent the ground distance at which they are located.

Table C-1 - Procedural Steps to simulate flight TP348.

ACFT_ID	Step Number	Step Type	Thrust Rating	Flap_ID	End Point Altitude (ft)	Rate Of Climb (ft/min)	End Point CAS (kt)
A320-211	1	Takeoff	MaxTakeoff	1+F			170
A320-211	2	Climb	MaxTakeoff	1+F	1600		
A320-211	3	Accelerate	MaxTakeoff	1+F		1200	197
A320-211	4	Climb	MaxTakeoff	1+F	2200		
A320-211	5	Accelerate	MaxTakeoff	1		1000	250
A320-211	6	Climb	MaxClimb	ZERO	5000		
A320-211	7	Climb	MaxClimb	ZERO	8000		
A320-211	8	Accelerate	MaxClimb	ZERO		1230,7	280
A320-211	9	Climb	MaxClimb	ZERO	11000		

Figure C-1 - Modeled and Real Flight Paths for TP348.

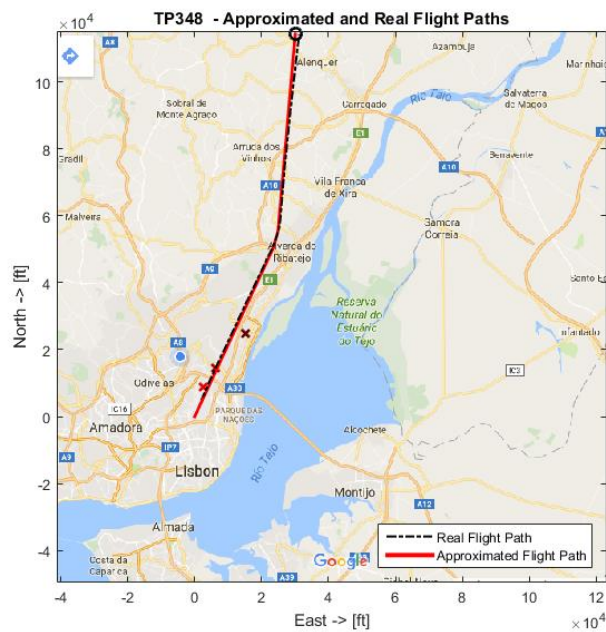


Figure C-2 - Position Error in function of the ground distance traveled.

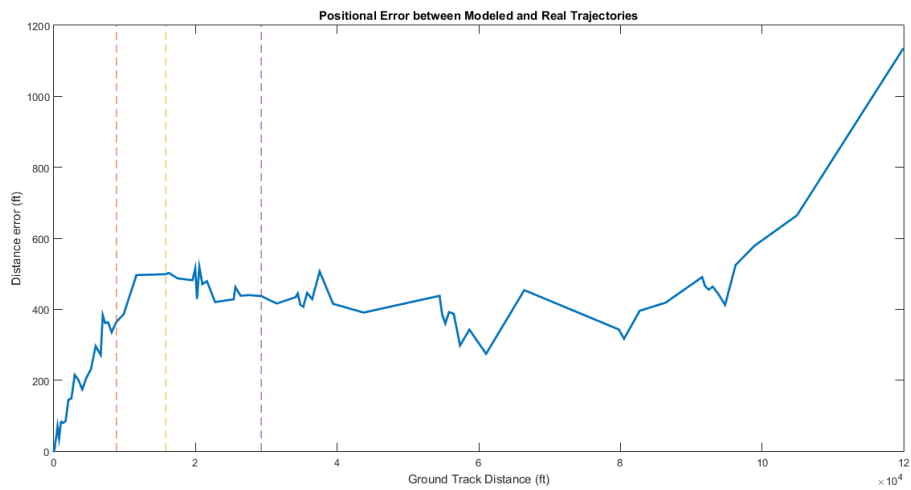


Figure C-3 - True Airspeed error in function of the ground distance traveled.

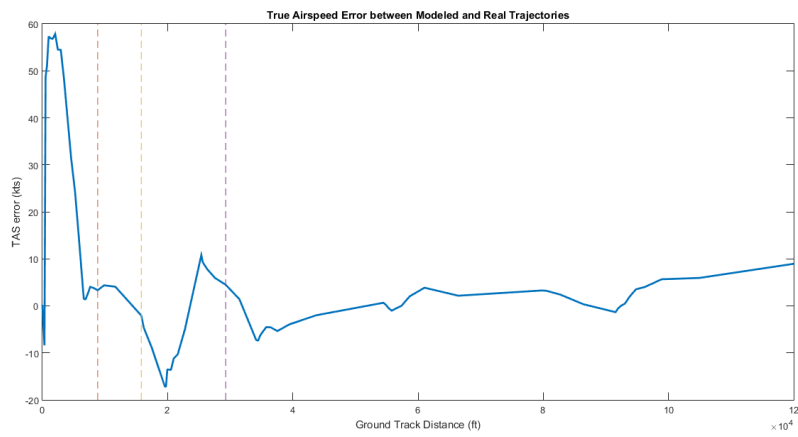
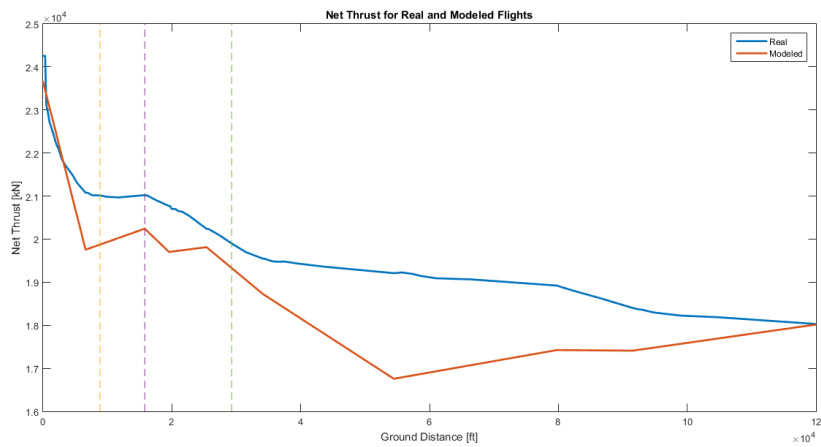


Figure C-4 - Noise-related Power parameter (Net Thrust) for Real and Modeled paths in function of ground distance.

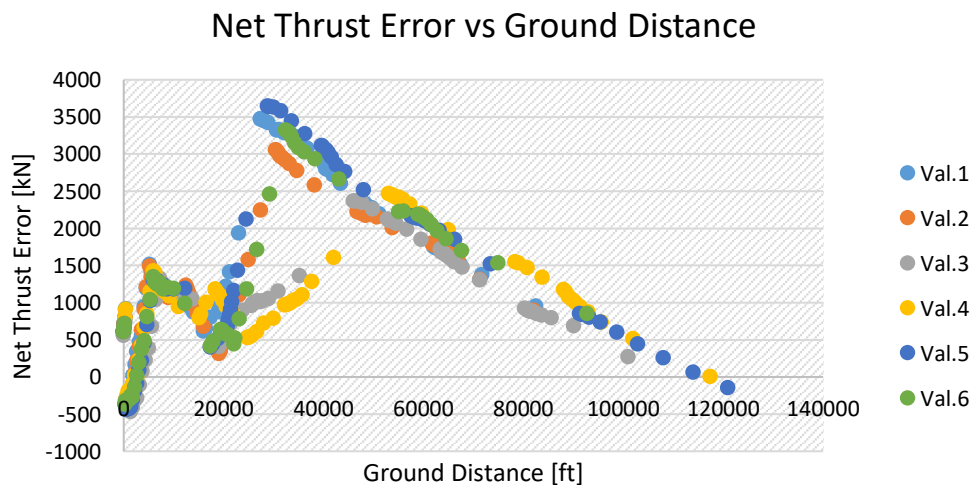


D. Validation Results

Table D-1 - Results obtained for the procedures defined in the model for segmentation and noise validation.

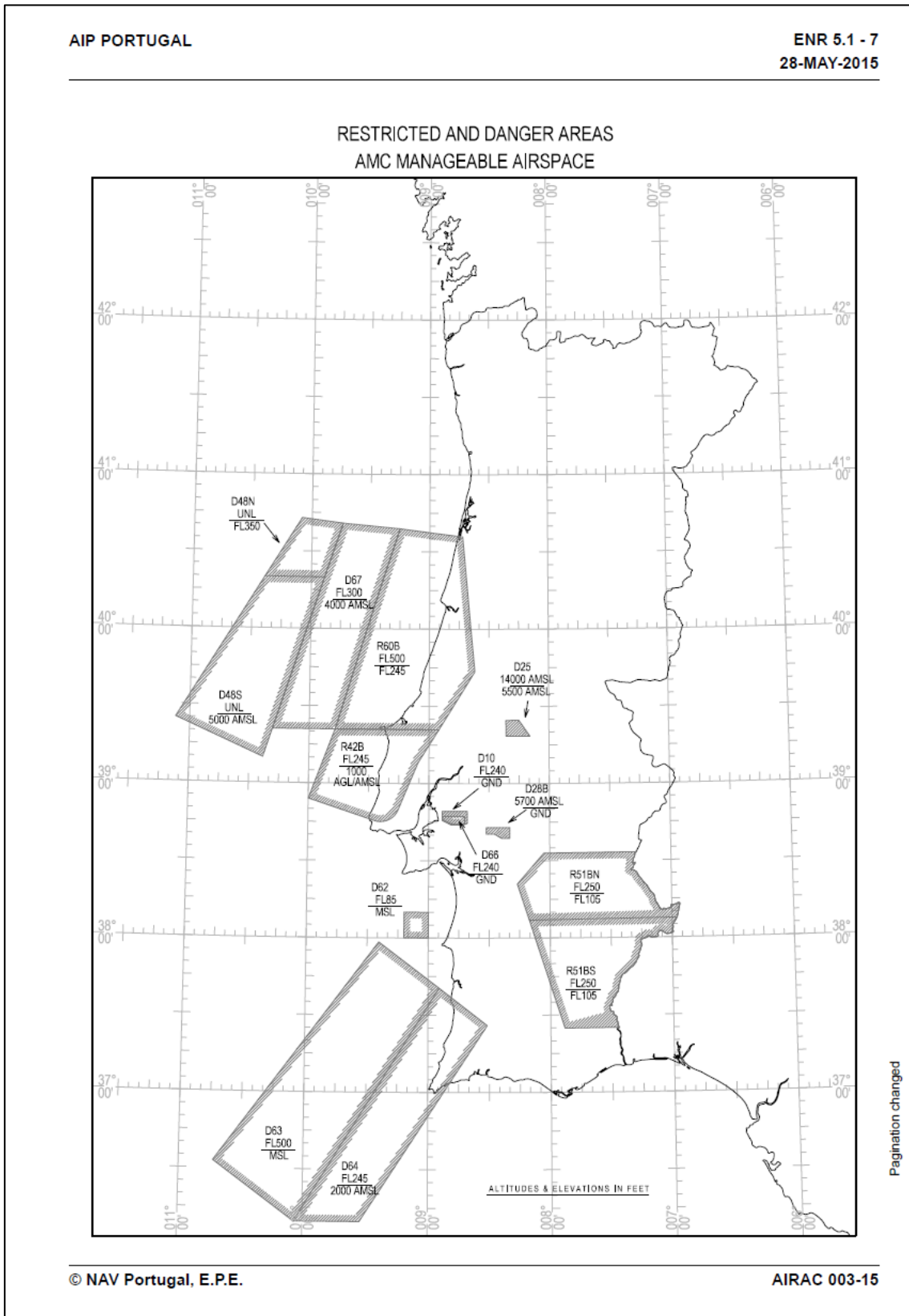
Flight	St.	Errors			Real (dBA)	Uncorr. (dBA)	Uncorr. Error (dBA)	Corrected (dBA)	Corr. Error (dBA)
		X (ft)	S (kt)	P (kN)					
TP616	7	164.36	-0.67	1153,14	82.8	81,39	1,41	80,99	1,81
	3	372.49	-2.39	672,39	75.7	78,71	-3,01	76,29	-0,59
	1	405.9	3.66	3438,02	71.6	63,56	8,04	63,56	8,04
TP544	7	332.69	1.64	1124	83.8	80,8	3	80,38	3,42
	3	384.42	-0.71	718,62	77.1	79,23	-2,13	76,8	0,3
	1	146.34	-8.09	3146,52	69.6	69,84	-0,24	69,84	-0,24
TP434	7	143.96	1.41	1180,21	83.7	79,51	4,19	79,57	4,13
	3	142.98	-0.41	906,45	79.4	82,12	-2,72	80,23	-0,83
	1	484.29	-0.84	1048,81	74.8	72,15	2,65	72,15	2,65
TP348	7	407.8	2.87	1090,48	84.9	80,73	4,17	80,47	4,43
	3	487.99	-4.89	836,4	80.3	80,51	-0,21	78,32	1,98
	1	476.57	0.59	650,24	68	67,8	0,2	67,8	0,2
TP784	7	335.97	-0.23	1193,68	83.9	80,79	2,01	80,26	2,54
	3	409.55	0.21	558,92	78.9	80,22	-1,82	78,33	0,07
	1	193.54	-2.68	3644,6	74	63,77	3,63	63,77	3,63
TP1024	7	397.24	-1.93	1170,17	82.8	80,7	3,2	80,38	3,52
	3	257.9	1.71	591,18	78.4	80,36	-1,46	78,47	0,43
	1	397.61	0.72	2423,35	67.4	72,91	1,09	72,91	1,09

Figure D-1 - Noise related power parameter (net thrust) error in function of ground distance traveled.



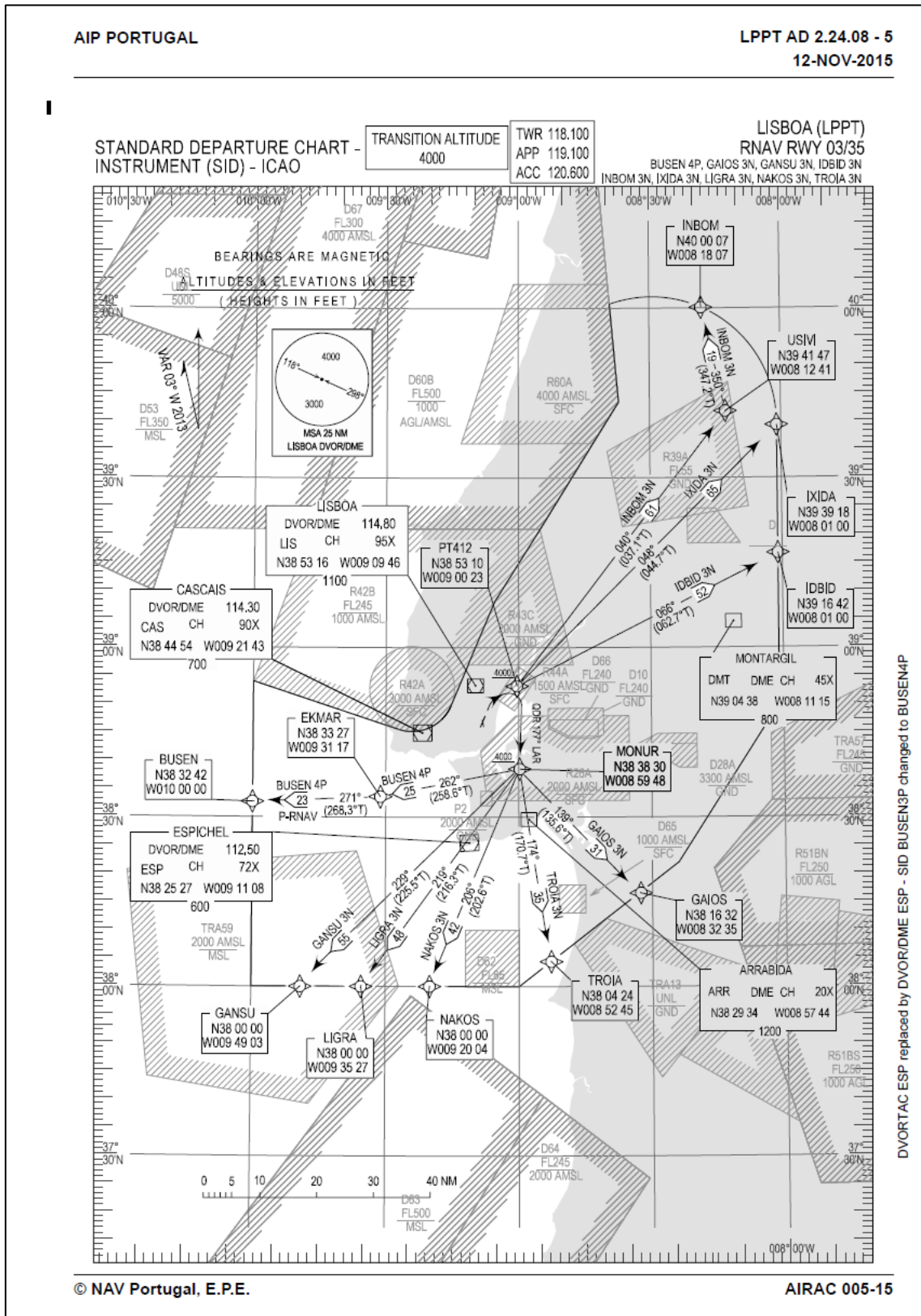
E. Lisbon Restricted and Danger Areas

Figure E-1 - Restricted and Danger Areas in Lisbon TMA



F. RNAV SIDs for Lisbon (LPPT) RWY 03/35

Figure F-1 - RNAV SID for LPPT RWY 03/35



G. FlightRadar24 data - TP348

Figure G-1 - Trajectory for flight TP348, as obtained from Flightradar24.com.

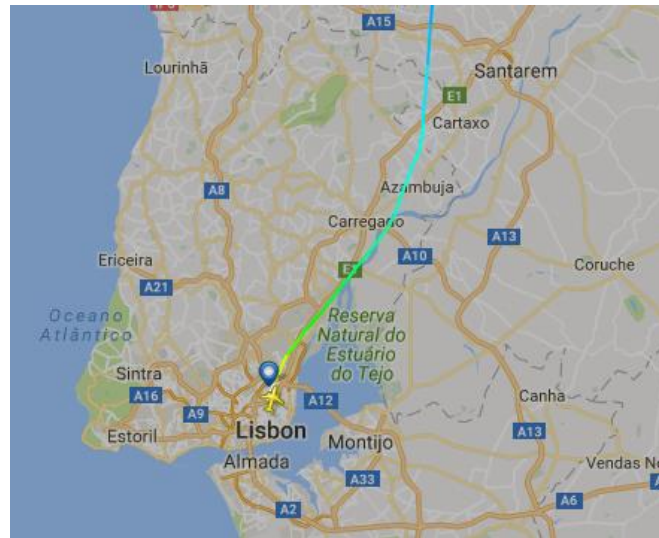
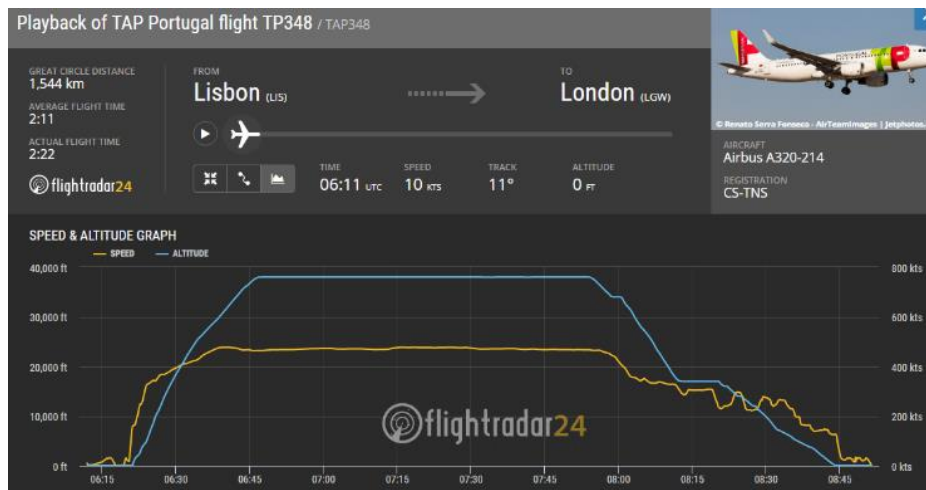


Figure G-2 - Speed and Altitude over duration of flight graphs for flight TP348, as obtained from Flightradar24.com.



H. Departure trajectories - FlightRadar24 data

Figure H-1 - All departing flights from Ryanair.

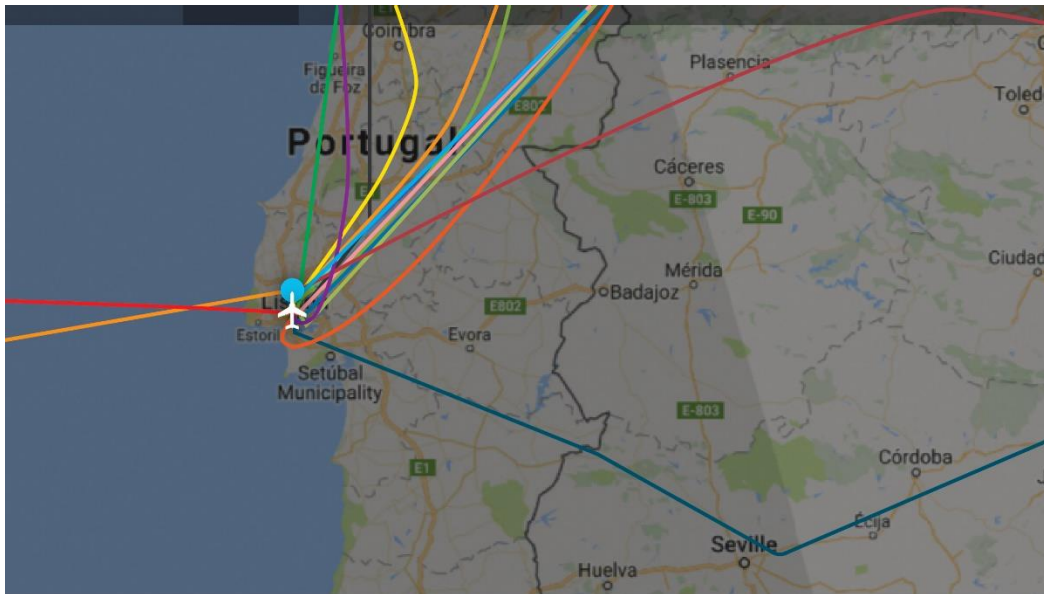
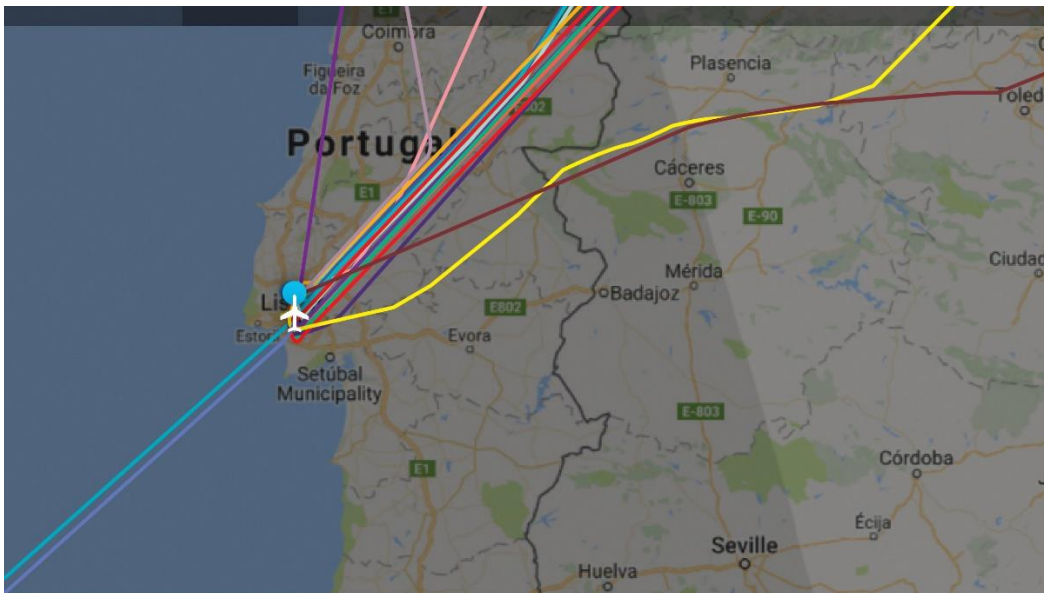


Figure H-2 - All departing flights from EasyJet.



I. Flight Schedules

Table I-1 - Schedule as obtained from ANA for Ryanair and EasyJet.

Hour	Destination	ICAO	Airline	Flight No.	Aircraft	SID Route
615	Berlin, Schoenefeld	SFX	EasyJet	EZY7651	A319-111	IXIDA 3N
630	London, Stansted	STN	Ryanair	FR 1885	737-8AS	IXIDA 3N
640	London, Gatwick	GTW	EasyJet	EZY8716	A320-214	INBOM 3N
640	Paris, Beauvais	BVA	Ryanair	FR 1083	737-8AS	IXIDA 3N
700	Madrid	MAD	EasyJet	EZY7611	A319-111	IDBID 3N
710	Madeira	FNC	EasyJet	EZY7603	A319-111	GANSU 3N
745	Hamburg	HAM	Ryanair	FR 2941	737-8AS	IXIDA 3N
755	Porto	OPO	Ryanair	FR 2094	737-8AS	INBOM 3N
840	Parris, Ch. De Gaulle	CDG	EasyJet	EZY3760	A319-111	IXIDA 3N
1000	Bristol	BRS	EasyJet	EZY6254	A320-214	IXIDA 3N
1000	Frankfurt, Hahn	HHN	Ryanair	FR 1787	737-8AS	IXIDA 3N
1000	Dublin	DUB	Ryanair	FR 7329	737-8AS	INBOM 3N
1040	Milan/Bergamo	BGY	Ryanair	FR 2086	737-8AS	IXIDA 3N
1045	Nantes	NTE	EasyJet	EZY7641	A319-111	INBOM 3N
1100	London, Luton	LTN	EasyJet	EZY2366	A319-111	IXIDA 3N
1100	Rome, Ciampino	CIA	Ryanair	FR 2097	737-8AS	IDBID 3N
1100	Ponta Delgada	PDL	Ryanair	FR 2623	737-8AS	BUSEN 3N
1100	Brussels	BRU	Ryanair	FR 2926	737-8AS	IXIDA 3N
1140	Bordeaux	BOD	EasyJet	EZY7637	A319-111	IXIDA 3N
1235	Porto	OPO	Ryanair	FR 1671	737-8AS	INBOM 3N
1330	Geneva	GVA	EasyJet	EZY1448	A320-214	IXIDA 3N
1340	Milan, Malpensa	MLX	EasyJet	EZY2716	A319-111	IXIDA 3N
1435	Marseille	MRS	Ryanair	FR 2077	737-8AS	IXIDA 9S
1505	Madrid	MAD	EasyJet	EZY7615	A319-111	IDBID 3N
1550	London, Luton	LTN	EasyJet	EZY2368	A319-111	IXIDA 9S
1550	Liverpool	LPL	EasyJet	EZY7084	A319-111	IXIDA 9S
1640	Luxembourg	LUX	EasyJet	EZY7655	A319-111	IXIDA 9S
1640	Basel	BSL	EasyJet	EZY7687	A319-111	IXIDA 9S
1730	Brussels	BRU	Ryanair	FR 2932	737-8AS	IXIDA 9S
1740	Manchester	MAN	Ryanair	FR 2253	737-8AS	IXIDA 9S
1805	Rome, Ciampino	CIA	Ryanair	FR 2693	737-8AS	GAIOS 5S
1820	Amsterdam	AMS	EasyJet	EZY7663	A319-111	IXIDA 9S
1825	Eindhoven	EIN	Ryanair	FR 3092	737-8AS	IXIDA 9S
1850	Madeira	FNC	EasyJet	EZY7607	A319-111	GANSU 3N
1855	Lyon, St. Exupery	LYS	EasyJet	EZY4434	A319-111	IXIDA 3N
1925	Paris, Ch. De Gaulle	CDG	EasyJet	EZY3764	A319-111	IXIDA 9S
2020	Porto	OPO	Ryanair	FR 2096	737-8AS	INBOM 3N
2030	London, Gatwick	GTW	EasyJet	EZY8720	A320-214	INBOM 3N
2055	London, Stansted	STN	Ryanair	FR 1883	737-8AS	IXIDA 3N
2220	Ponta Delgada	PDL	Ryanair	FR 2625	737-8AS	BUSEN 3N

J. Standard ANP Departure Procedures

Standard procedures ANP: Default, ICAO-A and ICAO-B for A320-211

Table J-1 - ANP standard procedure (Default) for Airbus A320-211.

ACFT_ID	Profile_ID	Stage Length	Step Number	Step Type	Thrust Rating	Flap_ID	End Point Altitude (ft)	ROC (ft/min)	End Point CAS (kt)
A320-211	DEFAULT	1	1	Takeoff	MaxTakeoff	1+F			
A320-211	DEFAULT	1	2	Climb	MaxTakeoff	1+F	1000		
A320-211	DEFAULT	1	3	Accelerate	MaxTakeoff	1+F		1150,5	186,2
A320-211	DEFAULT	1	4	Accelerate	MaxTakeoff	1		1300,7	208,1
A320-211	DEFAULT	1	5	Climb	MaxClimb	ZERO	3000		
A320-211	DEFAULT	1	6	Accelerate	MaxClimb	ZERO		1230,7	250
A320-211	DEFAULT	1	7	Climb	MaxClimb	ZERO	5500		
A320-211	DEFAULT	1	8	Climb	MaxClimb	ZERO	7500		
A320-211	DEFAULT	1	9	Climb	MaxClimb	ZERO	10000		

Table J-2 - ANP standard ICAO-A procedure for Airbus A320-211.

ACFT_ID	Profile_ID	Stage Length	Step Number	Step Type	Thrust Rating	Flap_ID	End Point Altitude (ft)	ROC (ft/min)	End Point CAS (kt)
A320-211	ICAO_A	1	1	Takeoff	MaxTakeoff	1+F			
A320-211	ICAO_A	1	2	Climb	MaxTakeoff	1+F	1500		
A320-211	ICAO_A	1	3	Climb	MaxClimb	1+F	3000		
A320-211	ICAO_A	1	4	Accelerate	MaxClimb	1+F		812,1	186,1
A320-211	ICAO_A	1	5	Accelerate	MaxClimb	1		933,5	201,2
A320-211	ICAO_A	1	6	Accelerate	MaxClimb	ZERO		1119,7	228,2
A320-211	ICAO_A	1	7	Accelerate	MaxClimb	ZERO		1240,5	250
A320-211	ICAO_A	1	8	Climb	MaxClimb	ZERO	5500		
A320-211	ICAO_A	1	9	Climb	MaxClimb	ZERO	7500		
A320-211	ICAO_A	1	10	Climb	MaxClimb	ZERO	10000		

Table J-3 - ANP standard ICAO-B procedure for Airbus A320-211.

ACFT_ID	Profile_ID	Stage Length	Step Number	Step Type	Thrust Rating	Flap_ID	End Point Altitude (ft)	ROC (ft/min)	End Point CAS (kt)
A320-211	ICAO_B	1	1	Takeoff	MaxTakeoff	1+F			
A320-211	ICAO_B	1	2	Climb	MaxTakeoff	1+F	1000		
A320-211	ICAO_B	1	3	Accelerate	MaxTakeoff	1+F		1150,5	186,2
A320-211	ICAO_B	1	4	Accelerate	MaxTakeoff	1		1300,7	208,1
A320-211	ICAO_B	1	5	Climb	MaxClimb	ZERO	3000		
A320-211	ICAO_B	1	6	Accelerate	MaxClimb	ZERO		1230,7	250
A320-211	ICAO_B	1	7	Climb	MaxClimb	ZERO	5500		
A320-211	ICAO_B	1	8	Climb	MaxClimb	ZERO	7500		
A320-211	ICAO_B	1	9	Climb	MaxClimb	ZERO	10000		